# Stratigraphic evolution of the Neoproterozoic Callison Lake Formation: Linking the break-up of Rodinia to the Islay carbon isotope excursion

# STRATIGRAPHIC EVOLUTION OF THE NEOPROTEROZOIC CALLISON LAKE FORMATION: LINKING THE BREAK-UP OF RODINIA TO THE ISLAY CARBON ISOTOPE EXCURSION

JUSTIN V. STRAUSS*, *****, FRANCIS A. MACDONALD*, GALEN P. HALVERSON**, NICHOLAS J. TOSCA***, DANIEL P. SCHRAG*, and ANDREW H. KNOLL*, ****

*Department of Earth and Planetary Sciences, Harvard University, 20 Oxford Street, Cambridge, Massachusetts 02138 USA

**Department of Earth and Planetary Sciences/Geotop, McGill University, 3450 University Street, Montreal, QC H3A 0E8 CANADA

***Department of Earth Sciences, University of Oxford, South Parks Road, Oxford, OX1 3AN UK

****Department of Organismic and Evolutionary Biology, Harvard University, 24 Oxford Street, Cambridge, Massachusetts 02138 USA

*****Present address: Department of Earth Sciences, Dartmouth College, HB6105 Fairchild Hall, Hanover, New Hampshire 03755 USA

**ABSTRACT. The ~780-540 Ma Windermere Supergroup of western North America records the protracted development of the western Laurentian passive margin and provides insights into the nature, timing, and kinematics of Rodinia's fragmentation. Here we present a refined tectono- and chemo-stratigraphic model for circa 780–720 Ma sedimentation in NW Canada through a study of the Callison Lake Formation**

**(formalized herein) of the Mount Harper Group, spectacularly exposed in the Coal Creek and Hart River inliers of the Ogilvie Mountains of Yukon, Canada. Twenty-one stratigraphic sections are integrated with geological mapping, facies analysis, carbon and oxygen isotope chemostratigraphy, and Re-Os geochronology to provide a depositional reconstruction for the Callison Lake Formation. Mixed siliciclastic, carbonate, and evaporite sediments accumulated in marginal marine embayments formed in discrete hangingwall depocenters of a prominent Windermere extensional fault zone. Deposition of the Windermere Supergroup in NW Canada post dates the eruption of the circa 780 Ma Gunbarrel Large Igneous Province by ~30 million years, is locally associated with compressional or transpressional tectonism, and predates the successful rift-drift transition by ~200 million years. In order to accommodate evidence for coeval extensional and compressional tectonism, abrupt facies change, and Neoproterozoic fault geometries, we propose that NW Laurentia experienced strike-slip deformation during the ~740–660 Ma early fragmentation of the supercontinent Rodinia. Sequence stratigraphic data from the Callison Lake Formation and other basal Windermere successions in the northern Canadian Cordillera delineate three distinct depositional sequences, or transgressive-regressive (T-R) cycles, that are coeval with similar stratigraphic packages in the ~780–720 Ma Chuar-Uinta Mountain-Pahrump basins of the western United States. The global circa 735 Ma Islay carbon isotope excursion is consistently present in carbonate strata of the third T-R cycle and is interpreted to represent a primary perturbation to the global carbon cycle, possibly driven by the uplift and weathering of extensive shallow epicontinental seaways and evaporite basins.**

Key words: Windermere Supergroup, Neoproterozoic chemostratigraphy, Islay carbon isotope excursion, Mount Harper Group, Callison Lake Formation

## INTRODUCTION

Neoproterozoic sedimentary deposits of western North America provide a critical record of the protracted breakup of the supercontinent Rodinia (Stewart, 1972; Young and others, 1979; Ross, 1991; Yonkee and others, 2014) and form the backbone to many global geochemical, paleontological, and geochronological compilations (Narbonne and others, 1994; Halverson and others, 2005; Rooney and others, 2015, Cohen and Macdonald, 2015). The tectonic setting and evolution of these sedimentary succesions also provide essential geological context for Neoproterozoic climate change. For instance, Rodinia's fragmentation at low latitude may have set the stage for runaway global cooling that resulted in global Cryogenian glaciation (Kirshvink, 1992; Hoffman and others, 1998; Hoffman and Schrag, 2002; Schrag and others, 2002). Recent interpretations for the initiation of these glaciations point to the consumption of $CO_2$ and $O_2$ via uplift and weathering of extensive continental flood basalts, many of which were centered along the Neoproterozoic margins of Laurentia (Goddéris and others, 2003; Donnadieu and others, 2004; Macdonald and others, 2010; Halverson and others, 2014; Rooney and others, 2014). Furthermore, high-precision U-Pb chemical abrasion-isotope dilution-thermal ionization mass spectrometry (CA-ID-TIMS) zircon ages on volcanic tuffs and Re-Os organic-rich rock (ORR) ages on black shale and carbonate interbedded with Neoproterozoic marine strata from NW Canada have recently established firm temporal constraints on critical events in Neoproterozoic Earth history, including the onset of the Sturtian glaciation and its relationship to the global Islay carbon isotope excursion (ICIE; also called the “Islay anomaly”) (Macdonald and others, 2010; Rooney and others, 2014; Strauss and others, 2014a). Yet, many aspects of the early tectonic and environmental evolution of the western Laurentian margin remain controversial, such as the temporal and spatial record of extension, the exact timing of rift-drift transition, and the paleogeographic arrangement of circum-Laurentian continents in Rodinia.

Building on the stratigraphic compilations of Gabrielse (1967) and Crittenden and others (1971), Stewart (1972) was the first Cordilleran geologist to highlight the “Windermere Group” and equivalent rocks as recording the rift phase of the western Laurentian passive margin. The <6 km thick Windermere Supergroup encompasses ca. 780–540 Ma rocks of the Canadian Cordillera (Sequence C of Young and others, 1979), but stratigraphic equivalents of these deposits span the length of North America from Mexico to Alaska (Wheeler and McFeely, 1991). The concept of Neoproterozoic extensional opening of the paleo-Pacific Ocean persisted for over a decade until papers using backstripping techniques to generate subsidence curves for the early Paleozoic passive margin indicated that the rift-drift transition occurred at ~540 Ma, ~200 million years after the major expression of Windermere Supergroup rift-related sedimentation and volcanism at ~780–680 Ma (Armin and Mayer, 1983; Bond and others, 1983; Bond and Kominiz, 1984; Devlin and Bond, 1988; Levy and Christie-Blick, 1989). Therefore, most recent reconstructions (for example, Colpron and others, 2002) indicate a protracted two-stage rift history for the western margin of Laurentia (ca. 780–700 and ca. 575–540

Ma), with localized pulses of extension persisting into the early Paleozoic (for example, Goodfellow and others, 1995; Cecile and others, 1997; Pyle and Barnes, 2003).

Mid-Neoproterozoic (Tonian–Cryogenian) Laurentian basins provide a particularly important record of the nature, timing, and driving mechanisms for Rodinia's initial fragmentation and inform the development of a viable kinematic model for Cordillera-wide extension. The evolution of these geographically isolated sedimentary deposits has been attributed to subsidence associated with mantle plume activity and emplacement of the ca. 780 Ma Gunbarrel Large Igneous Province (LIP) (Li and others, 1999; 2008; Harlan and others, 2003; Macdonald and others, 2012; Sandeman and others, 2014; Yonkee and others, 2014). In the western United States, these strata include the Chuar Group (Gp) of Arizona, the Pahrump Gp of California, and the Uinta Mountains Gp and Big Cottonwood Formation (Fm) of Utah, which are collectively referred to as the ChUMP basins (Dehler and others, 2010 and references therein). Equivalent strata in NW Canada, which are the focus of this study, include the Coates Lake Gp of the Mackenzie Mountains, Northwest Territories (NWT), and the Mount Harper Gp of the Ogilvie Mountains, Yukon (for example, Jefferson and Parrish, 1989; Mustard and Roots, 1997; Macdonald and others, 2012). In this contribution, we refine the record of early Windermere Supergroup sedimentation in the Ogilvie Mountains of Yukon, Canada, through an integrated study of the Callison Lake Fm (previously called the Callison Lake dolostone; table 1) of the Mount Harper Gp. We present new geological mapping combined with detailed measured stratigraphic sections, sequence stratigraphy, and carbon and oxygen isotope chemostratigraphy to develop a depositional model for the

Callison Lake Fm, provide an updated interpretation for mid-Neoproterozoic extension in NW Canada, and assess the origin of the ICIE.

## GEOLOGICAL BACKGROUND AND PREVIOUS WORK

Proterozoic sedimentary strata in northwest Canada are discontinuously exposed throughout the Cordilleran fold and thrust belt and in erosional inliers through Phanerozoic strata (fig. 1A). Although crystalline basement is not exposed in Yukon, Proterozoic sedimentary successions further to the east in the NWT rest unconformably on the ca. 1880–1840 Ma western Bear Province of the Wopmay Orogen (Hoffman, 1989; Villeneuve and others, 1991; Bowring and Grotzinger, 1992). Young and coworkers (1979) divided the Proterozoic sedimentary successions of NW Canada into three discrete unconformity bounded "sequences" (fig. 1): Sequence A (~1.7–1.2 Ga Wernecke Supergroup and equivalents), Sequence B (~1.2–0.78 Ga Mackenzie Mountains Supergroup and equivalents), and Sequence C (~0.78–0.54 Ga Windermere Supergroup and equivalents). Over the past three decades, this classification has been refined and subdivided following the recognition of regional unconformities, unique basin forming events, and new radiometric age constraints (Cook and Maclean, 1995; Thorkelson and others, 2005; Turner and others, 2011; Macdonald and others, 2012; Furlanetto and others, 2013; Medig and others, 2014; Thomson and others, 2014; 2015a).

The Callison Lake Fm of the Mount Harper Gp (Windermere Supergroup) is part of the Mackenzie-Ogilvie Platform, a paleogeographic feature of the Foreland Belt of the Canadian Cordillera (Gordey and Anderson, 1993; Cecile and others, 1997; Norris, 1997). More specifically, these strata are exposed in the Coal Creek and Hart River inliers of the

Yukon Block (see Yukon Stable Block of Jeletsky, 1962), an independent lithospheric block that underlies most of north-central Yukon from the Alaskan border to the Richardson Fault Array near the Yukon-NWT border (fig. 1; Jeletsky, 1962; Lenz, 1972; Roots and Thompson, 1992; Abbott, 1997; Cecile and others, 1997; Morrow, 1999; Thorkelson and others, 2005). The Dawson Fault (also known as the Dawson Thrust) and Richardson Fault Array bound the Yukon Block to the south and east, respectively (fig. 1); both of these long-lived structural features delineate a platform-to-basin transition – the Richardson Trough to the east and the Selwyn Basin to the south (for example, Gordey and Anderson, 1993; Abbott, 1997; Cecile and others, 1997). The northern and western boundaries of the Yukon Block are not as clearly defined.

Proterozoic strata of the Yukon Block are superbly exposed in the Tatonduk, Coal Creek, Hart River, and Wernecke inliers of Yukon, all of which share a similar, yet distinct, depositional history. Despite synsedimentary tectonism and associated complex facies change (for example, Aitken, 1981; 1991; Eisbacher, 1981; 1985; Jefferson, ms, 1983; Jefferson and Parrish, 1989; Abbott, 1997; Thorkelson and others, 2005; Turner and Long, 2008; Turner and others, 2011; Macdonald and others, 2012), recent work has begun to shed light on interregional correlations among the Proterozoic inliers of Yukon and strengthen connections to the well documented successions of the Mackenzie Mountains and Amundsen Basin (fig. 2; Rainbird and others, 1996; Abbott, 1997; Thorkelson and others, 2005; Macdonald and Roots, 2010; Macdonald and others 2010; 2011; 2012; Medig and others, 2010; 2014; Turner, 2011; Turner and others, 2011; Halverson and others, 2012; Cox and others, 2013; Furlanetto and others, 2013; van Acken and others, 2013; Kunzmann and others, 2014; Thomson and others, 2014; 2015a).

For the purposes of this contribution, we will not discuss the geology of the Tatonduk inlier any further because basal Windermere Supergroup strata are not well developed and exposed in this region (Macdonald and others, 2011). Importantly, there is a clear difference in equivalent Proterozoic strata across the Richardson Fault Array, particularly the Snake River and Knorr faults mapped by Aitken and Cook (1974), Eisbacher (1977; 1981), and Norris (1982). Stratigraphic correlation of Yukon Block inliers to the adjacent Mackenzie Mountains requires significant facies change and some component(s) of tectonic rotation and strike-slip displacement along the ancestral Richardson Fault Array (figs. 1, 2; Wheeler, 1954; Gabrielse, 1967; Aitken and Cook, 1974; Eisbacher, 1977; 1978; 1981; Bell, 1982; Jefferson, ms, 1983; Jefferson and Parrish, 1989; Aitken and McMechan, 1992; Park and others, 1992; Abbott, 1997; Thorkelson, 2000; Thorkelson and others, 2005).

### *Hart River Inlier*

The Hart River inlier is located in the southeastern Ogilvie Mountains (figs. 1, 2, 3) and contains Proterozoic strata of the Wernecke, Pinguicula, Fifteenmile, Rapitan, and Mount Harper groups. Green's (1972) regional mapping of the Dawson (116B and C), Larsen Creek (116A), and Nash Creek (106D) map areas established the regional stratigraphic and structural framework for the Ogilvie Mountains, upon which Abbott (1993; 1997) added detailed mapping of the Mark Creek area (fig. 3). The oldest strata exposed in the Hart River inlier comprise mixed siliciclastic and carbonate strata of the Quartet and Gillespie Lake groups (Wernecke Supergroup), which were most likely deposited in a Mesoproterozoic intracratonic basin or along a poorly understood passive continental margin (Green, 1972; Abbott, 1993; 1997; Delaney and others, 1981; Thorkelson and others, 2000; 2005; Furlanetto and others, 2013). The Hart River basalts unconformably overlie the Wernecke Supergroup and are assumed to be extrusive equivalents of the circa 1380 Ma Hart River sills (Abbott, 1997). These volcanic rocks are unconformably overlain by ~2.5 km of mixed siliciclastic-carbonate strata of the Pinguicula and Fifteenmile groups, which consist of two separate successions defined by map units PPA–C and PPD1–3 and separated by a prominent angular unconformity (figs. 2, 3; Abbott, 1997). Halverson and others (2012), following Medig and others (2010), correlated the upper Pinguicula Gp of the Hart River inlier (map units PPD1-3) with the informal Gibben and Chandindu formations of the lower Fifteenmile Gp of the Coal Creek inlier and the Hematite Creek Gp of the Wernecke inlier (figs. 2, 3).

In the Hart River inlier, the Callison Lake Fm rests with an angular unconformity on Pinguicula, Wernecke, and lower Fifteenmile Gp strata, suggestive of significant tectonic uplift and erosion prior to deposition (fig. 3; Abbott, 1997; Macdonald and Roots, 2010; Macdonald and others, 2010; Halverson and others, 2012). Abbott (1993; 1997) was the first to recognize the Callison Lake Fm and described it as a well-bedded, light gray weathering dolomite unit characterized by stromatolites, pisolites, intraformational breccias, “cryptalgal” laminations, and abundant chert lenses. No stratigraphic sections of the Callison Lake Fm were measured, and Abbott (1997) tentatively correlated these strata with the upper Fifteenmile Gp (map unit PF1) of the Coal Creek inlier and the Little Dal Gp of the Mackenzie Mountains. Based on similarities in lithology and stratigraphic position, Macdonald and Roots (2010) subsequently correlated the Callison Lake Fm with the upper Fifteenmile Gp of the Coal Creek inlier (map units PF2 and PF3).

The Callison Lake Fm is disconformably or erosionally overlain by conglomerate, glacial diamictite, or mixed carbonate-siliciclastic strata of the Mount Harper, Rapitan, Hay Creek, and 'upper' groups (figs. 2, 3; Abbott, 1997; Macdonald and Roots, 2010; Macdonald and others, 2010).

### *Coal Creek Inlier*

The Coal Creek inlier is located in the south-central Ogilvie Mountains (figs. 1, 2, 4) and contains Proterozoic strata of the Wernecke, Pinguicula, Fifteenmile, Rapitan, Mount Harper, Hay Creek, and "upper" groups. Following Green's (1972) establishment of the regional geologic framework for the Dawson (116B and C) map sheet, subsequent detailed mapping and stratigraphic projects by Thompson and Roots (1982), Blaise and Mercier (1984), Thompson and others (1987; 1994), Roots (ms, 1987), Mercier (1989), Mustard (ms, 1990; 1991), and Mustard and Roots (1997) subdivided the Proterozoic stratigraphic succession and established the informal Mount Harper and Fifteenmile groups. The oldest rocks exposed in the Coal Creek inlier comprise mixed siliciclastic and carbonate strata of the Fairchild Lake, Quartet, and Gillespie Lake groups (Wernecke Supergroup) (fig. 4). The overlying Fifteenmile Gp was originally subdivided into lower (PR1–5) and upper (PF1–3) subgroups with five and three map units (Thompson and others, 1994), respectively, that locally unconformably overlie the Pinguicula Gp and Wernecke Supergroup. Macdonald and Roots (2010) and Macdonald and others (2011; 2012) recently revised the Fifteenmile Gp sedimentary succession and discarded many informal map units used by Thompson and others (1994). According to this new scheme, the Fifteenmile Gp can be subdivided into an ~1 km thick "Reefal assemblage" (previous map units PR1–5 and PF1a) of mixed shale and carbonate strata. Zircon extracted from a quartz-phyric tuff interbedded with shale in the upper portion of the Reefal assemblage constrains its depositional age to 811.51 ± 0.25 Ma (CA-ID-TIMS; Macdonald and others, 2010). Halverson and others (2012) proposed a tripartite subdivision of the Fifteenmile Gp into the Gibben and Chandindu formations and the Reefal assemblage to clarify correlations among Proterozoic inliers, including the relationship between the Fifteenmile and Pinguicula groups. Macdonald and others (2012) and Kunzmann and others (2014) expanded upon this by providing a detailed description of the basin forming mechanism and regional correlations of these strata. Lower Fifteenmile Gp strata are gradationally overlain by the "Craggy dolostone" (informal term; formerly map unit PF1), an ~500 m thick, massive and highly silicified dolostone unit (Thompson and others, 1994; Macdonald and others, 2012). The Craggy dolostone is overlain by the Callison Lake Fm (formerly map units PF2 and PF3; table 1). Although this contact was previously considered gradational (Thompson and others, 1994; Mustard and Roots, 1997), here we document evidence for subaerial exposure, paleokarst development, and angular stratigraphic discordance along this contact (fig. 5A-C). The recognition in both the Coal Creek and Hart River inliers of a significant exposure surface and angular unconformity separating the Callison Lake Fm from the underlying Fifteenmile Gp (Abbott, 1997) suggests that the Callison Lake Fm is more closely related to the overlying Mount Harper Gp, which forms the base of the Windermere Supergroup (Macdonald and Roots, 2010; Macdonald and others, 2011; Strauss and others, 2014a).

## STRATIGRAPHIC FRAMEWORK AND FORMALIZATION OF THE MOUNT HARPER GROUP

The Mount Harper Gp of the Coal Creek inlier consists of three separate units (fig. 2): the ~500 m thick mixed siliciclastic-carbonate Callison Lake Fm that is described herein (table 1), an ~1100 m thick rift-related siliciclastic succession called the Seela Pass Fm (previously termed the “lower Mount Harper Group” or “Mount Harper conglomerate” but formalized herein; table 2), and an ~1200 m thick bimodal volcanic suite called the Mount Harper volcanics (previously termed the “Mount Harper Volcanic Complex”) (Strauss and others, 2014b and references therein). The overlying ~300–1400 m thick siliciclastic and carbonate succession, previously referred to as the “upper Mount Harper Group,” has been correlated with distinct portions of the Rapitan, Hay Creek, and “upper” groups of the Mackenzie Mountains and has been abandoned (Macdonald and others, 2011; Strauss and others, 2014b). The Mount Harper Gp stratigraphic succession in the Hart River inlier is not as well characterized (Abbott, 1997); however, our preliminary geological mapping differentiates the Mount Harper Gp from the overlying Rapitan, Hay Creek, and “upper” groups (fig. 4).

The Seela Pass Fm (table 2) is composed of up to ~1100 m of continental strata intimately associated with a syndepositional, north-side-down normal fault (fig. 5E; Thompson and others, 1987; Mustard, ms, 1990; Mustard, 1991; Mustard and Donaldson, 1990; Mustard and Roots, 1997; Strauss and others, 2014b). Mustard and Donaldson (1990) and Mustard (1991) describe the contact of the Seela Pass and Callison Lake formations as a distinct disconformity marked by up to ~100 m of paleorelief and thick paleokarst breccias. A thick tapering wedge of fault-derived breccia (Mustard, 1991), distinct from the laterally equivalent karst breccia, is preserved along the down-dropped side of the Harper Fault (Mustard, ms, 1990; Mustard, 1991; Mustard and Donaldson, 1990; Mustard and Roots, 1997). This geographically isolated wedge grades both northward and eastward into massive and disorganized beds of coarse-grained boulder to gravel conglomerate interpreted as upper- to mid-fan alluvial fan debris flows (Mustard, 1991). Farther to the northeast, alluvial fan deposits of the Seela Pass Fm grade laterally into conglomerate, sandstone, and mudstone of distal fan delta deposits that yield northward directed paleocurrent directions (Mustard, 1991). This maroon mudstone facies assemblage records a distinct coarsening-upwards package, which Mustard (1991) interpreted as evidence for progradation of Seela Pass alluvial fans into a lacustrine or marginal marine setting. Clastic deposition of the Seela Pass Fm ceased with the onset of Mount Harper volcanism (Mustard, 1991; Mustard and Roots, 1997).

The ancestral Harper Fault dips 50-60º northward and delineates the southernmost exposure of geographically isolated outcrops of the Seela Pass and Callison Lake formations in the Coal Creek inlier (figs. 4, 5E; Mustard and Roots, 1997). Detailed mapping suggests these limited regional exposures are of primary depositional origin, outlining the remnants of an ~10 (N-S) X ~80-100 (E-W) km Proterozoic half graben (Roots, ms, 1987; Mustard, 1991; Mustard and Roots, 1997; Strauss and others, 2014b). The footwall of the Harper Fault is composed of crenulated quartzite and shale of the Quartet Gp and tectonized carbonate of the Gillespie Lake Gp (Wernecke Supergroup) (fig. 4; Thompson and others, 1994; Mustard and Roots, 1997; Strauss and others, 2014b), providing a maximum ~4 km vertical offset assuming the sub-Mount Harper Gp succession in the hanging wall is of similar thickness to the eroded remnants of the footwall (Mustard, 1991). A minimum offset is ~1100 m, as indicated by the composite measured thickness of the Seela Pass Fm directly north of the Harper Fault (Mustard, 1991). Evidence for maximum progressive downward denudation of the footwall fault scarp is supported by inverted stratigraphy in fault-proximal Seela Pass conglomerates (Mustard, 1991; Macdonald and others, 2011).

The bimodal Mount Harper volcanics are divided into six informal units and two distinct compositional suites (fig. 4; Roots, ms, 1987; Mustard and Roots, 1997; Cox and others, 2013). The basal volcanic suite, members A–C, forms an ~1200 m thick basaltic edifice that conformably overlies Seela Pass strata in the hangingwall of the Harper Fault and unconformably overlies Quartet and Gillespie Lake strata in the footwall, attesting to uplift and erosion of the footwall block prior to volcanism (Mustard and Roots, 1997). These mafic lavas formed in both subaerial and subaqueous settings and most likely initially erupted subaqueously onto damp substrate of the Seela Pass Fm, judging from reworked volcaniclastics, convolute internal stratification, entrained clasts in lowermost lava flows, and loading structures in the uppermost Seela Pass Fm (Roots, ms, 1987; Mustard, 1991; Mustard and Roots, 1997; Cox and others, 2013). The upper suite is characterized by intermediate andesites and rhyolites of members D–F that were dated by U-Pb CA-ID-TIMS on zircon at 717.43 ± 0.14 Ma (Macdonald and others, 2010). The Mount Harper Volcanics are overlain conformably by, and locally interfinger with, conglomerate, sandstone, and glacial diamictite of the informal Eagle Creek formation (Strauss and others, 2014b) of the Rapitan Gp (Macdonald and others, 2010; 2011; Strauss and others, 2014b).

As noted above, Abbott (1993; 1997) was the first to recognize the Callison Lake Fm in the Hart River inlier, but no measured sections were presented in the literature until Macdonald and Roots (2010) and Macdonald and others (2010; 2011) presented preliminary coarse stratigraphic descriptions and carbon isotope chemostratigraphy from one section in the Coal Creek inlier. Subsequently, Tosca and others (2011) described the mineralogy of unusual sedimentary talc deposits from the lower Callison Lake Fm and Strauss and others (2014a) reported 739.9 ± 6.1 Ma vase-shaped microfossil (VSM) assemblages from black shale in upper Callison Lake strata (fig. 2). More recently, Rooney and others (2015) presented another Re-Os ORR age of 752.7 ± 5.5 Ma from the lower Callison Lake Fm (fig. 2). Here, we place all of these previous descriptions and geochronological constraints into a refined stratigraphic context while formalizing the Callison Lake Fm (table 1).

## METHODS

Geological mapping was undertaken in the Coal Creek inlier over two- to four-week summer field seasons from 2009–2013 and in the Hart River inlier during the summers of 2009, 2011, and 2012. Twenty-one detailed stratigraphic sections of the Callison Lake Fm were logged by measuring stick, tape measure, and Jacob staff at m- to cm-scale during mapping projects from 2009–2013 (coordinates of logged sections are provided in table DR1 of the AJS supplementary data file[1]). Owing to the constraint of available exposure, some of these measured sections are composite (figs. 6, 7). The

[1]All GPS coordinates for stratigraphic sections (table DR1) and carbon and oxygen isotope data (table DR2) are presented online as a supplementary electronic data file (http://earth.geology.yale.edu/~ajs/SupplementaryData/xxx/xxx).

measured sections are divided into siliciclastic, carbonate, and diagenetic lithofacies based on composition, texture, bedding style, and sedimentary structures (table 3). Paleocurrent analysis was not performed due to the general paucity of reliable current indicators.

We present 1222 new carbonate carbon ($\delta^{13}C_{carb}$) and oxygen ($\delta^{18}O_{carb}$) isotopic measurements from specified stratigraphic sections (all raw data are presented in table DR2 of the AJS supplementary data file[1]). Fist- to golf ball-sized hand samples were collected at 0.5–2 m resolution through measured sections for carbonate carbon and oxygen isotope chemostratigraphy. $\delta^{13}C_{carb}$ and $\delta^{18}O_{carb}$ isotopic results are reported in per mil notation of $^{13}C/^{12}C$ and $^{18}O/^{16}O$, respectively, relative to the standard VPDB (Vienna-Pee-Dee Belemnite). Carbonate samples were cut perpendicular to bedding and primary lithofacies were carefully microdilled (~2-10 mg of powder) to avoid secondary veins, cements, and siliciclastic components. $\delta^{13}C_{carb}$ and $\delta^{18}O_{carb}$ isotopic data were acquired simultaneously on a VG Optima dual inlet isotope ratio mass spectrometer coupled with a VG Isocarb preparation device (Micromass, Milford, MA) in the Laboratory for Geochemical Oceanography at Harvard University. Approximately 1 mg of sample powder was reacted in a common, purified phosphoric acid ($H_3PO_4$) bath at 90°C. The evolved $CO_2$ was collected cryogenically and analyzed using an in-house reference gas. Measured data were calibrated to VPDB using the Cararra marble standard (CM2). Total analytical errors ($1\sigma$) are better than ± 0.1‰ for both $\delta^{13}C_{carb}$ and $\delta^{18}O_{carb}$ based on repeat analysis of standards and samples. Increasing the reaction time to eleven minutes for dolomite samples minimized “memory effects” resulting from the common acid bath system, with the total memory effect estimated at <0.1‰ based on reproducibility of standards run directly after samples.

## SEDIMENTOLOGY AND STRATIGRAPHY OF THE CALLISON LAKE FORMATION

The Callison Lake Fm is divided here into four informal members (Heterolithic, Talc, Ramp, and Transitional) that can be correlated between the Coal Creek and Hart River inliers, albeit with differences in thickness, lithofacies, and preservation under erosional unconformities (figs. 6, 7). Member contacts define regionally significant sequence boundaries and/or distinct paleoenvironmental shifts, but they are not always distinguishable at a map scale, so we have elected to keep them informal. Below, we describe the primary lithofacies of each member, followed by a brief paleoenvironmental interpretation, and then summarize our findings in a regional tectono-stratigraphic synthesis put forth in the Discussion.

Lowermost strata of the Callison Lake Fm are heterogeneous along depositional strike and in the different inliers (figs. 6, 7). The basal surface is either marked by a significant disconformity with evidence for subaerial exposure, paleokarst development, and intense silicification, or a stratigraphic truncation of underlying units with subtle (<2°) to profound (>30°) angular discordance (fig. 5A-C). In the Coal Creek inlier, the upper contact is either gradational into overlying siliciclastic rocks of the Seela Pass Fm or marked by a profound erosional unconformity with overlying glaciogenic rocks of the Eagle Creek Fm (figs. 4, 6). In the Hart River inlier, the upper Callison Lake Fm is either truncated by imbricate Mesozoic and younger thrust faults or marked by an erosional unconformity with various younger units (figs. 3, 7).

### *Heterolithic member – Description*

The Heterolithic mb, named for its diverse lithological composition, is 23.5 to 155.9 m thick. A mixed suite of siliciclastic deposits (Facies F1, F2, F3, F4; table 3) characterize the bulk of this unit, but it also contains a distinct package of stromatolitic biostromes and bioherms (F7) that are present in both the Coal Creek and Hart River inliers (figs. 5H, 6, 7). The base of the Heterolithic mb rests on extensively silicified carbonate strata of the Craggy dolostone and is commonly marked by a thin (0.05–0.45 m), clast-supported chert and quartz pebble conglomerate unit (F1; fig. 8A). Thick- to medium-bedded and locally channelized sandstone deposits (F2), interbedded with variegated shale and siltstone (F3), overlie this coarse-grained unit in a series of stacked fining-upwards packages that range from ~10–70 cm thick (fig. 8B). The fine- to coarse-grained sandstone beds are moderately- to well-sorted, consist of quartz or chert arenite and wacke, and are characterized by crude parallel lamination and sparse symmetrical ripple- to unidirectional dune-scale trough cross-bedding with abundant shale-chip clasts. The variegated siltstone and shale facies (F3) contains mudcracks (fig. 8C), planar lamination, flaser bedding, and rare ball-and-pillow structures. Locally, there are clear erosional surfaces in the siltstone and shale units capped by crudely normal-graded and coarser-grained (up to granule size) sandstone beds that eventually fine-upwards back into mudcracked shale- and siltstone-dominated intervals; these m-scale, coarser-grained packages tend to have lenticular, channel-like geometries (fig. 5G).

The sandstone-dominated interval gradationally transitions into variegated shale and siltstone (F3) interbedded with dolomitic stromatolite biostromes and bioherms (F7), which are capped by a prominent interval of black shale (F4) (figs. 5, 6, 7, 8D-F). The bright yellow-orange to buff-white bioherms and biostromes generally range from ~0.2 to 42.8 m thick and are composed of morphologically diverse stromatolites, including conical forms, low inheritance branching structures (fig. 8D), laterally linked and/or high relief domal structures (fig. 8F), and high inheritance digitate forms, all of which have silty dolomudstone intercolumnar fill and local synoptic relief. The doloboundstone units also contain rare frosted quartz grains, and petrographic examination of stromatolite laminae yields zones of disseminated organic matter with dolomitized cyanobacterial sheaths (fig. 8G) and VSMs (fig. 8H). Notably, the Mount Harper East section (J1301) has a much thicker (~40 m thick) stromatolitic buildup than the rest of the sections (figs. 5H, 6) – this composite structure appears to comprise multiple superimposed stromatolitic bioherms and could be classified as a reef (*sensu* Geldsetzer and others, 1988).

The overlying black shale interval commonly drapes the distinct stromatolitic horizons and is up to ~60 m thick. A VSM-bearing shale layer at the base of this unit in the Mount Harper East section (J1301) has been dated with ORR Re-Os geochronology at 752.7 ± 5.5 Ma (fig. 6; Rooney and others, 2015). These strata are characterized by laminated, organic-rich black shale interbedded with thin intervals of gray-green silicified siltstone, planar laminated and silt-rich yellow-orange dolomudstone, and altered zones with abundant hematite, pyrite, sphalerite, and ankerite (figs. 6, 7). The black shale interval in the Coal Creek inlier also contains a thin (~2–25 cm), matrix-supported conglomerate bed with mm- to cm-scale poorly sorted and angular clasts of olive-green shale, chert-replaced isopachous and botryoidal cements, unusual chert spherules, and abundant cm-scale cubic pyrite. In the Hart River inlier, almost all of the fine-grained siliciclastic strata of the Heterolithic mb contain a prominent penetrative cleavage and are difficult to distinguish from underlying deposits of the Fifteenmile Gp equivalents (for example, map unit PPD3; fig. 3); however, this member is consistently present in the two inliers, albeit with prominent thickness and facies variation (figs. 6, 7). The contact with the overlying Talc mb is commonly marked by an abrupt transition into light gray microbial dolostone and/or talc-rich black shale.

*Heterolithic member – Interpretation*

Mixed siliciclastic and carbonate deposits of the Heterolithic mb record a decameter-scale fining-upwards package from the basal conglomeratic unit into thick black shale deposits. The base of the Heterolithic mb most likely records marine transgression over pre-existing irregular paleokarst topography formed in the underlying Craggy dolostone; in particular, the basal conglomeratic unit is interpreted here to represent a transgressive lag associated with regional deepening in the Callison Lake basin(s). As highlighted below, we tentatively interpret the Heterolithic mb to record sedimentation in a tidal flat to lagoonal depositional setting characterized by low topographic relief; however, the regional poor exposure of the Heterolithic mb, as well as the lack of paleocurrent data and poor preservation of internal bedding structures in sandstone units, precludes a very detailed paleoenvironmental interpretation.

The general fine grain size of basal Heterolithic mb deposits reflects predominant deposition from suspension; however, this low-energy depositional regime was clearly disrupted by intervals of higher-energy, bed-load sedimentation characterized by channelized, medium- to fine-grained sandstone units with basal erosional scours and abundant shale-chip conglomerate. The abundance of mudcracks in the variegated shale and siltstone facies (F3), and the presence of discrete shale partings with mudcracks between planar laminated sandstone beds, suggests these fine-grained deposits were commonly exposed to subaerial conditions. This evidence for periodic desiccation, in combination with the presence of local flaser bedding and symmetrical ripple cross-lamination in siltstone and sandstone units, provides support for a potential tidal influence on basal Heterolithic mb strata. Furthermore, the m-scale, crudely cross-bedded, and channelized sandstone units potentially represent intertidal dunes, or tidal bars (for example, Allen and Homewood, 1984; Ashley, 1990), which is supported by the the lateral transition of these coarser-grained units into the episodically-exposed variegated shale and siltstone facies (F3; fig. 5G). These combined features could also reflect low-energy fluvial sedimentation on a coastal plain; however, the fine-grained nature of the deposits, the facies stacking pattern of the entire Heteroltihic mb, and the presence of a basal conglomeratic lag all lend greater support to the development of a distinct transgressive, tide-dominated marine succession (Cattaneo and Steel, 2003; Dalrymple, 2010; Desjardins and others, 2012 and references therein). Unfortunately, the lack of paleocurrent data precludes the identification of bimodal versus unidirectional current indicators, as well as the development of a precise geometrical configuration for the paleoshoreline.

The upsection loss of coarser-grained siliciclastic deposits suggests a gradational transition into a zone of consistent suspension deposition, either due to relative deepening in the basin(s) below fair weather wave base (FWWB) or through the development of an outboard protective barrier to wave action (that is, shoal complex, sand ridge, or barrier island complex). The lack of current-generated bedforms in the upper Heterolithic mb and the development of laterally extensive, thick organic-rich black shale deposits is suggestive of a lagoonal or shelf interior depositional environment. This change in bathymetry is also consistent with the development of high relief and ornate stromatolitic bioherms and biostromes with minimal evidence for reworking through current or wave action. The bounding lithofacies composition and facies architecture in both the basal Heterolithic and overlying Talc members, in combination with the presence of VSMs in both stromatolitic laminae and encasing black shale units (figs. 6, 7, 8H), also implies a marine depositional setting for the upper Heterolithic mb (for example, Porter and Knoll, 2000).

*Talc member – Description*

The Talc mb, named for its unusual mineralogical composition (Tosca and others, 2011), ranges from 44.9 to 108.8 m in thickness. These strata are characterized by extreme lateral and vertical facies heterogeneity on a cm- to m-scale (figs. 6, 7, 9); therefore, we have simplified the main talc-rich facies into two categories (table 3) that include strata characterized by mm- to m-thick talc-rich black shale (F5) and intervals containing interbedded talc-rich shale and dolostone (F6). Other volumetrically significant facies that characterize this mb include stromatolitic and microbial dolostone

(F8, 9), intraclast grainstone and wackestone (F10), and oolitic or peloidal dolograinstone (F11) (figs. 6, 7, 9; table 3).

Talc-rich shale strata (F5) are dark-gray to jet-black, have a distinctive vitreous luster (fig. 9A), and locally contain abundant black chert nodules or silicified horizons (mm- to cm-thick). The shale is locally truncated by erosional surfaces, which are generally overlain by channelized bodies of shale-clast, matrix-supported conglomerate (F6; fig. 9B) or oolitic and oncolitic dolograinstone (F11). No crossbedding has been identified in these channelized deposits, but crude sub-parallel to inclined lamination is visible in finer-grained oolitic and intraclast dolograinstone lithologies.

Most dolostone units in the Talc mb are composed of mm- to cm-scale nodular dolomudstone (F6), planar to wavy laminated doloboundstone with morphologically diverse stromatolites (F8, F9; fig. 9C), or oncolitic and oolitic dolograinstone (F11). The stromatolites are characterized by a diverse morphological spectrum from cm-scale digitate and cuspate structures to large (>2.45 m thick) domal or conical buildups that have clear synoptic relief (fig. 9C); most stromatolitic laminae are coated with thin drapes of talc-rich shale. These microbially influenced and planar laminated dolostone horizons are commonly interbedded with, or grade laterally into, stromatolite-clast rudstone and wackestone, locally overturned stromatolitic mounds suspended in talc-rich shale (fig. 9D), and ptygmatically-folded dolostone laminites (fig. 9E). Other dolostone facies in the Talc mb include lenticular, m-scale deposits of medium- to thick-bedded, trough crossbedded oolitic and pisolitic dolograinstone (F11).

The Talc mb also contains tepees (*sensu* Kendall and Warren, 1987), mudcracks, and minor matrix-supported carbonate breccias (F14) at various stratigraphic levels in the carbonate-dominated strata (figs. 6, 7, 9). Dolomite pseudomorphs after gypsum ($CaSO_4 \bullet 2H_2O$) are locally present, as evidenced by cm-scale disc-shaped crystals and vertically oriented fibrous textures that resemble selenite, or satin spar. Dolomitic replacement fabrics after anhydrite ($CaSO_4$) are also common in the Talc mb, including nodular bedding resembling chickenwire texture (fig. 9F), discrete zones of enterolithic folding (*sensu* Butler and others, 1982), and isolated to coalesced displacive growth structures (fig. 9F). No primary evaporite minerals were recognized in the Talc mb; however, chert-replaced nodular structures after anhydrite with μm-scale relict anhydrite clusters, zebraic and length-slow chalcedony in megaquartz (Milliken, 1979; Folk and Pittman, 1971; Ulmer-Scholle and Scholl, 1994; Ulmer-Scholle and others, 1993), and small (< 200 μm) gypsum laths suspended in organic matter are present in thin section.

The Talc mb facies belt is traceable, albeit discontinuous, between the Coal Creek and Hart River inliers (>150 km) with discrete intervals characterized by subtle cyclicity and vertically stacked facies associations (figs. 6, 7, 9). For example, ~0.70–1.45 m thick parasequences composed of talc-rich shale, stromatolitic doloboundstone, microbialite, and mudcrack-dominated talc-rich shale and nodular carbonate are present in almost every section (figs. 6, 7, 9). Recrystallized sucrosic dolostone and pervasive silicification in the form of chert nodules (mm- to cm-scale) and stratiform chert horizons are also common features of dolomitic strata in the Talc mb.

### *Talc member – Interpretation*

As highlighted below, the Talc mb likely records deposition in a stable, episodically restricted marginal marine setting. The presence of evaporite pseudomorphs, tepees, mudcracks, and the intimate association of microbial dolostone and organic-rich fine-grained strata all suggest deposition in a subaerially exposed, but periodically flooded, peritidal mud flat, or sabkha, similar to the modern Trucial Coast of the Arabian Gulf (for example, Purser, 1973, Bathurst, 1975; Schreiber and others, 1986).

The predominance of laminated, talc-rich shale deposits, the lack of distinct wave-generated bedforms, and the abundance of microbial dolostone suggests consistent low-energy suspension and precipitation-based deposition in subtidal to supratidal depositional environments. The isopachous “stromatolitic” laminites of the Talc mb resemble subtidal evaporitic textures previously described by Pope and others (2000) in other Precambrian carbonate-evaporite sedimentary successions. There is also evidence for episodic high-energy events in the Talc mb that are responsible for channel incision, oolitic to oncolitic grainstone deposition, the deformation of microbial and/or suspension-load laminites, and the development of shale-chip conglomerate and stromatolitic/intraclast rudstone. The m-scale, channelized oolitic grainstones (F11) and shale-chip conglomerates (F6) most likely represent tidal channel avulsion and migration, whereas the presence of stromatolitic intraclast grainstone and wackestone and local synsedimentary deformation is more suggestive of episodic storm or seismic activity.

A marine paleoenvironmental setting characterized by alternation of subtidal and supratidal deposition is also supported by the abundance of microbial dolostone fabrics, from supratidal, planar-laminated microbialite to subtidal, m-scale stromatolitic buildups with synoptic relief. The distinct parasequence architecture of the Talc mb likely reflects marine shoaling cycles from subtidal talc-rich shale deposits into supratidal microbialite with subaerial exposure surfaces (fig. 9). This parasequence architecture is similar to those described from examples of modern and ancient marine peritidal deposits (for example, Purser, 1973; Grotzinger, 1989; Grotzinger and James, 2000 and references therein). Finally, the stratigraphic architecture of subjacent Heterolithic and Ramp mb strata also supports a model of tidal flat progradation, which is also characteristic of modern and ancient sabkha depositional reconstructions (for example, Pratt, 2010 and references therein).

The most distinctive component of the Talc mb is its namesake – the widespread presence of talc as an authigenic sedimentary mineral. Tosca and others (2011) performed X-Ray diffraction (XRD) analyses and experiments to show that talc was not only the main constituent of these unusual shale units, but also derived from an early authigenic precipitate due to its distinctive crystallographic disorder. The presence of talc in the Callison Lake Fm is most likely a result of relatively late (burial?) diagenetic transformation from a hydrated Mg-clay precursor such as kerolite ($Mg_3Si_4O_{10}(OH)_2 \bullet H_20$), sepiolite ($Mg_2Si_6O_{15}(OH)_2 \bullet 4H_2O$), or stevensite ($Na_{0.15}Mg_3Si_4O_{10}(OH)_4$), all of which are metastable relative to talc (Tosca and others, 2011). Most descriptions of modern Al-free Mg-clay occurrences are from evaporitic and alkaline lacustrine basins (Calvo and others, 1999 and references therein); however, they are also described in open marine environments, pedogenic horizons, hydrothermal settings, and weathering profiles of mafic volcanic rocks (Millot, 1970; Weaver and Beck, 1977; Stoessell and Hay, 1978; Yan et al., 2005; Dekov et al., 2008; Galán and Pozo, 2011; Tosca, 2015 and references therein). The significance of the widespread distribution, impressive thickness, and unique depositional fabrics of Callison Lake talc deposits is being presented elsewhere.

*Ramp member – Description*

The Ramp mb is the thickest and most laterally extensive unit in the Callison Lake Fm, measuring up to ~518 m thick near Mount Harper in the Coal Creek inlier (section J1210; fig. 6). The contact between the Talc and Ramp members is marked by the loss of talc-rich shale and a transition into light- to dark-gray thinly bedded dolomudstone with bright red to maroon shale partings (figs. 6, 7, 10B). Exposures of the Ramp mb average ~400 m thick and are overlain by an erosional unconformity (figs. 6, 7), except in localities in the eastern Coal Creek inlier where the overlying Transitional mb is conformable with the Seela Pass Fm (fig. 5).

Relatively homogeneous light- to dark-gray and medium- to thick-bedded dolostone characterizes the Ramp mb. These dolostones locally appear massive and structureless due to a combination of fabric-destructive dolomitization and surficial caliche precipitation and lichen growth. Characteristic facies include microbial and stromatolitic dolostone (F7-9), oolitic and peloidal dolograinstone (F11), stromatolitic intraclast grainstone and wackestone (F10), laminated dolomudstone and dolosiltite (F12), and diagenetic facies such as pervasively recrystallized dolostone (F13) and carbonate breccia (F14). Similar to microbial structures described in the underlying strata, Ramp mb microbial dolostone is characterized by a pronounced diversity in morphology and size, including flat, crinkly laminated microbialite with fenestral fabrics, laterally-linked to high-relief domal structures (fig. 10E), high-inheritance columnar forms, and m-scale broad domal buildups (fig. 10F).

One of the most common features in the Ramp mb is the abundance of stromatolite clast grainstone, wackestone, and floatstone (F10; figs. 6, 7, 10E); these cm- to m-scale crudely laminated and poorly sorted deposits are commonly associated with erosional surfaces in underlying stromatolite or microbialite units (for example, fig 10E). Other possible microbial features in the Ramp mb include cm- to m-thick intervals of mm- and cm-scale "clotted" fabrics with irregularly shaped cavities filled by multiple generations of dolomitic cement (fig. 10C). These unusual "clotted" fabrics resemble features described as "thrombolitic" by Harwood and Sumner (2011; 2012) from the Neoproterozoic Beck Spring Dolomite of Death Valley and putative microbial fabrics mentioned by Turner and others (2011) in the correlative Coppercap Fm of the Mackenzie Mountains, NWT (fig. 2); however, the origin of these structures remains ambiguous in the Callison Lake Fm because we lack clear petrographic evidence for a non-diagenetic origin. The Ramp mb also contains multiple, m-thick, massive oncolitic dolograinstones and floatstones that locally contain pendant cements (fig. 10D).

The Ramp mb contains medium- to thick-bedded, fine- to coarse-grained, and trough and tabular cross-bedded dolograinstone horizons (F11; figs. 6, 7, 10A). Giant ooids (Swett and Knoll, 1989; Grotzinger and James, 2000), peloids, pisoids, and various intraclasts are the predominant clasts in these grainstone deposits. The geometries of these deposits are difficult to reconstruct on single ridgeline exposures in the Ogilvie Mountains, but in some instances, one can document distinct along-strike transitions into finer-grained deposits of dolosiltite, dolomudstone, or stromatolitic doloboundstone (figs. 6, 7). As noted above, the dolosiltite and dolomudstone units (F12) are generally thin-bedded and contain ferruginous clay partings and local erosional scours (fig. 10B); no distinct grading has been recognized in these intervals. These finer-grained deposits, as well as the microbialite units (F9), locally display irregular ptygmatic folds and convolute bedding (for example, Mount Gibben East, section J1302; figs. 6, 7, 10G).

Grainstone deposits of the Ramp mb (F10, 11) tend to be the locus of late-stage, fabric-destructive diagenetic recrystallization (F13), most likely due to their elevated primary porosity. These sucrosic dolostones are generally thick-bedded or massive, and commonly devoid of sedimentary structures in outcrop (figs. 6, 7). Some of the massive dolostone units underlie massive carbonate breccias (F14, figs. 6, 7, 10H). The buff-colored, matrix-supported breccias range from ~0.7 to 4.2 m thick and are generally composed of a fitted fabric of angular dolostone clasts (locally silicified) in a matrix of terriginous silt, dolosiltite, or pure coarse-grained dolomite spar (fig. 10H). Finally, black to dark gray chert is another ubiquitous diagenetic feature in carbonate deposits of the Ramp mb.

*Ramp member – Interpretation*

As described below, the Ramp mb lithofacies record a mixture of subtidal to supratidal depositional environments. Thick intervals of chaotic, ptygmatically-folded and laminated dolosiltite and microbialite (for example, Mount Gibben East, section J1302; figs. 6, 10G) suggest that Ramp mb strata were subject to episodic synsedimentary deformation and seismic activity. Concordant and planar-laminated strata bound these convoluted intervals, so the deformation was not post-depositional and younger in origin.

The basal fine-grained strata of the Ramp mb most likely reflect sub-wave base suspension deposits; the discrete ferruginous clay laminae could record episodic pulses of very-fine-grained siliciclastic delivery into the basin and/or the development of basinal hardgrounds and authigenic iron silicate precipitation. Stratigraphically higher intervals of dolomudstone and dolosiltite deposits interfinger with doloboundstone and oolitic dolograinstone units, which is suggestive of deposition in the lee of topographically elevated subtidal features. In support of this interpretation, several components of the Ramp mb record evidence for peritidal deposition and episodic subaerial exposure. For example, the abundance of planar, crinkly laminated microbialite with abundant fenestral fabrics is a characteristic feature of peritidal carbonate deposits (for example, Pratt, 2010 and references therein). These supratidal features, and their intimate association with interbedded dolograinstone and doloboundstone facies, suggests that these represent small emergent tidal flats that formed in the lee of topographic barrier complexes such as oolitic shoals or stromatolitic build ups similar to the Trucial Coast (for example, Purser, 1973).

The abundance of stromatolite intraclast grainstone in the majority of Ramp mb deposits, as well as coarse-grained grainstone of variable allochem composition, is suggestive of a generally high-energy depositional setting above storm wave base (SWB). This is confirmed by distinct erosional scours in doloboundstone facies (for example, fig. 10E), as well as trough cross-bedded oolitic grainstone deposits that require relatively constant subtidal wave action; however, the preservation of poorly sorted intraclast dolowackestone and ornate stromatolitic and microbialite textures between erosional surfaces requires episodes of stromatolite proliferation and lower-energy suspension deposition. This is also supported by the widespread development of m-scale, high relief domal stromatolitic structures in close association with wackestone deposits (figs. 6, 7, 10F). Therefore, these somewhat disparate facies associations most likely reflect deposition at different water depths on a carbonate ramp with the localized development of patch reefs and microbial buildups (*sensu* Read, 1982).

The massive carbonate breccia units in the Ramp mb are interpreted as paleokarst horizons developed during subaerial exposure episodes of the carbonate depositional system. Similar to the peritidal carbonate fabrics, most of these horizons are relatively thin and difficult to trace along strike between individual sections; however, near Mount Harper there is evidence for an extensive ~60 m thick paleokarst unit that defines the upper boundary of the Ramp mb (section J1210; figs. 4, 6; Mustard and Donaldson, 1990). This interval was previously considered to define a major disconformity between the Fifteenmile and Mount Harper groups (Mustard and Donaldson, 1990; Mustard, 1991; Mustard and Roots, 1997); but, approximately 7.5 km along depositional strike at Mount Harper East (section J1301) there is no karst horizon and the Ramp-Transitional mb contact is conformable (fig. 6), reflecting a diachronous contact between these two members.

*Transitional member – Description*

Previous workers (for example, Thompson and others, 1994; Mustard, 1991; Mustard and Roots, 1997; Macdonald and others, 2010; 2011) included the Transitional mb in the basal part of the Seela Pass Fm because the upper Ramp mb contact delineates a distinct map-scale lithological boundary; however, we demonstrate here that these strata are not only tied to the Callison Lake Fm, but also record one of the most critical geochemical and tectonic transitions in the Mount Harper Gp.

The Transitional mb consists of a relatively thin (19.4 to 43.4 m thick) and discontinuous package of mixed siliciclastic and carbonate rocks that only outcrop in the eastern part of the Coal Creek inlier and define a coarsening upwards trend into maroon shale, sandstone, and conglomerate of the Seela Pass Fm (figs. 4, 6). West of Mount Harper the Ramp-Transitional mb contact is either truncated by overlying younger units or marked by a significant disconformity and paleokarst horizon (figs. 3, 6; Mustard and Donaldson, 1990); in contrast, east of Mount Harper, this contact appears to be conformable, although with some component of stratigraphic onlap as discussed below. In the conformable sections, the member contact is typically marked by an abrupt transition from interbedded oolitic dolograinstone and doloboundstone (F8, 9, 11) of the upper Ramp mb into very-thin-bedded dolomudstone and dolosiltite (F12; fig. 6). These fine-grained deposits range from 5–70 cm thick and are characterized by wavy and tabular bed geometries with 0.1–0.9 cm thick maroon clay partings and abundant black chert nodules.

The bulk of Transitional mb deposits generally consist of interbedded dark-gray stromatolitic dolostone (F8) and black shale (F4). Stromatolites of this interval are characterized by a variety of digitate columnar forms (fig. 11A), high-inheritance and laterally linked domal structures (fig. 11B), and irregularly shaped branching morphologies; most of these stromatolites are locally affected by zones of convolute lamination, slumped features, or healed synsedimentary, cm-scale normal faults (fig. 11B). The stromatolites also tend to be in primary growth position, contain significant fine-grained terriginous silt and clay components, and lack erosional surfaces. These deposits are then overlain by a package of laminated and silicified black shale and siltstone (F4) that ranges from 9.8 to 11.3 m thick (fig. 6). On an outcrop scale, these poorly exposed and organic-rich siliciclastic deposits appear to be homogeneous and very-fine grained; however, in thin section they are clearly composed of poorly sorted and crudely stratified mud, silt, and very-fine sand-sized particles (fig. 11C) – no evidence for grading has been documented. At Mount Gibben East (section J1204; fig. 6), a black shale layer from this interval yielded a Re-OS age of 739.9 ± 6.1 Ma and contained assemblages of diverse VSMs (figs. 6, 11C; Strauss and others, 2014a).

There are exceptions to this general lithofacies progression. For example, at Mount Harper (J1210) the Ramp-Transitional mb contact is marked by an abrupt transition from massive silicified breccia into interbedded black shale (F4) and very thin- to medium-bedded, extensively fractured orange-yellow laminated dolomudstone and dolosiltite (F12; fig. 6). This interval is both cut by numerous mafic sills of the Mount Harper Volcanics (fig. 6) and sheared between rheologically stiff bounding units (Ramp mb and Seela Pass Fm); however, it appears to be equivalent to the prominent black shale horizon midway through the Transitional mb and is therefore missing the basal carbonate-shale sequence (fig. 6).

The uppermost Transitional mb consists of interbedded microbialite (F9), stromatolite doloboundstone (F8), stromatolite intraclast grainstone and wackestone (F10), and silicified breccias (F14) (fig. 6). Microbial and stromatolitic dolostones are light- to dark-gray and consist of stratiform crinkly lamination and laterally-linked, low relief stromatolitic domal structures up to 35 cm tall. These microbialites are locally truncated and interbedded with thin- to medium-bedded stromatolite intraclast wackestone and grainstone that fill topographic relief above erosional scours. Some of these microbialite intervals display fenestral fabrics, mudcracks, and tepee structures (fig. 6). At Mount Gibben East (J1203 and J1204), these carbonate strata are capped by enigmatic, ~4-10 m thick silicified dolostone breccia units. The massive matrix-supported breccias are characterized by poorly sorted, pebble- to boulder-sized angular to subrounded clasts of extensively silicified dolostone that resemble facies of the underlying Ramp and Transitional mb strata (fig. 11D). The base of the overlying Seela Pass Fm is defined herein as the first appearance of sandstone or conglomerate, which is laterally variable in stratigraphic location due to the NE-directed progradation of Seela Pass alluvial systems over Transitional mb deposits (for example, Mustard, 1991).

### *Transitional member – Interpretation*

The abrupt shift from upper Ramp mb mixed subtidal and supratidal deposits into finer-grained strata of the basal Transitional mb records a prominent deepening into a zone of low-energy suspension sedimentation. We interpret the ferruginous clay partings to represent a combination of hardground cementation and episodic fine-grained siliciclastic rainout. The overlying interval of interbedded black shale and stromatolitic doloboundstone lacks erosional surfaces, storm deposits, and wave- or current-generated bedforms, which suggests these strata were either deposited below SWB or isolated from wave action through the development of a topographic barrier (for example, shoal complex, sand ridge, or barrier island complex). Onlap of these strata onto the prominent paleokarst horizon at Mount Harper suggests base-level rise was involved in this distinct facies shift, and the development of a protected lagoonal or shelf interior depositional setting is supported by the absence of a transition through distinct shoreface deposits and the along-strike development of extensive organic-rich black shale deposits. Continuous deepening below SWB and/or increased isolation from wave action coupled with drowning of the carbonate factory or burial due to siliciclastic influx is consistent with the upsection loss in carbonate and deposition of laminated black shale and siltstone. However, this deepening may also be the result of local synsedimentary faulting as suggested by the abundance of siliciclastic material in the stromatolitic units and the presence of cm-scale healed normal faults and convolute lamination, as well as the limited geographic range of this unit.

The upper part of the Transitional mb records shallowing from the underlying suspension-dominated subtidal environments into a zone of supratidal carbonate sedimentation. The reappearance of stromatolitic doloboundstone with erosional scours, intraclast wackestone and grainstone, and fenestral microbialite with sparse mudcracks and tepees is characteristic of subtidal to supratidal depositional settings. The development of subaerial conditions is consistent with the eventual widespread progradation of Seela Pass alluvial fan and fan delta deposits over the Transitional mb. Although one could interpret the silicified breccias at Mount Harper East as paleokarst units, the presence of clasts from the underlying Ramp and Transitional members makes these breccias difficult to explain as *in situ* dissolution breccias. Another possibility that we discuss below is that they represent matrix-supported debrites, consisting of reworked fault talus from localized, basin-bounding structures associated with the onset of regional extension.

## SEQUENCE STRATIGRAPHY OF THE CALLISON LAKE FORMATION

Sequence stratigraphy has been applied previously to Proterozoic sedimentary successions in NW Canada to correlate amongst disparate stratigraphic sections in geographically isolated basins (Grotzinger, 1986; Bowring and Grotzinger, 1992; Rainbird, 1993; Long and others, 2008; Macdonald and others, 2012; Thomson and others, 2015a). Here, we provide a basic sequence stratigraphic framework for the Callison Lake Fm based on the recognition and interpretation of transgressive-regressive (T-R) cycles in outcrop exposures from the Coal Creek and Hart River inliers. T-R cycles (that is, depositional sequences) are comprised of discrete packages of strata deposited during a full cycle of change in accommodation or sediment supply (*sensu* Catuneanu and others, 2009; 2011). These cycles are bounded by subaerial unconformities, flooding surfaces, shoreline ravinement surfaces, or regressive marine erosional surfaces, and they contain a transgressive phase that records an upward deepening event and a regressive phase that records an upward shallowing event (for example, Johnson and Murphy, 1984; Johnston and others, 1985; Embry and Johannessen, 1992; Embry, 1995; 2009). Here, we follow the terminology put forth by Catuneanu and others (2011) to define subaerial unconformities, maximum flooding surfaces, maximum regressive surfaces, and transgressive ravinement surfaces.

The Callison Lake Fm records three discrete T-R cycles (fig. 12; labeled T-R6, T-R7, and T-R8). This terminology builds upon previous sequence stratigraphic work in NW Canada from Long and others (2008) and Thomson and others (2015) in the correlative upper Shaler Supergroup of the Amundsen Basin, NWT. The basal Heterolithic mb deepening over the Craggy dolostone-Callison Lake subaerial unconformity records the onset of T-R6. We interpret the conglomeratic lag at the base of the Heterolithic mb to represent a transgressive ravinement surface associated with T-R6, and the maximum flooding surface (MFS) is recorded in black shale deposits just above the prominent stromatolitic bioherms and biostromes of the middle Heterolithic mb (figs. 6, 7, 12). The overlying Talc mb belongs to the regressive part of T-R6 and records a distinct episode of tidal flat progradation and parasequence development (fig. 12).

The base of T-R7 is marked by a sharp transition from evaporitic dolostone and talc-rich shale of the Talc mb into non-restricted carbonate deposits of the Ramp mb (fig. 12). This boundary most likely represents a maximum regressive surface (*sensu* Embry, 2009), as it records the onset of marine transgression over evaporitic strata of the Talc mb. A thin interval of thin-bedded, laminated dolomudstone and dolosiltite at the base of the Ramp mb represent the transgressive phase of T-R7 (figs. 6, 7, 12). The MFS of T-R7 is difficult to place, but the regressive phase of T-R7 is clearly defined by the thick and extensive progradational carbonate strata of the Ramp mb (fig. 12). A local subaerial unconformity defines the Ramp-Transitional mb contact and marks the top of T-R7 (figs. 6, 12).

T-R8 is complicated by local extensional tectonism during the Callison Lake-Seela Pass transition. Transgressive deposits associated with T-R8 include thin-bedded dolomudstone and interbedded microbial dolostone and black shale of the basal Transitional mb (fig. 12). The MFS of T-R8 is somewhere in the prominent black shale deposits of the middle Transitional mb, which locally drape the subaerial unconformity surface in the western part of the Coal Creek inlier (fig. 6). Regressive deposits of T-R8 are represented by the transition back into microbial carbonate deposition at the top of the

Transitional mb; the upper T-R8 boundary is most likely represented by a local subaerial unconformity at the Callison Lake-Seela Pass formational boundary (fig. 12).

## *CARBONATE CARBON AND OXYGEN ISOTOPE RESULTS*

Previously published $\delta^{13}C_{carb}$ and $\delta^{18}O_{carb}$ chemostratigraphic data for the Callison Lake Fm are reported from two stratigraphic sections in the Coal Creek inlier and define a trend from relatively enriched background $\delta^{13}C_{carb}$ values (~5‰) to a negative anomaly down to approximately -6‰ (Mount Harper and Mount Gibben East, fig. 4; Macdonald and others, 2010; Strauss and others, 2014a). Here, we present 1222 new $\delta^{13}C_{carb}$ and $\delta^{18}O_{carb}$ measurements from the Coal Creek and Hart River inliers that range from -5.8 to 6.1‰ and -11.4 to 4.0‰, respectively, and are shown in stratigraphic context in figures 6 and 7. Figure 13 provides a compilation of $\delta^{13}C_{carb}$ vs. $\delta^{18}O_{carb}$ crossplots for the different members of the Callison Lake Fm.

Carbon and oxygen isotope data from the Heterolithic mb range from -1.6 to 5.4‰ and -11.4 to 3.8‰, respectively (figs. 6, 7, 13). The majority of $\delta^{13}C_{carb}$ values are moderately enriched (average = 2.2‰) and almost exclusively come from the stromatolitic biohermal and biostromal intervals in the central portion of the Heterolithic mb; few data come from isolated thin-bedded dolomudstone interbedded with thicker siliciclastic-dominated intervals, most of which tend to be slightly depleted in $\delta^{13}C_{carb}$. Oxygen isotope data from the Heterolithic mb, and the Callison Lake Fm in general, are very enriched compared to average Neoproterozoic limestone data and normal to slightly enriched in comparison to average dolostones (for example, Jacobsen and Kaufman, 1999; Jaffrés and others, 2007; Prokoph and others, 2008). Contrary to all the other members in the Callison Lake Fm, $\delta^{13}C_{carb}$ and $\delta^{18}O_{carb}$ weakly covary in the Heterolithic mb (fig. 13).

Talc mb $\delta^{13}C_{carb}$ and $\delta^{18}O_{carb}$ data are more variable with values ranging from -5.6 to 5.5‰ and -7.1 to 3.8‰, respectively, and do not covary. The majority of Talc mb strata commence with moderately enriched $\delta^{13}C_{carb}$ values and trend towards more depleted isotopic compositions upsection (figs. 6, 7). In the Hart River inlier, there is a distinct negative $\delta^{13}C_{carb}$ isotope anomaly in the upper Talc mb down to values as low as -5.61‰; this trend is evident in the Coal Creek inlier as well, although it is not as clearly developed. Some stratigraphic sections appear to record a series of $\delta^{13}C_{carb}$ shifts in the Talc mb (for example, section J1302, Mine Camp, fig. 6), portions of which could be captured in other sections given the profound thickness differences and sampling resolution.

Ramp mb $\delta^{13}C_{carb}$ and $\delta^{18}O_{carb}$ values range from -1.8 to 6.1‰ and -8.2 to 5.5‰, respectively. $\delta^{13}C_{carb}$ data generally record a reproducible positive-drifting trend just above the Talc-Ramp mb transition and remain between 2–5‰ for the entirety of the Ramp mb (figs. 6, 7). However, the middle portion of the Ramp mb in the Hart River inlier displays a distinct interval of stratigraphically consistent depleted $\delta^{13}C_{carb}$ values that range from 0 to -1.8‰; this feature is not seen in correlative strata of the Coal Creek inlier. $\delta^{18}O_{carb}$ values from the Ramp mb are variable, but also are enriched (ave. = -0.2‰) with $\delta^{13}C_{carb}$ vs. $\delta^{18}O_{carb}$ data displaying a lack of covariance (fig. 13).

Carbon and oxygen isotope data from the Transitional mb range from -5.8 to 4.2‰ and -9.0 to 4.0‰, respectively. Carbon isotope values from these strata record a prominent ~10‰ negative carbon isotopic excursion that has been previously correlated with the global ca. 735 Ma Islay anomaly (Prave and others, 2009; Macdonald and others, 2010; Rooney and others, 2014; Strauss and others, 2014a). Here, we report $\delta^{13}C_{carb}$ and $\delta^{18}O_{carb}$ data from four parallel sections through this anomaly that reproduce a prominent trend from enriched $\delta^{13}C_{carb}$ values of the upper Ramp mb into variably depleted $\delta^{13}C_{carb}$ isotopic compositions in the middle Transitional mb (fig. 6). All of these sections display distinct structure to the negative $\delta^{13}C_{carb}$ anomaly, in which the nadir of the excursion is generally associated with m-scale variation between approximately -2 and -5‰ and then a distinct return to enriched values up to 0.8‰ in the uppermost Transitional mb strata. Carbon and oxygen isotope data from the Transitional mb do not covary (fig. 13), and $\delta^{18}O_{carb}$ values are similar to those reported in underlying members of the Callison Lake Fm.

## DISCUSSION

### *Tectono-stratigraphic Model for the Callison Lake Formation*

The development of a regional angular unconformity beneath the Mount Harper Gp, coupled with previous documentation of fault-controlled sedimentation in the Seela Pass Fm, provides evidence for mid-Neoproterozoic (late Tonian) extensional tectonism in Yukon (Mustard, 1991; Abbott, 1997; Mustard and Roots, 1997; Thorkelson and others, 2005; Macdonald and Roots, 2010; Macdonald and others, 2012). Previous studies placed the onset of extension in the Seela Pass Fm and overlying Mount Harper volcanics of the Mount Harper Gp (for example, Mustard, 1991; Mustard and Roots, 1997), but we suggest the Callison Lake Fm represents an earlier manifestation of regional extension in NW Canada associated with the onset of Windermere Supergroup sedimentation. Therefore, the 752.7 ± 5.5 Ma Re-Os depositional age from the maximum flooding interval of the Heterolithic mb (fig. 12; Rooney and others, 2015) provides an important new temporal constraint for an episode of regional extension in Yukon. Below, we use the sedimentological data described above to reconstruct a depositional model for the Callison Lake Fm (fig. 14); this is followed by a review of regional map patterns and correlations to help refine our kinematic model for mid-Neoproterozoic extensional tectonism in NW Canada and the greater North American Cordillera.

The precise geometry of the original Callison Lake basin is difficult to reconstruct due to limited exposure and subsequent erosional truncation and fault reactivation; however, many of the sedimentological features and map patterns point to deposition in semiarid, marine-influenced extensional sub-basins. Evidence for fault related sedimentation includes lateral and longitudinal basin-fill asymmetry, abrupt facies and thickness change, sedimentary structures interpreted as indicating synsedimentary deformation, and the development of localized disconformities and topographic relief. The general increase in member thickness from NNW to SSE in both the Coal Creek and Hart River inliers suggests regional deepening to the SSE towards hypothesized ancestral basin-bounding structures (figs. 6, 7, 14). The lack of exposure between the Hart River and Coal Creek inliers makes it difficult to assess whether these two areas were originally linked by a single, >110 km long extensional basin or if they formed as independent half graben separated by an accommodation, or transfer zone. Given the common segmentation of large, active fault zones (for example, Jackson and White, 1989), we consider these two regions as representing discontinuous marine embayments, or gulfs, formed in hangingwall depocenters and associated with discrete, ~20-40 km-long basin-bounding fault segments of an evolving border fault zone.

The general fine-grained nature of Heterolithic mb strata and the lack of locally preserved alluvial fan deposits suggests that the preserved portions of the Callison Lake hangingwall depocenters were relatively distal to basin-bounding structures and ancestral topographic highlands (fig. 14A). Heterolithic mb siliciclastic strata record deposition in a tidally influenced nearshore or coastal plain setting whose sediment supply was potentially sourced by axial fluvial systems and/or hangingwall fans (fig. 14A). The transition from these marginal marine deposits into the upper Heterolithic mb black shale and stromatolitic bioherm facies records regional deepening and the development of a protected lagoonal or interior shelf depositional environment. Shallower, intertidal lithofacies are recorded from sections in the NW Coal Creek inlier (for example, Mine Camp (J1302) and Talc Falls (F926-8); figs. 6, 9), which could represent the local transition into nearshore, supratidal depositional environments. Interestingly, Carr and others (2003) describe very similar fine-grained lithofacies in the early Miocene Nukhul Fm of the Egyptian Suez Rift (Red Sea), which consists of estuary mouth sandstone facies interbedded with estuary funnel and deltaic variegated mudstone and sandstone facies deposited in narrow hangingwall depocenters. Although there is no evidence for the development of such narrow basins in the Callison Lake Fm, we argue that this paleoenvironmental setting potentially provides a good analog for early Heterolithic mb sedimentation.

The abrupt paleoenvironmental shift from suspension-dominated deposits of the upper Heterolithic mb into peritidal deposits of the Talc mb most likely represents regional shoaling and subsequent tidal flat progradation over the shelf/lagoonal depositional system, similar to the Holocene development of the Abu Dhabi sabkhas (for example, Purser, 1973). There are a number of important characteristics of the Talc mb that indicate a marine depositional setting despite some of the ambiguity derived from the presence of abundant authigenic Mg-clay minerals (for example, Calvo and others, 1999). First, the Talc mb facies belt is unlike classic bulls-eye evaporite patterns developed in continental settings (for example, Warren, 1989). Furthermore, there is no evidence for the precipitation of bittern salts or saline carbonates in the Talc mb and the close association of organic-rich, microbially influenced dolostone with sulfate evaporite replacement fabrics is a classic feature of marine-fed sabkhas (for example, Schreiber and El Tabakh, 2000 and references therein). For example, the abundance of dolomite-replaced evaporite pseudomorphs, chaotic displacement fabrics, and m-scale parasequences are all indicative features of intra-sediment sulfate evaporite precipitation and the development of evaporitic cycles, which are ubiquitous features of modern and ancient marine sabkhas (for example, Shearman, 1978; Butler and others, 1982; Kirkham, 1997). Building upon the analog depositional setting of African-Arabian extension in the Red Sea, the Talc mb shares many similarities with early Miocene discontinuous sulfate evaporite deposits of the Gulf of Suez and NW Red Sea, which were deposited in marine-influenced hangingwall depocenters during the earliest phases of Oligo-Miocene extension (Orszag-Sperber and others, 1998 and references therein).

The abrupt transition from evaporitic strata of the Talc mb into laminated dolomudstone of the basal Ramp mb records a prominent flooding event that initiates non-restricted carbonate sedimentation in the Callison Lake Fm (fig. 14B). This base-level transgression was most likely driven by near- or far-field extensional tectonism, which may be locally evidenced by a concentration of seismically disrupted strata near the top of the Talc mb in certain sections (figs. 6, 7). Despite the erosional truncation of the Ramp mb in the Coal Creek inlier, one can still reconstruct a facies progression of NNW-to-SSE deepening from thinner peritidal-dominated sections (Mine Camp (J1302), fig. 6) to extensive subtidal-dominated sections (Mount Harper East (J1301), fig. 6). This depositional pattern appears to reflect the local development of a hangingwall carbonate ramp (fig. 14B; Read, 1982; Leeder and Gawthorpe, 1987; Bosence, 1998); however, we cannot rule out the possibility that this pattern instead reflects the development of local subaqueous topography in an extensive, rimmed platform-type setting (for example, Read, 1982; Tucker, 1985). Unfortunately, the key deposits to assess these different facies models would have been situated closer to the eroded (or displaced) ancestral basin-bounding fault (fig. 14), where one would expect to either encounter distal starved basin deposits (ramp) or proximal nearshore strata (rimmed platform). Depositional models consistent with the Red Sea analog include either the development of small carbonate depocenters in blind-headed gulfs, similar to upper portions of the Early Miocene Nukhul and Tayran formations of the Gulf of Suez and NE Red Sea (Hughes and others, 1992; Montenat and others, 1998; Bosworth and other, 2005 and references therein), or a temporary divergence to broad rift subsidence recorded in the Rudeis, Burqan, and Habab formations and lower Maghersum Gp of the Red Sea region (Bosworth and others, 2005 and references therein).

The Ramp-Transitional mb boundary represents the onset of tectonic reorganization in the Callison Lake basin(s) that eventually evolved into widespread extensional faulting and volcanism associated with the Seela Pass Fm and Mount Harper volcanics (fig. 14C). The increase in subaerial exposure surface frequency, the development of local topographic highs, and the widespread evidence for soft-sediment deformation in the upper Ramp mb (figs. 6, 7) provides sedimentological evidence for regional emergence and disruption of carbonate ramp sedimentation. In the Coal Creek inlier, the onset of this synsedimentary tectonism is marked by the coeval development of subaerial exposure and karst in the western uppermost Ramp mb deposits and apparently synchronous rapid deposition of basal Transitional mb strata in the eastern portion of the inlier (fig. 6). These divergent depositional histories indicate rotational motion of the ancestral basin-bonding structure (and its hangingwall depocenter) about a vertical W-E or NW-SE axis. Syntectonic Transitional mb strata were deposited in an evolving and complex paleoenvironmental setting possibly characterized by a narrow, marine gulf fed by antecedent fluvial systems that were eventually buried by alluvial fan and fan delta deposits of the Seela Pass Fm (fig. 14C). The maximum flooding interval of the Transitional mb black shale deposits has been dated with Re-Os geochronology at 739.9 ± 6.1 Ma (Strauss and others, 2014a), which provides an important age constraint for the timing of syntectonic sedimentation close to the Callison Lake-Seela Pass contact.

Fault-associated rotation of the Coal Creek hangingwall depocenter could have been driven by a number of local extensional processes, including uplift at the western fault tip or segment boundary, the regional development or activation of accommodation zone faulting in the western Coal Creek inlier associated with some component of oblique extension, and/or uplift and doming associated with the emplacement of the Mount Harper volcanics at depth (fig. 14C). This phase of syn-Callison Lake tectonism was possibly presaged by motion along blind structures at depth – the thinning of Ramp mb carbonate strata towards the NW could represent the development of a hangingwall monocline above a blind fault and the thickening of strata to the SE could indicate the coeval growth of a hangingwall syncline (for example, Gawthorpe and Leeder, 2000; Sharp and others, 2000). Interestingly, regional map patterns highlight a distinct synform in pre-Seela Pass strata in the Coal Creek subsurface – this previously buried structure possibly daylights in Seela Pass time as the "Trap Door" fault (fig. 4; Strauss and others, 2014b). Post ~740 Ma, northward-directed progression of the ancestral basin bounding structures and coeval segmentation of the Callison Lake depocenter(s) is marked by the development of the Harper Fault and Seela Pass syn-rift deposits in the Coal Creek inlier (figs. 4, 14C; Mustard, 1991; Mustard and Roots, 1997). This newly developed extensional half-graben contains its own unique history of fault-related sedimentation, volcanism, and dike emplacement (Roots, ms, 1987; Mustard, 1991; Mustard and Roots, 1997). Seela Pass equivalent rift-related sedimentation is also present in the Hart River inlier but has not been documented at the same level of detail (Abbott, 1997). In conclusion, the Callison Lake basin setting is similar to initial sedimentary deposits in the Oligo-Miocene northern Red Sea and Gulf of Suez extensional systems, recording no evidence for widespread doming or significant relief from rift flank uplift, a distinctly fine-grained siliciclastic syn-rift fill with early carbonate and sulfate evaporites in wedge-shaped half-grabens, and no apparent relationship to plume-related rifting.

### *Regional Correlations of the Windermere Supergroup*

The Mount Harper Gp shares a similar history of stratigraphic interpretation with the Coates Lake Gp of the Mackenzie Mountains: both units were also originally placed in the Mackenzie Mountains Supergroup and then relocated to the basal Windermere Supergroup after recognition of their rift-related nature (fig. 2; Young and others, 1979; Aitken, 1981; Jefferson, ms, 1983; Jefferson and Ruelle, 1986; Jefferson and Parrish, 1989; Abbott, 1997; Thorkelson and others, 2005; Macdonald and Roots, 2010; Macdonald and others, 2011; 2012; Turner and others, 2011). Coates Lake strata are subdivided into the Thundercloud, Redstone River, and Coppercap formations, and they are separated from the underlying Little Dal Gp by a significant erosional unconformity and discontinuous outcrops of the Little Dal basalt (figs. 1, 2, 15; Jefferson, ms, 1983). Previously published age constraints for the Little Dal basalt (fig. 2) are through geochemical correlation to a fault-bounded 777.8 +2.5/-1.8 Ma quartz diorite (U-Pb zircon; Jefferson and Parrish, 1989) and the 779.5 ± 2.3 Ma Tsezotene sills (U-Pb baddeleyite; Harlan and others, 2003); however, Milton and others (2015) recently reported a new U-Pb CA-ID-TIMS zircon age of 774.93 ± 0.54 for these mafic flows. The Little Dal basalt and Tsezotene sills have been correlated with the Hottah sheets of the Wopmay Orogen, suggesting a link to the ca. 780 Ma Gunbarrel LIP (Ootes and others, 2008; Sandeman and others, 2014).

The Coates Lake Gp was deposited in a series of marine embayments formed in extensional half-grabens (Jefferson, ms, 1983). The Thundercloud and Redstone River formations are characterized by abrupt lateral facies change between talc-bearing sulfate evaporites (Abercombie, ms, 1978), conglomerate, sandstone, and thin carbonate units, which are suggestive of deposition in proximal to distal alluvial fans, fan deltas, and marginal marine to playa lake settings (Ruelle, 1982; Jefferson, ms, 1983; Jefferson and Ruelle, 1986). These heterolithic strata gradationally transition into deep-water carbonate-dominated deposits of the Coppercap Fm (Jefferson, ms, 1983), which has been dated with Re-Os geochronology at 732.2 ± 3.9 Ma (figs. 1, 2, 15; Rooney and others, 2014). Various strata of the ~717–662 Ma Rapitan Gp (Macdonald and others, 2010; Rooney and others, 2014) unconformably overlie Coates Lake Gp strata with local angular discordance, attesting to synsedimentary tectonism throughout Coates Lake and Rapitan time (Eisbacher, 1977; 1981; Helmstaedt and others, 1979; Aitken, 1981; Jefferson, ms, 1983; Jefferson and Parrish, 1989; Turner and others, 2011).

Mount Harper equivalent strata of the Shaler Supergroup in the Minto inlier of Victoria Island include the Kilian and Kuujjua formations (figs. 1, 2, 15; Macdonald and others, 2011; 2012; Thomson and others, 2014), which were deposited in the intracratonic Amundsen Basin (Young, 1981; Rainbird, ms, 1991). The Kilian Fm consists of mixed siliciclastic, evaporite, and carbonate strata that record subtidal to peritidal sedimentation in a carbonate ramp and sabkha depositional setting (Young, 1981; Jefferson, 1985; Rainbird, ms, 1991; Rainbird, 1993; Jones and others, 2010). The overlying Kuujjua Fm is dominated by coarse-grained quartz arenite and minor interbedded fine-grained sandstone, shale, and dolomitic siltstone and represents a profound shift to fluvial sedimentation (Young, 1981; Jefferson, 1985; Rainbird, ms, 1991; 1992). Extensive continental flood basalts of the Natkusiak Fm (Thorsteinsson and Tozer, 1962) unconformably to conformably overlie the Kilian and Kuujjua formations and have been dated with baddeleyite on coeval sills at 723 +4/-2 Ma (U-Pb TIMS; Heaman and others, 1992) and 716.33 ± 0.54 Ma (CA-ID-TIMS; Macdonald and others, 2010); these mafic volcanics, and their associated gabbroic sills and dikes, represent remnants of the Franklin LIP (Heaman and others, 1992). Both the Kilian and Kuujjua formations display erosional truncation, NE stratigraphic thinning, and local evidence for extensional faulting, which have been attributed to pre-eruptive thermal uplift associated with the emplacement of the Franklin LIP (Rainbird, 1993). A maximum age constraint for the Kilian Fm comes from a Re-Os ORR age of 761 ± 41 Ma in the underlying Wynniat Fm (van Acken and others, 2013) and ca. 800 Ma detrital zircon grains in sandstone from the basal Kilian Fm (figs. 1, 2, 15; Rayner and Rainbird, 2013).

Preliminary sequence stratigraphic correlations among Neoproterozoic strata in NW Canada are still being developed (Long and others, 2008; Macdonald and others, 2012; Thomson and others, 2015a). There is no published sequence stratigraphic data from the Coates Lake Gp and previous work has retained the Kilian and Kuujjua formations in Sequence B of Young and others (1979) (Rainbird, 1993; Long and others 2008; Thomson and others, 2015a). Given the significance of the Mackenzie Mountains-Windermere Supergroup boundary throughout NW Canada, we argue that the Kilian and Kuujjua formations should be stratigraphically placed in Sequence C of Young and others (1979) (see discussion by C.W. Jefferson in Long and others, 2008); therefore, we abandon the sequence stratigraphic nomenclature of Long and others (2008) that retains these units in “sub-sequence sB5 of Sequence B” and develop a preliminary T-R cycle correlation scheme based on the work of Rainbird (1993). We also use the detailed sedimentological and stratigraphic data of Jefferson (ms, 1983) to provide a template for preliminary sequence stratigraphic interpretations in the Coates Lake Gp (fig. 15).

Rainbird (1993) documented four submergent-emergent cycles in the Kilian Fm, the fourth of which was interrupted by an abrupt shift to fluvial sedimentation in the Kuujjua Fm. The scale and style of these cycles, as well as their association with basin-wide subaerial exposure surfaces, suggests similarity to the T-R cycles described herein from the Callison Lake Fm. We posit that the three depositional sequences in the Callison Lake Fm (T-R6, T-R7, and T-R8; fig. 12) are equivalent to the initial three cycles of Rainbird (1993) (fig. 15). This is supported by the presence of the Islay Carbon Isotope Excursion (ICIE) in the upper part of T-R8 in both the Callison Lake and Kilian formations (fig. 15; Jones and others, 2010; Macdonald and others, 2010; Prince, 2014; Strauss and others, 2014a; Thomson and others, 2015b). Interestingly, Eisbacher (1977; 1981) and Jefferson (ms, 1983) independently documented three unconformity-bound depositional cycles in the Coates Lake Gp, each later divided into distinct formation boundaries (Jefferson, ms, 1983). The ICIE, which has already been correlated geochonologically between the Coppercap and Callison Lake formations (Strauss and others, 2014a), is also preserved in the third depositional cycle (T-R8) of the Coates Lake Gp (fig. 15). Although this integrated sequence stratigraphic and chemostratigraphic correlation scheme is speculative, it provides an appealing alternative to simplified lithostratigraphic correlation in these tectonically active basins.

Regional sequence stratigraphic correlations of younger depositional cycles in NW Canada are potentially complicated by the onset of diachronous regional extension associated with the emplacement of the Franklin LIP (fig. 15). The base of cycle T-R9 in the Mount Harper Gp is most likely marked by the transition to fault-related sedimentation in the Seela Pass Fm (figs. 12, 15), whereas cycle T-R9 in the Shaler

Supergroup is quite similar in stratigraphic architecture to underlying T-R cycles in the Kilian Fm (Rainbird, 1993). The abrupt shift from marginal marine to fluvial sedimentation at the Kilian-Kuujjua contact most likely represents a younger depositional cycle boundary (that is, base of T-R10) and could be similarly driven by the onset of regional extension-related faulting in the Shaler Supergroup (Rainbird, 1993; Prince, 2014; Thomson and others, 2015a). This may be indicative of diachronous, NE-propagating mid-Neoproterozoic extension across NW Canada during the break-up of Rodinia, culminating with the emplacement of the Franklin LIP (for example, Rainbird and others, 2014). Sequence T-R9 does not appear to be present in the Coates Lake Gp due to erosional truncation beneath the Rapitan Gp (fig. 15; Jefferson, ms, 1983). Despite previous studies that suggest a eustatic origin for these T-R cycles (Rainbird, 1993; Long and others, 2008; Thomson and others, 2015a), the regional correlation of these sequence boundaries in NW Canada and their clear association with extension-related unconformities is perhaps more suggestive of a greater tectonic driving mechanism.

Application of this tectono-stratigraphic correlation scheme to other mid-Neoproterozoic strata of the Windermere Supergroup in Laurentia, such as the ChUMP basins of the western U.S., enables a margin-wide comparison. A preliminary sequence stratigraphic scheme for the Uinta Mountain Gp was proposed by Dehler and others (2010) and expanded upon by Kingsbury-Stewart and others (2013), both of which concluded that Uinta Mountain Gp (and correlative Big Cottonwood Fm) siliciclastic strata record three, km-scale fining-upwards depositional sequences (*composite* sequences of Kingsbury-Stewart and others, 2013). A preliminary four-fold, km-scale sequence stratigraphic framework was also proposed for the Chuar Gp (Dehler and others, 2001), although the recognition of ca. 780 Ma detrital zircons in the Nankoweap Fm requires an update to the sequence stratigraphic architecture of these strata (Dehler and others, 2012). No sequence stratigraphy has been reported from the Pahrump Gp of Death Valley; however, recent work by Macdonald and others (2013b), Mahon and others (2014), and Smith and others (2015) has documented an equivalent basal Windermere Supergroup tectono-stratigraphic package that comprises the Horse Thief Springs Fm, Beck Spring Dolomite, and unit KP1 of the Kingston Peak Fm (tectonostratigraphic unit two (TU2) of Macdonald and others, 2013b). The presence of the ICIE in the uppermost Beck Spring Dolomite (Horodyski and Knauth, 1994; Prave, 1999; Corsetti and Kaufman, 2003; Macdonald and others, 2013b; Strauss and others, 2014a; Smith and others, 2015), coupled with these distinct formational boundaries, suggests a comparable sequence stratigraphic architecture for the Pahrump Gp. Notably, the sudden influx of fine-grained siliciclastic strata of unit KP1 into the Pahrump basin(s) is comparable in stratigraphic location (that is, post-dates the ICIE) to the T-R9 and T-R10 fault-related sedimentation in the Callison Lake and Kuujjua formations of NW Canada.

### *Mid-Neoproterozoic Tectonic Evolution of NW Canada and Laurentia*

The Laurentian paleocontinent holds an analogous central position in Rodinia to Africa in Pangea (for example, Hoffman, 1991) – both share protracted extensional histories with the development of continent fringing passive margins and distinct relationships with plume-related continental flood basalt volcanism. Gondwana’s break-up was characterized by the development of extensive, plume-related continental flood basalts (for example, Cox, 1978; Morgan, 1981; Encarnatión and others, 1996) whose impact on the greater extensional history is still debated (Courtillot and others, 1999). Interestingly, this is very similar to the relationship between Neoproterozoic LIPs and the break up of Rodinia (for example, Li and others, 1999; 2008; Macdonald and others, 2012; Sandeman and others, 2014; Yonkee and others, 2014).

The widespread development of a prominent subaerial unconformity, volcanism, and rift-related sedimentation at the Mackenzie Mountains-Windermere Supergroup boundary in NW Canada appears to be contemporaneous with the emplacement of the Gunbarrel LIP around 780 Ma (Armstrong and others, 1982; Park and others, 1995; Dudás and Lustwerk, 1997; Harlan and others, 2003; Ootes and others, 2008; Sandeman and others, 2014). The Fifteenmile-Mount Harper Gp boundary in Yukon may be a local manifestation of this event; however, there is no evidence for Gunbarrel magmatism in Yukon and the new Re-Os and U-Pb ages from the Mount Harper Gp suggest that syntectonic units record pronounced extensional tectonism and sedimentation from ~750–720 Ma. This apparent ~30 Ma gap between Gunbarrel magmatism and regional extension in Yukon raises the interesting possibility of important ~750-730 Ma Laurentian tectono-sedimentary events (Evanchick and others, 1984; Parrish and Scammell, 1988; McDonough and Parrish, 1991; Crowley, 1997; Karlstrom and others, 2000) that are completely unrelated to the Gunbarrel LIP and perhaps even more important in the long-term evolution of the western margin of Laurentia.

In the Coal Creek inlier, Mustard (1991) and Mustard and Roots (1997) noted the development of diachronous, opposing basin geometries between the NNE-oriented Seela Pass and SSW-directed Eagle Creek half-grabens. Mustard (1991) predicted a discrete NW-SE-oriented extensional accommodation zone between these sub-basins that was also responsible for localizing Mount Harper volcanism, similar to the spatial relationship between volcanism and accommodation zones in the East African Rift (Bosworth, 1985; 1987; Ebinger, 1989). The existence of this transfer zone is supported by the dense concentration of NW-oriented mafic dikes along the trace of this structure (fig. 4), as well as its documented role in dictating sedimentation patterns in the Coal Creek inlier and influencing the rotational motion of the Callison Lake depocenter during the Callison Lake-Seela Pass transition (fig. 14C).

The general pattern of propagating half-graben, coupled with the development of oblique intervening accommodation zones, is characteristic of the principal displacement zone of strike-slip extensional systems (Christie-Blick and Biddle, 1985 and references therein). Oblique extension in the Coal Creek inlier is possibly supported by the narrow rhomboidal map patterns in Windermere Supergroup deposits, distinct latitudinal and longitudinal basin asymmetries, apparently rapid subsidence of fault-related deposits, and the localized development of unconformities and abrupt lateral facies change (fig. 4; Mustard and Roots, 1997). More regionally, the lack of evidence for thermally driven post-rift subsidence in any of the Windermere sedimentary successions, even including the informal upper group, is also a characteristic feature of strike-slip sedimentation (Reading, 1980; Mann and others, 1983; Christie-Blick and Biddle, 1985 and references therein). Although Mustard (1991) opposed a model of oblique extension in the Coal Creek inlier, many of his arguments were based on non-unique sedimentological observations, such as the predominance of conglomeratic fill and the consistent orientation of paleocurrents transverse to the basin margin.

In the Hart River inlier, Abbott (1997) documented evidence for syntectonic Mount Harper Gp sedimentation and coeval E-W-oriented mid-Neoproterozoic normal and reverse faults. In the en echelon fault belt of the Callison Lake and Rae Creek faults (fig. 3), Abbott (1997) noted a prominent difference in the erosional level of south-dipping Proterozoic strata beneath the Cambro-Ordovician Bouvette Fm. This observation, coupled with the consistent south-dipping orientation of steeply inclined structures and their apparent overlap by Rapitan-equivalent strata requires some degree of post-Callison Lake, pre-Rapitan reverse offset (fig. 3). Extremely localized zones of m- to km-scale folding of Fifteenmile and Pinguicula units are also present in the vicinity of relatively undeformed younger Neoproterozoic strata (for example, Penetration Lake, fig. 3), although it is currently unclear if these structures are related to Mesozoic deformation. The restriction of Mount Harper Gp strata to south of the Callison Lake Thrust, along with the omission of units and opposing displacements across the Marc Creek Fault, suggests that these two structures are Neoproterozoic graben-bounding faults that were reactivated during the Mesozoic (fig. 3; Abbott, 1997). Importantly, all of these structural and stratigraphic configurations could be generated in a strike-slip setting where both normal and reverse fault separations are present in the same evolving fault system (for example, Nilsen and McLaughlin, 1985). In summary, map patterns, sedimentological observations, and structural arguments from both the Coal Creek and Hart River inliers support a reconstruction of initial dip-slip or slight oblique extension during deposition of the Callison Lake Fm followed by localized transtension and transpression during the development of ~740–660(?) Ma Seela Pass–Rapitan basins. Following previous suggestions for a Proterozoic origin of the Dawson Fault (Thrust) (Roots and Thompson, 1992; Abbott, 1996), we argue that this long-lived structure represents a fundamental trace of an ancient strike-slip fault zone in Yukon (fig. 14C).

Eisbacher (1978; 1981) documented evidence for localized pre- to syn-Windermere Supergroup contractional deformation in the Wernecke inlier (fig. 2), which was characterized by WSW-directed thrust faults involving the Wernecke Supergroup and Pinguicula Gp and capped by massive alluvial fan conglomerates of the Rapitan and Hay Creek groups. In the same region, Thorkelson (2000) mapped a number of related W- and SW-oriented thrust faults and overturned folds in the Pinguicula and Hematite Creek groups that were clearly truncated by overlying Windermere Supergroup conglomerates; Thorkelson (2000) termed this compressional event the “Corn Creek Orogeny”. These observations, in combination with the radiating orientation of Windermere Supergroup-related normal fault geometries and the regional angular unconformity between the Mackenzie Mountains and Windermere supergroups, led Eisbacher (1977; 1978; 1981) to interpret the Wernecke inlier as a discrete transpressional zone in a larger Windermere dextral strike-slip system.

Significant mid-Neoproterozoic angular unconformities and localized contractional structures are also described in the Coates Lake and Rapitan groups of the Mackenzie Mountains and regionally associated with the “Hayhook Orogeny” of Young and others (1979), or “Hayhook extensional event” of Jefferson and Parrish (1989) (Aitken and Cook, 1974; Helmstaedt and others, 1979; Jefferson, ms, 1983). The Hayhook event is a local manifestation of basal Windermere Supergroup extensional tectonism and is defined by discrete extensional faults and rift-related sedimentation in the Coates Lake and Rapitan groups (Young and others, 1979; Jefferson, ms, 1983;

Jefferson and Parrish, 1989). Although Eisbacher (1981) suggested that the compressional structures of the Wernecke inlier were synchronous with this basal Windermere rift-related sedimentation throughout NW Canada, Thorkelson (2000) mapped E-W-trending normal faults attributed to the Hayhook event that apparently crosscut the older thrust faults of the Corn Creek Orogeny, providing ambiguity to the proposed temporal link between Windermere Supergroup extension and compression. Alternatively, the normal faults of Thorkelson (2000) could represent tear faults in lateral thrust ramp complexes (*sensu* Thomas, 1990) and Eisbacher's (1981) original interpretation could still hold. Unfortunately, the direct connection between the enigmatic Corn Creek Orogeny and the Hayhook extensional event in the Wernecke inlier remains ambiguous; however, the presence of discrete regions characterized by transpressional and transtensional tectonism throughout NW Canada lends credence to the tectonic reconstructions proposed by Eisbacher (1977; 1981). In fact, many workers have proposed models of mid-Neoproterozoic strike-slip motion along the ancestral Richardson Fault Array and during deposition of the Coates Lake and Rapitan groups (Bell, 1982; Norris, 1982; Jefferson, ms, 1983; Jefferson and Ruelle, 1986; Jefferson and Parrish, 1989; Aitken and McMechan, 1992; Abbott, 1996).

When extrapolated south through the remainder of the North American Cordillera, NW Canada highlights a much more complex Neoproterozoic tectonic framework than simple dip-slip extension in Laurentian intracratonic basins (for example, Yonkee and others, 2014). A number of permissible scenarios could rectify these along-strike inconsistencies, including a different tectonic setting for NW Canadian versus ChUMP basins in the actively extending margin, diachronous extension and basin development, the localization of Gunbarrel plume-related thermal anomalies and related subsidence, and/or a distinct transition in the style and orientation of extensional tectonism along the length of ancestral North America. The consistency in stratigraphic architecture, sequence stratigraphy, $\delta^{13}C_{carb}$ chemostratigraphy, and radiometric age constraints appears to rule out diachroneity as an explanation for the earliest stages of Windermere Supergroup basin development; therefore, we hypothesize that this requires latitudinal (and possibly longitudinal) variability in extensional regimes, consistent with synchronous E-W or SE-NW dip-slip ChUMP extension coupled with NW-SE strike-slip extension in NW Canada (in present coordinates). Regional differences in the geometry of the basins may be due to the local tectonic fabric in the underlying basement (for example, Lund and others, 2010 and references therein); particularly, the ChUMP basins are present along reactivated Mesoproterozoic basins (for example, Macdonald and others, 2013b). Whether or not oblique extension also played a role in the subsequent development of ~720–660 Ma extensional basins throughout the western U.S. and Canada remains to be substantiated, although the distinct lack of tilted strata, modest extension (~25-40%), narrow basin geometries, lack of substantial volcanism, local detrital zircon sources, variable tectonic subsidence patterns, and lack of broad thermal subsidence permits a different interpretation from the current models of Neoproterozoic pure shear extension (Lund, 2008; Turner and Long, 2008; Lund and others, 2010; Yonkee and others, 2014). We suggest that the zigzag geometry of the Cordilleran rift system is an inherent Paleozoic feature (Hansen and others, 1993; Cecile and others, 1997) and need not have defined the extensional framework of western Laurentia for over 200 million years.

*Implications for Neoproterozoic Chemostratigraphy and the Origin of the Islay Carbon Isotope Excursion (ICIE)*

The $\delta^{13}C_{carb}$ profile from the Callison Lake Fm is bracketed with U-Pb and Re-Os geochronology and has been used to correlate among regional and global pre-Sturtian basins (Macdonald and others, 2010; Strauss and others, 2014a). The chemostratigraphic data presented herein confirm previously published isotopic results and further demonstrate that the Callison Lake $\delta^{13}C_{carb}$ and $\delta^{18}O_{carb}$ data are reproducible within individual members and along depositional strike. An additional feature brought out with this study is a negative $\delta^{13}C_{carb}$ interval in ~750 Ma Talc mb strata (figs. 6, 7). Smith and others (2015) recently reported a similar negative $\delta^{13}C_{carb}$ interval from the correlative Horse Thief Springs Fm of the Pahrump Gp of the southwest United States, and an equivalent shift towards depleted $\delta^{13}C_{carb}$ values is recorded in the lower Russøya Mb of the Elbrobreen Fm of Svalbard (Halverson and others, 2004; 2005).

Despite the possible correlation of the Talc mb $\delta^{13}C_{carb}$ profile with other Neoproterozoic successions, Talc mb carbon isotope data remain somewhat ambiguous due their heterogeneity, as well as the depositional setting and complex paragenetic history of host carbonate strata. Sabkhas are characterized by complex early diagenetic environments involving the widespread precipitation, dissolution, and replacement of carbonate and sulfate minerals (Butler and others, 1982; Schreiber and El Tabkah, 2000; Warren, 2006 and references therein); these reactions commonly involve remineralization of organic matter through microbial sulfate reduction coupled with authigenic carbonate precipitation (Pierre and Rouchy, 1988; Anadón and others, 1992; Kendall, 2001; Machel, 2001). Syndepositional recrystallization to more stable carbonate minerals (for example, Reid and Macintyre, 1998) and penecontemporaneous dolomitization in sabkha environments contributes to the homogenization of authigenic and primary DIC isotopic compositions. Mixed carbonate-evaporite successions are also commonly affected by extensive thermochemical sulfate reduction during burial dolomitization (Machel, 2001 and references therein). Therefore, although we focused our sampling on the thickest exposures of pure microbial dolostone (figs. 6, 7), we cannot rule out based on the depositional setting that some, if not all, of the isotopic heterogeneity recorded in the Talc mb is a product of these early- and late-stage diagenetic processes. Importantly, many of the Talc mb stratigraphic sections remain predominantly enriched in $\delta^{13}C_{carb}$ (fig. 6), and these data appear to be more consistent with $\delta^{13}C_{carb}$ values from the bounding Heterolithic and Ramp members, as well as other coeval global successions (Halverson, 2006). It is worth noting that carbonate strata of the Horse Thief Springs Fm were also deposited in a sabkha-like depositional setting (Mahon and others, 2014), so the depleted $\delta^{13}C_{carb}$ values reported by Smith and others (2015) could be a result of similar processes involving the recrystallization of authigenic and primary carbonate phases.

The pervasive enrichment of $\delta^{18}O_{carb}$ throughout the Talc and Ramp members (fig. 13) lends further geochemical support to sedimentological evidence of evaporitic conditions throughout the Coal Creek and Hart River inliers. Although the chemostratigraphic utility of $\delta^{18}O_{carb}$ data is controversial, distinct $\delta^{18}O_{carb}$ enrichments are common in modern and ancient restricted settings (Friedman, 1980; McKenzie, 1981; Gat and Bowser, 1991; Kah and others, 1999; Frank and Lyons, 2000; Kah, 2000; Jaffrés and others, 2007; Wilson et al., 2010). Early dolomitization in Precambrian carbonate successions aids in the reduction of pore space (Tucker, 1982) and thereby may restrict subsequent fluid interactions; however, it is also likely that $\delta^{18}O$ enrichments in ancient dolomites may simply be a function of the most recent pore-fluid composition and its formation temperature during precipitation, as well as some contribution from calcite-dolomite equilibrium isotope fractionation (for example, Land, 1983). Therefore, although it is difficult to distinguish between possible primary $\delta^{18}O_{carb}$ data and those that are imparted during subsequent diagenetic overprinting, the consistently enriched $\delta^{18}O_{carb}$ data of the Callison Lake Fm is at least consistent with primary modification of episodically restricted basin waters.

Predominantly enriched Ramp mb $\delta^{13}C_{carb}$ values from the Coal Creek inlier contrast with correlative strata in the Hart River region that display multiple, isotopically depleted intervals (figs. 6, 7). Some of these negative $\delta^{13}C_{carb}$ data appear to be associated with distinct paleokarst horizons (for example, Mark Creek, section J907; fig. 7); however, calling upon meteoric diagenesis as a driver for these depleted carbon isotope data (for example, Allan and Matthews, 1992; Knauth and Kennedy, 2009; Swart and Kennedy, 2012) is difficult to reconcile with the lack of evidence for a Neoproterozoic terrestrial biomass capable of generating abundant $^{13}C$-depleted, soil-derived $CO_2$ (Jones and others, 2015). Other explanations include: 1) early diagenetic reactions involving evaporite replacement, dolomitization, or *in situ* microbial anaerobic respiration of organic carbon, 2) localized delivery and oxidation of detrital organic carbon, or 3) post-depositional alteration associated with burial dolomitization. High-energy intertidal to supratidal deposits of the Ramp mb are unusual lithofacies for pronounced authigenic carbonate production associated with anaerobic remineralization of organic matter (for example, Irwin and others, 1977; Reimers and others, 1996; Schrag and others, 2013; Sun and Turchyn, 2014). Furthermore, there is no sedimentological or petrographic evidence for a sustained detrital organic carbon flux into the Hart River basin during Ramp mb sedimentation; this scenario would also require localized organic matter oxidation and carbonate precipitation (for example, Lloyd, 1964; Patterson and Walter, 1994) to outpace buffering through air-sea gas exchange. Although no distinct evaporite textures have been recognized in the Ramp mb, the m-scale breccias could represent isolated dissolution of precursor evaporite deposits (Pope and Grotzinger, 2003) and the supratidal depositional setting of these strata support episodic evaporitic conditions. Many of these depleted $\delta^{13}C_{carb}$ data are also associated with m-scale intervals of massively recrystallized dolostone, the origins of which are most likely related to fabric destructive burial-zone diagenesis. Therefore, we hypothesize that the minor divergence in compositional data between the Hart River and Coal Creek inliers most likely reflects local, platform-scale processes involving the early- and post-depositional interaction of evaporite recrystallization, organic matter oxidation, and dolomitization.

From predominantly enriched data in the Ramp mb, $\delta^{13}C_{carb}$ values of the Transitional mb drop to a nadir of -5.8‰ in a prominent negative excursion that has been previously correlated to the global ICIE due to its reproducibility in multiple sections and its covariation with $\delta^{13}C_{org}$ (fig. 6; Macdonald and others, 2010; Strauss and others, 2014a). This pre-Sturtian carbon isotope excursion was first recognized beneath the glaciogenic Port Askaig Fm in the Islay (Lossit) Limestone of Scotland (Brasier and Shields, 2000; McCay and others, 2006; Prave and others, 2009). It has also been documented in the Black River Fm of Tasmania (Calver, 1998), Mwashia Subgroup of the Roan Gp in Zambia (Bull and others, 2011), Beck Spring Dolomite of Death Valley (Horodyski and Knauth, 1994; Prave, 1999; Corsetti and Kaufman, 2003; Macdonald and others, 2013b; Smith and others, 2015), bed group 19 of NE Greenland (Fairchild and others, 2000), Russøya Mb of the Elbobreen Fm of Svalbard (Halverson and others, 2004; Hoffman and others, 2012), Coppercap Fm of the Mackenzie Mountains (Halverson, 2006; Rooney and others, 2014), and the Kilian Fm of Victoria Island (Jones and others, 2010; Prince, 2014; Thomson and others, 2015b). Previous explanations for the ICIE were mechanistically linked to global glaciation due to the presence of isotopically depleted carbonate strata directly beneath circa 716-660 Ma Sturtian glacial deposits (Hoffman and others, 2012 and references therein); however, this relationship has recently been severed by syn-Islay Re-Os ages of 739.9 ± 6.1 Ma and 732.2 ± 3.9 Ma from the Callison Lake and Coppercap formations, respectively, which demand >10 Myr between the termination of the $\delta^{13}C_{carb}$ excursion and onset of glaciation (fig. 15; Rooney et al., 2014; Strauss et al., 2014a). These new ages are also consistent with the observation that many pre-glacial carbonate successions, including the Callison Lake Fm, contain a recovery to enriched $\delta^{13}C_{carb}$ values predating the onset of glaciation (fig. 6; Prave and others, 2009; Hoffman and others, 2012; Strauss and others, 2014a). Although a number of recent studies invoke diagenetic models for high amplitude Neoproterozoic $\delta^{13}C_{carb}$ excursions (for example, Knauth and Kennedy, 2009; Derry, 2010; Swart and Kennedy, 2012), Hoffman and others (2012) documented $\delta^{13}C_{carb}$–$\delta^{13}C_{org}$ covariation and a lack of $\delta^{18}O_{carb}$ covariance in the ICIE of Svalbard as evidence for a primary seawater DIC origin. These same isotopic covariance relationships are also present in the

Beck Spring Dolomite and Coppercap and Callison Lake formations (Corsetti and Kaufman, 2003; Rooney and others, 2014; Strauss and others, 2014a).

The relationship documented herein between circa 740 Ma tectonism, marine transgression, and the ICIE in Laurentia is consistent with a mechanistic link between tectonics, weathering, ocean geochemistry, and relative sea level change. Halverson and others (2014) highlighted the possible importance of Neoproterozoic continental flood basalt weathering in modulating the long-term carbon cycle during the protracted ca. 830–720 Ma low-latitude break-up of Rodinia. Here, we explore another feature of this pre-Sturtian tectonic background condition – the development and subsequent demise of extensive shallow epicontinental seaways and evaporite basins.

Despite the lack of consensus on the exact arrangement of paleocontinents in Rodinia (for example, Li and others, 2008; Evans, 2009), every hypothetical reconstruction necessitates significant marine extensional basins situated between larger continental fragments (Li and others, 2013) and paleocontinents that were episodically submerged beneath massive epicontinental seaways (for example, Centralian Superbasin of Australia; Walter and others, 1995; Lindsay, 2002). As noted above, the western margin of Laurentia was characterized by a series of extensional basins that were episodically linked to interior evaporitic epicontinental seaways such as the Amundsen Basin of Victoria Island (Young, 1981). Pre-Sturtian evaporite deposition in NW Canadian basins spans two discrete intervals (~900–811 Ma Minto Inlet-Ten Stone and ~780–740 Ma Kilian-Redstone River-Callison Lake) over an interpolated basin size >3 X $10^6$ $km^2$ (Evans, 2006 and references therein). The coeval Centralian Superbasin of central Australia and Adelaide foldbelt of southern Australia represent an intermittentlylinked, extensive epicontinental seaway on the order of 2 X $10^6$ $km^2$ (Lindsay, 2002) that was also characterized by two protracted phases of coeval evaporite deposition (>802 Ma Curdimurka-Bitter Springs-Browne-Sunbeam and ~780–720 Ma Skillogalee) (Hill and Walter, 2000; Lindsay, 2002; Grey and others, 2011). Other volumetrically significant Neoproterozoic evaporitic basins include the ~880(?)–720 Ma Roan Gp of the central-African Copperbelt covering an estimated 0.5 X $10^6$ $km^2$ (Jackson and others, 2003; Armstrong and others, 2005; Selley and others, 2005; Bull and others, 2011) and the circa 800–720 Ma Duruchaus Fm of the Kalahari craton that covered an estimated 0.3 X $10^6$ $km^2$ (Evans, 2006; Miller, 2008 and references therein). These enormous evaporite basins likely represent mere fractions of much larger epicontinental seaways that once existed between Rodinian paleocontinental fragments (for example, Li and others, 2013), many of which were eventually tectonically dismembered during the fragmentation of Rodinia.

How might the development and demise of these epicontinental seaways drive the ICIE and affect the long-term Neoproterozoic carbon cycle? If the ICIE is analogous to the Paleocene-Eocene Thermal Maximum (PETM) negative $\delta^{13}C_{carb}$ excursion and lasted for a duration comparable to the mixing and residence times of carbon in the oceans (1-10s kyr), then a plausible driving mechanism involves the extensive subaerial oxidation of organic matter associated with the uplift and erosion of these evaporite basins (*cf.* Higgins and Schrag, 2006). If, however, the ICIE turns out to have lasted on a timescale greater than the residence time of carbon in the oceans (>100 kyr), a massive carbon oxidation explanation is less likely given the required oxidant budgets (for example, Bristow and Kennedy, 2008) and scenarios involving changes in the fractional burial of organic carbon (Kump, 1991) and authigenic carbonate (Schrag and others, 2013) or shifts in the composition of weathering products (Kump and others, 1999) provide more reasonable explanations. Epicontinental seaways characterized by extensive sabkha and basinal evaporite deposits not only represent an important sink for authigenic carbonate and organic carbon burial, but also act as critical regulators of marine sulfate inventories during precipitation and dissolution events (for example, Wortmann and Paytan, 2012).

Similar to records of enhanced organic matter preservation in large Mesozoic epicontinental seaways (for example, Slingerland and others, 1996; Fisher and Arthur, 2002; Riboulleau and others, 2003), Rodinian extensional basins likely provided a locus for elevated organic matter and authigenic carbonate burial, as evidenced by the consistently enriched background $\delta^{13}C_{carb}$ data in the early Neoproterozoic (for example, Knoll and others, 1986; Schrag and others, 2002; Halverson and others, 2005). As an example, evaporitic strata in the Talc mb of the Callison Lake Fm contain organic-rich black shale horizons with up to 4 wt.% total organic carbon in association with authigenic carbonate with depleted $\delta^{13}C_{carb}$ values (figs. 6, 7). On short timescales, the desiccation of even some small fraction of these massive epicontinental seaways during the discrete ~740 Ma episode of regional extension discussed above would have resulted in the widespread oxidation of labile marine organic carbon through interactions with oxygenated meteoric systems, sulfate-rich brines, and exposure to aerobic microbial respiration (for example, Hartnett and others, 1998; Hedges and others, 1999; Moodley and others, 2005; Bouchez and others, 2010). Higgins and Schrag (2006) estimated that assuming >90% of the total sedimentary organic carbon is oxidized during an episode of uplift and exposure, the desiccation of the top ~30 m of an ~3 X $10^6$ $km^2$ epicontinental seaway with 5 wt.% organic carbon would result in the release of ~5000 Gt C to the ocean-atmosphere system. This hypothetical seaway is essentially the same size as only one of the major *preserved* Rodinian epicontinental basins, the majority of which display abundant sedimentological evidence for sub-Sturtian erosional unconformities (for example, Jefferson, ms, 1983; Rainbird, 1993; Prave and others, 2009; Hoffman and others, 2012 and many others).

Given this framework and based on simple mass balance calculations considering the modern ocean-atmosphere system, the approximate amount of oxidized organic carbon ($\delta^{13}C$= –25‰) required to generate a ~10‰ negative $\delta^{13}C_{carb}$ excursion is ~22,000 Gt. This calculation neglects effects such as $CaCO_3$ dissolution and carbonate speciation that would likely require even larger initial carbon inputs; however, the exact magnitude of the required Islay-related $CO_2$ flux also depends on many critical features that remain poorly constrained in the Neoproterozoic, such as the size of the ocean-atmosphere-biosphere carbon pool, the composition of seawater ($Ca^{2+}$, alkalinity, et cetera), the attendant distribution of $CO_2$ throughout the carbonate system, and its final consumption by biological productivity. One would assume that the uplift of Rodinian evaporite basins and rift flanks would have also initiated weathering of sulfate evaporites and remnants of Neoproterozoic continental flood basalt provinces, thereby possibly limiting the total $CO_2$ release generated by widespread organic matter oxidation through enhanced nutrient delivery and biological uptake of $CO_2$ (for example, Tziperman and others, 2011).

One prediction of this organic matter oxidation model is that the ICIE should be marked by rapid warming and sea level rise due to the thermal expansion of seawater. The consistent association of the ICIE with marine transgression in extensional basins of

Laurentia (fig. 12) provides preliminary support for a hypothetical flooding event, which may be mirrored in other global successions (for example, Prave and others, 2009; Bull and others, 2011; Hoffman and others, 2012; Smith and others, 2015); however, the Laurentian sea level record is difficult to disentangle from extensional tectonism as a primary driver for regional base level rise (see above). Given the predicted sea level response, this hypothesis also requires rapid uplift rates to expose evaporite basins while simultaneously isolating them from warming-related marine transgression (Higgins and Schrag, 2006). Although this may appear challenging to explain in extensional settings, the combined effects of plume-related uplift (Saunders and others, 2007), dynamic topography, and oblique extension during the break-up of Rodinia may have promoted the widespread development of basinal sills (for example, Duggen and others, 2003) and facilitated relatively rapid (for example, Vogl and others, 2014) isolation, uplift, and weathering of pre-Sturtian evaporite basins.

The observation in the Callison Lake Fm and other global successions that the ICIE spans 10s of m of mixed carbonate and siliciclastic strata and contains variable internal structure (figs. 6, 15) possibly supports a longer duration for the $\delta^{13}C_{carb}$ excursion. In order to circumvent oxidant mass balance complications associated with driving long lived $\delta^{13}C_{carb}$ excursions with organic matter burial, Schrag and others (2013) proposed that authigenic carbonate production provides a sink for $^{13}C$-depleted carbon in Proterozoic oceans characterized by low $O_2$ and alkalinity-primed anoxic pore fluids (for example, Higgins and others, 2009). Due to the relatively consistent magnitude of the excursion and its $\delta^{13}C_{carb}$–$\delta^{13}C_{org}$ covariation, the ICIE could be related to a global decline in the fractional burial of authigenic carbonate (category 1 of Schrag and others,

2013) due to a transient perturbation to surface redox conditions or seawater carbonate saturation state, an abrupt sea level fluctuation, and/or a shift in the loci of global organic carbon remineralization in marine basins. The margin-wide ~ 740 Ma extensional episode and marine transgression in Laurentia may have temporarily altered the locus of sediment column organic carbon remineralization (for example, by shoaling the zone of anaerobic oxidation of methane) or shifted the primary location of organic carbon burial and remineralization in Rodinian extensional basins. One criticism of the authigenic carbonate model is the difficulty in identifying the exact nature and location of the depleted carbonate sink – significant volumes of sulfate and authigenic carbonate could have been sequestered in the vast epicontinental basins of Rodinia. Therefore, the episodic dissection of these basins during regional tectonic events may have delivered light carbon and sulfate to the oceans through a combination of direct oxidation of organic matter and weathering of authigenic carbonate reservoirs, while simultaneously affecting the sinks of authigenic carbonate and organic carbon burial in isolated extensional basins.

Sulfur isotope data support a hypothetical evaporite weathering hypothesis for the ICIE. Sulfur isotopic data from pre-Sturtian sedimentary deposits display profound variability (for example, Gorjan and others, 2000; Hurtgen and others, 2002; Halverson and Hurtgen, 2007), consistent with low marine $SO_4^{2-}$ concentrations possibly associated with ca. 850-720 Ma global evaporative drawdown. Moreover, $\delta^{34}S$ data from sulfate deposits of the Kilian Fm record a ~15‰ positive anomaly that covaries with the ICIE (Kaufman and others, 2007; Jones and others, 2010), which is consistent with the dissolution of freshly exposed sulfate evaporites and attendant increase in pyrite burial through elevated microbial sulfate reduction (*sensu* Wortmann and Paytan, 2012). Set upon a backdrop of low latitude continental configurations, the coincidence in timing of other high amplitude Neoproterozoic $\delta^{13}C_{carb}$ anomalies (for example, ca. 811 Ma Bitter Springs anomaly) with distinct episodes of intra-Rodinian extensional tectonism suggests that this evaporative drawdown and weathering hypothesis may have far reaching implications for Neoproterozoic global climate and biogeochemical cycles.

## CONCLUSIONS

The Callison Lake Fm (formalized herein) of the Coal Creek and Hart River inliers of Yukon, Canada, records a complex subsidence history, in which episodic basinal restriction and abrupt facies change can be tied to mid-Neoproterozoic (Tonian) extensional tectonism and rift-related sedimentation (Windermere Supergroup) throughout NW Canada. The syn-tectonic, circa 753 Ma Heterolithic mb of the basal Callison Lake Fm is dominated by fine-grained siliciclastic sedimentation in a marginal marine depositional setting and locally includes discontinuous stromatolitic bioherms with poorly preserved VSMs. These strata are sharply overlain by a progradational sabkha succession (Talc mb) dominated by talc-rich black shale interbedded with evaporitic microbial dolostone, which transition upsection into a thick package of subtidal to supratidal dolostone (Ramp mb) and mark the development of a carbonate ramp. In some stratigraphic sections in the Coal Creek inlier, Ramp mb carbonate strata grade up-section into interbedded microbial dolostone and organic-rich black shale deposits of the Transitional mb, which contains a diverse VSM assemblage constrained by a Re-Os depositional age of 739.9 ± 6.1 Ma. In other stratigraphic sections, this same depositional interval is marked by a significant paleokarst horizon, which is suggestive of differential subsidence and uplift associated with a major phase of ~740 Ma extensional tectonism in Yukon.

Stratigraphic, structural, and geochronological data from the Callison Lake Fm demonstrate that these strata are correlative with at least part of the ~780–720 Ma Coates Lake Gp of the Mackenzie Mountains, both of which were potentially deposited during ~740–720 Ma transtension and transpression along the northwestern margin of Laurentia. New sequence stratigraphic data described herein from the Callison Lake Fm highlights three distinct depositional sequences, or transgressive-regressive (T-R) cycles, that are coeval with similar stratigraphic packages in the Coates Lake Group of the Mackenzie Mountains, Shaler Supergroup of Victoria Island, and Chuar-Uinta Mountain-Pahrump basins of the western United States. The global, circa 735 Ma Islay carbon isotope excursion (ICIE) is consistently present in the third T-R cycle and is interpreted to represent a primary perturbation to the global carbon cycle based on its reproducibility in regional and global basins and covariance in carbonate and organic carbon isotopes. Here, we explore a new model for the origin of the ICIE that links this negative carbon isotope excursion to the uplift and weathering of extensive shallow epicontinental seaways and evaporite basins associated with the break-up of Rodinia.

## ACKNOWLEDGMENTS

JVS was supported by the National Science Foundation (NSF) Graduate Research Fellowship Program. FAM thanks the MIT NASA Astrobiology Institute node, NSF Sedimentary Geology and Paleobiology (EAR-1148058), and NSF Tectonics (EAR-

1049463) for support. We thank Charlie Roots, Maurice Colpron, Don Murphy, Tiffani Fraser, Steve Israel, David Moynihan, Grant Abbott, and Carolyn Relf of the Yukon Geological Survey for their continued support of this research. Fireweed and TransNorth Helicopters provided safe and reliable transportation in Yukon. We thank Phoebe Cohen, Erik Sperling, Athena Eyster, Esther Kennedy, Lyle Nelson, Alex Gould, Grant Cox, Marcus Kunzmann, and Danielle Thomson for assistance in the field. Greg Eischeid, Sierra Peterson, Sarah Manley, and Kate Dennis are thanked for help in the Laboratory for Geochemical Oceanography at Harvard University. David Johnston, Alan Rooney, Paul Myrow, Paul Hoffman, John Taylor, Tim Gibson, Emmy Smith, Uyanga Bold, Andrew Masterson, Tom Laakso, Wil Leavitt, Tony Prave, Ian Fairchild, Andrey Bekker, and Noah Planavsky are thanked for providing stimulating conversations. Rob Rainbird and Elizabeth Turner provided extremely constructive reviews and comments on an earlier version of this manuscript. Finally, we thank associate editors Danny Rye and David Evans at *American Journal of Science* for providing fantastic editorial advice.

## REFERENCES

Abbott, J. G., 1993, Revised stratigraphy and new exploration targets in the Hart River area (NTS 116A/10, 116A/11), southeastern Yukon, *in* Yukon Exploration and Geology 1992: Exploration and Geological Services Division, Yukon, Indian and Northern Affairs Canada, p. 13-23.

Abbott, J. G., 1996, Implications of probable Late Proterozoic dextral strike-slip movement on the Snake River Fault, *in* Cook, F.A. and Erdmer, P., editors, Slave – Northern Cordillera Lithospheric Evolution (SNORCLE) Transect: Lithoprobe Report 50, p. 138-140.

Abbott, G., 1997, Geology of the upper Hart River area, eastern Ogilvie Mountains, Yukon Territory (116A/10, 116A/11): Exploration and Geological Services Division, Yukon Region, Bulletin 9, p. 1-76.

Abercombie, H.J., ms, 1978, Mineralogy and environment of deposition of a Precambrian evaporite deposit, Mackenzie Mountains, Northwest Territories: B.Sc. thesis, University of British Columbia, 45 p.

Aitken, J.D., 1981, Stratigraphy and sedimentology of the upper Proterozoic Little Dal Group, Mackenzie Mountains, Northwest Territories, *in* Campbell, F.H.A., editor, Proterozoic basins of Canada: Geological Survey of Canada Paper 81-10, p. 47-71.

Aitken, J.D., 1991, The Ice Brook Formation and post-Rapitan, Late Proterozoic glaciation, Mackenzie Mountains, Northwest Territories: Geological Survey of Canada Bulletin 404, 43 p.

Aitken, J.D., and Cook, D.G., 1974, Geological maps, northern part of Mount Eduni and Bonnet Plume Lake map-areas, District of Mackenzie: Geological Survey of Canada Open File Report 221, scale 1:250,000.

Aitken, J.D., and McMechan, M.E., 1992, Middle Proterozoic Assemblages, *in* Gabrielse, H., and Yorath, C.J., editors, Geology of the Cordilleran Orogen in Canada: Geological Survey of Canada, Geology of Canada, n. 4, p. 97-124. (also Geological Society of America, The Geology of North America, v. G-2).

Allen, P.A., and Homewood, P., 1984, Evolution and mechanics of a Miocene tidal dune: Sedimentology, v. 31, p. 62-81.

Anadón, P., Rosell, L., and Talbot, M.R., 1992, Carbonate replacement of lacustrine gypsum deposits in two Neogene continental basins, eastern Spain: Sedimentary Geology, v. 78, p. 201-216.

Armin, R.A., and Mayer, L., 1983, Subsidence analysis of the Cordilleran miogeocline: Implications for timing of late Proterozoic rifting and amount of extension: Geology, v. 11, p. 702-705.

Armstrong, R.A., Eisbacher, G.H., and Evans, P.D., 1982, Age and stratigraphic-tectonic significance of Proterozoic diabase sheets, Mackenzie Mountains, northwestern Canada: Canadian Journal of Earth Sciences, v. 19, no. 2, p. 316–323.

Armstrong, R.A., Master, S., and Robb, L.J., 2005, Geochronology of the Nchanga Granite, and constraints on the maximum age of the Katanga Supergroup, Zambian Copperbelt: Journal of African Earth Sciences, v. 42, p. 32-40.

Ashley, G.M., 1990, Classification of large scale subaqueous bedforms: a new look at an old problem: Journa of Sedimentary Petrology, v. 60, p. 160-172.

Bell, R.T., 1982, Comments on the geology and uraniferous mineral occurrences of the Wernecke Mountains, Yukon and District of Mackenzie: Current Research Part B, Geological Survey of Canada, Paper 1982-1B, p. 279-284.

Blaise, B., and Mercier, E., 1984, La sédimentation au Précambrien supérieur et au Paléozoique inférieur sur la marge de la plate-forme du Mackenzie (Monts Ogilvie, Territoire du Yukon): Current Research Part B, Geological Survey of Canada, Paper 84-1B, p. 85-92.

Bond, G.C., and Kominz, M.A., 1984, Construction of tectonic subsidence curves for the early Paleozoic miogeocline, southern Canadian Rocky Mountains: implications for subsidence mechanisms, age of breakup, and crustal thinning: Geological Society of America Bulletin,

v. 95, no. 2, p. 155.

Bond, G.C., Kominz, M.A., and Devlin, W.J., 1983, Thermal subsidence and eustasy in the Lower Paleozoic miogeocline of western North America: Nature, v. 306, no. 5945, p. 775–779, doi: 10.1038/306775a0.

Bond, G.C., Christie-Blick, N., Kominz, M.A., and Devlin, W.J., 1985, An early Cambrian rift to post-rift transition in the Cordillera of western North America: Nature, v. 315, no. 6022, p. 742–746, doi: 10.1038/315742a0.

Bosence, D.W.J., 1998, Stratigraphic and sedimentological models of rift basins, *in* Purser, B.H., and Bosence, D.W.J., editors, Sedimentation and Tectonics of Rift Basins: Red Sea–Gulf of Aden: London, Chapman and Hall, p. 9-28.

Bosworth, W., 1985, Geometry of propogating continental rifts: Nature, v. 316, p. 625-627.

Bosworth, W., 1987, Off-axis volcanism in the Gregory rift, east Africa: Implications for models of continental rifting: Geology, v. 15, p. 397-400.

Bosworth, W., Crevello, P., Winn Jr., R.D., and Steinmetz, J., 1998, Structure, sedimentation, and basin dynamics during rifting of the Gulf of Suez and northwestern Red Sea, *in* Purser, B.H., and Bosence, D.W.J., editors, Sedimentation and Tectonics of Rift Basins: Red Sea–Gulf of Aden: London, Chapman and Hall, p. 77-96.

Bosworth, W., Huchon, P., and McClay, K., 2005, The Red Sea and Gulf of Aden Basins: Journal of African Earth Sciences, v. 43, no. 1–3, p. 334–378.

Bowring, S.A., and Grotzinger, J.P., 1992, Implications of new chronostratigraphy for tectonic evolution of Wopmay Orogen, northwest Canadian Shield: American Journal of Science, v. 292, p. 1-20.

Braiser, M.D., and Shields, G., 2000, Neoproterozoic chemostratigraphy and correlation of the Port Askaig glaciation: Dalradian Supergroup of Scotland: Journal of the Geological Society of London, v. 157, p. 909-914.

Bristow, T.F., and Kennedy, M.J., 2008, Carbon isotope excursions and the oxidant budget of the Ediacaran atmosphere and ocean: Geology, v. 36, n. 11, p. 863-866.

Bull, S., Selley, D., Broughton, D., Hitzman, M., Cailteux, J., Large, R., and McGoldrick, P., 2011, Sequence and carbon isotopic stratigraphy of the Neoproterozoic Roan Group strata of the Zambian copperbelt: Precambrian Research, v. 190, p. 70-89.

Butler, G.P., Harris, P.M., and Kendall, C.G. St.C., 1982, Recent evaporites from the Abu Dhabi coastal flats, *in* Hanford, C.R., Loucks, R.G., and Davies, G.R., editors, Deposition and Diagenetic Spectra of Evaporites: Society of Economic Paleontologists and Mineralogists (SEPM) Core Workshop, v. 3, p. 33–64.

Calver, C.R., 1998, Isotope stratigraphy of the Neoproterozoic Togari Group, Tasmania: Australian Journal of Earth Sciences, v. 45, p. 865-874.

Calvo, J.P., Blanc-Valleron, M.M., Rodriguez-Arandia, J.P., Rouchy, J.M., and Sanz, M.E., 1999, Authigenic clay minerals in continental evaporitic environments: Special Publication of the International Associations of Sedimentologists, v. 27, p. 129–152.

Carr, I.D., Gawthorpe, R.L., Jackson, C.A.L., Sharp, I.R., and Sadek, A., 2003, Sedimentology and sequence stratigraphy of early syn-rift tidal sediments: The Nukhul Formation, Suez Rift, Egypt: Journal of Sedimentary Research, v. 73, n. 3, p. 407-420.

Cattaneo, A., and Steel, R.J., 2003, Transgressive deposits: a review of their variability: Earth-Science Reviews, v. 62, p. 187–228.

Catuneanu, O., Abreu, V., Bhattacharya, J.P., Blum, M.D., Dalrymple, R.W., Eriksson, P.G., Fielding, C.R., Fisher, W.L., Galloway, W.E., Gibling, M.R., Giles, K.A., Holbrook, J.M., Jordan, R., Kendall, C.G.St.C., Macurda, B., Martinsen, O.J., Miall, A.D., Neal, J.E., Nummedal, D., Pomar, L., Posamentier, H.W., Pratt, B.R., Sarg, J.F., Shanley, K.W., Steel, R.J., Strasser, A., Tucker, M.E., and Winker, C., 2009, Towards the standardization of sequence stratigraphy: Earth-Science Reviews, v. 92, p. 1-33.

Catuneanu, O., Galloway, W.E., Kendall, C.G.St.C., Miall, A.D., Posamentier, H.W., Strasser, A., and Tucker, M.E., 2011, Sequence Stratigraphy: Methodology and Nomenclature: Newsletters on Stratigraphy, v. 44, no. 3, p. 173–245, doi: 10.1127/0078-0421/2011/0011.

Cecile, M.P., Morrow, D.W., and Williams, G.K., 1997, Early Paleozoic (Cambrian to Early Devonian) tectonic framework, Canadian Cordillera: Bulletin of Canadian Petroleum Geology, v. 45, p. 54-74.

Cerling, T.E., 1994, Chemistry of closed basin lake waters: A comparison between African Rift Valley and some North American rivers and lakes, *in* Gierlowski-Kordesch, E., and Kelts, K., eds., Global Geological Record of Lake Basins: IGCP Monograph 219, v. 1, p. 29-30.

Christie-Blick, N., and Biddle, K.T., 1985, Deformation and basin formation along strike-slip faults, *in* Biddle, K.T., and Christie-Blick, N., editors, Strike-Slip Deformation, Basin Formation, and Sedimentation: Society of Economic Paleontologists and Mineralogists (SEPM) Special Publication, v. 37, p. 1-34.

Cohen, P.A., and Macdonald, F.A., 2015, The Proterozoic record of eukaryotes: Paleobiology, v. XX, p. 1-23.

Colpron, M., Logan, J., and Mortensen, J., 2002, U-Pb zircon age constraint for late Neoproterozoic rifting and initiation of the lower Paleozoic passive margin of western Laurentia: Canadian Journal of Earth Sciences, v. 39, no. 2, p. 133–143, doi: 10.1139/E01-069.

Cook, F.A., and MacLean, B.C., 1995, The intracratonic Paleoproterozoic Forward orogeny, and implications for regional correlations, Northwest Territories, Canada: Canadian Journal of Earth Science, v. 32, p. 1991–2008.

Cook, F.A., Varsek, J.L., and Clark, E.A., 1991, Proterozoic craton to basin crustal transition in western Canada and its influence on the evolution of the Cordillera: Canadian Journal of Earth Sciences, v. 28, no. 8, p. 1148–1158.

Cook, F.A., Dredge, M., and Clark, E.A., 1992, The Proterozoic Fort Simpson structural trend in northwestern Canada: Geological Society of America Bulletin, v. 104, p. 1121-1137.

Corsetti, F.A., and Kaufman, A.J., 2003, Stratigraphic investigations of carbon isotope anomalies and Neoproterozoic ice ages in Death Valley, California: Geological Society of America Bulletin, v. 115, n. 8., p. 916-932.

Courtillot, V., Jaupart, C., Manighetti, P., Tapponnier, P., and Besse, J., 1999, On causal links between flood basalts and continental breakup: Earth and Planetary Science Letters, v. 166, p. 177-195.

Cox, G.M., Roots, C.F., Halverson, G.P., Minarik, W.G., Macdonald, F.A., and Hubert-Theou, L., 2013, Mount Harper Volcanic Complex, Ogilvie Mountains: A far-flung occurrence of the Franklin Igneous Event?, *in* MacFarlane, K.E., Nordling, M.G., and Sack, P.J., editors, Yukon Exploration and Geology 2012: Yukon Geological Survey, p. 19-36.

Cox, K.G., 1978, Flood basalts, subduction and the break-up of Gondwanaland: Nature, v. 274, p. 47-49.

Crittenden, M.D., Jr., Schaeffer, F.E., Trimble, D.E., and Woodward, L.A., 1971, Nomenclature and correlation of some upper Precambrian and basal Cambrian sequences in western Utah and southeastern Idaho: Geological Society of America Bulletin, v. 94, p. 437-450.

Crowley, J.L., 1997, U-Pb geochronologic constrains on the cover sequence of the Monashee complex, Canadian Cordillera: Paleoproterozoic deposition on basement: Canadian Journal of Earth Science, v. 34, p. 1008-1022.

Dalrymple, R.W., 2010, Tidal depositional systems, *in* James, N.P., and Dalrymple, R.W., editors, Facies Models 4: Geological Association of Canada GEOtext 6, p. 201-231.

Dehler, C.M., Fanning, C.M., Link, P.K., Kingsbury, E.M., and Rybczynski, D., 2010, Maximum depositional age and provenance of the Uinta Mountain Group and Big Cottonwood Formation, northern Utah: Paleogeography of rifting western Laurentia: Geological Society of America Bulletin, v. 122, no. 9-10, p. 1686–1699, doi: 10.1130/B30094.1.

Dehler, C.M., Karlstrom, K.E., Gehrels, G.E., Timmons, M.J., and Crossey, L.J., 2012, Stratigraphic revision, provenance, and new age constraints of the Nankoweap Formation and Chuar Group, Grand Canyon Supergroup, Grand Canyon, Arizona: Geological Society of America Abstracts with Programs, v. 44, no. 6, p. 82.

Dekov, V.M., Cuadros, J., Shanks, W.C., and Koski, R.A., 2008, Deposition of talc, kerolite-smectite, smectite at seafloor hydrothermal vent fields: Evidence from mineralogical, geochemical and oxygen isotope studies: Chemical Geology, v. 247, p. 171–194.

Delaney, G.D., 1981, The mid-Proterozoic Wernecke Supergroup, Wernecke Mountains, Yukon Territory, *in* Campbell, F.H.A., editor, Proterozoic Basins of Canada: Geological Survey of Canada Paper 81-10, p. 1-23.

Desjardins, P.R., Buatois, L.A., and Mangano, M.G., 2012, Tidal flats and subtidal sand bodies, *in* Knaust, D., and Bromley, R.G., editors, Trace fossils as indicators of sedimentary environments: Developments of Sedimentology, v. 64, p. 529-561.

Devlin, W.J., and Bond, G.C., 1988, The initiation of the early Paleozoic Cordilleran miogeocline: evidence from the uppermost Proterozoic-Lower Cambrian Hamill Group of southeastern British Columbia: Canadian Journal of Earth Sciences, v. 25, no. 1, p. 1-19.

Donnadieu, Y., Godderis, Y., Ramstein, G., Nedelec, A., and Meert, J., 2004, A ‘snowball Earth’ climate triggered by continental break-up through changes in runoff: Nature, v. 428, p. 303–306.

Dudás, F.Ö., and Lustwerk, R.L., 1997, Geochemistry of the Little Dal basalts: continental tholeiites from the Mackenzie Mountains, Northwest Territories, Canada: Canadian Journal of Earth Science, v. 34, p. 50-58.

Duggen, S., Hoernle, K., van den Bogaard, P., Rupke, L., and Morgan, J.P., 2003, Deep roots of the Messinian salinity crisis: Nature, v. 422, p. 602-605.

Ebinger, C.J., 1989, Tectonic development of the western branch of the East African rift system: Geological Society of America Bulletin, v. 101, p. 885-903.

Eisbacher, G.H., 1977, Tectono-stratigraphic framework of the Redstone Copper Belt, District of Mackenzie, Report of Activities Part A: Geological Survey of Canada, Paper 77-1A, p. 229-234.

Eisbacher, G.H., 1978, Two major Proterozoic unconformities, northern Cordillera, Current Research Part A: Geological Survey of Canada, Paper 78-1A, p. 53-58.

Eisbacher, G.H., 1981, Sedimentary tectonics and glacial record in the Windermere Supergroup, Mackenzie Mountains, northwestern Canada: Geological Survey of Canada Paper 80-27, 40 p.

Eisbacher, G.H., 1985, Late Proterozoic rifting, glacial sedimentation, and sedimentary cycles in the light of Windermere deposition, western Canada: Palaeogeography, Palaeoclimatology, and Palaeoecology, v. 51, p. 231–254.

Embry, A.F., 1995, Sequence boundaries and sequence hierarchies: problems and proposals, *in* Steel, R.J., Felt, V.L., Johannessen, E.P., and Mathieu, C., editors, Sequence stratigraphy on the Northwest European Margin: Norwegian Petroleum Society (NPF), Special Publication 5, p. 1-11.

Embry, A.F., 2009, Practical Sequence Stratigraphy: Canadian Society of Petroleum Geologists, 79 p., online at www.cspg.org

Embry, A.F., and Johannessen, E.P., 1992, T-R sequence stratigraphy, facies analysis and reservoir distribution in the uppermost Triassic=Jurassic succession, western Sverdrup Basin, Arctic Canada, *in* Vorren, T.O., Bergsager, E., Dahl-Stamnes, O.A., Holter, E., Johansen, B., Lie, E., and Lund, T.B., editors, Arctic Geology and Petroleum Potential, Norwegian Petroleum Society, Special Publication, v. 2, p. 121-146.

Encarnatión, J., Fleming, T.H., Elliot, D.H., Eales, H.V., 1996, Synchronous emplacement of the Ferrar and Karoo dolerites and the early breakup of Gondwana: Geology, v. 24, p. 535-538.

Evanchick, C.A., Parrish, R.R., and Gabrielse, H., 1984, Precambrian gneiss and late Proterozoic sedimentation in north-central British Columbia: Geology, v. 12, p. 233-237.

Evans, D.A.D., 2006, Proterozoic low orbital obliquity and axial-dipolar geomagnetic field from evaporite palaeolatitudes: Nature, v. 444, p. 51-56.

Evans, D.A.D., 2009, The palaeomagnetically viable, long-lived and all-inclusive Rodinia supercontinent reconstruction: Journal of the Geological Society of London, Special Publications, v. 327, p. 371-404.

Fairchild, I.J., Spiro, B., Herrington, P.M., and Song, T.R., 2000, Controls on Sr and C isotopic compositions of Neoproterozoic Sr-rich limestones of East Greenland and North China, *in* Grotzinger, J.P., and James, N.P., editors, Carbonate Sedimentation and Diagenesis in the Evolving Precambrian World, Society of Economic Paleontologists and Mineralogists (SEPM) Special Publication, v. 67, p. 297-313.

Fisher, C.G., and Arthur, M.A., 2002, Water mass characteristics in the Cenomanian U.S. Western Interior Seaway as indicated by stable isotopes of calcareous organisms: Palaeogeography, Palaeoclimatology, and Palaeoecology, v. 188, p. 189-213.

Folk, R.L., and Pittman, J.S., 1971, Length-slow chalcedony: A new testament for vanished evaporites: Journal of Sedimentary Petrology, v. 41, no. 4, p. 1–14.

Frank, T.D., and Lyons, T.W., 2000, The integrity of $\delta^{18}O$ records in Precambrian carbonates: A Mesoproterzoic case study, *in* Grotzinger, J.P., and James, N.P., editors, Carbonate Sedimentation and Diagenesis in the Evolving Precambrian World: Society for Sedimentary Geology (SEPM) Special Publication, v. 67, p. 315–326.

Friedman, G.M., 1980, Dolomite is an evaporite mineral: evidence from the rock record and from sea-marginal ponds of the Red Sea, *in* Zenger, D.H., Dunham, J.D., and Ethington, R.L., editors, Concepts and Models of Dolomitization: Society of Economic Paleontologists and Mineralogists (SEPM) Special Publication, v. 28, p. 69–80.

Furlanetto, F., Thorkelson, D.J., Gibson, H.D., Marshall, D.D., Rainbird, R.H., Davis, W.J., Crowley, J.L., and Vervoort, J.D., 2013, Late Paleoproterozoic terrane accretion in northwestern Canada and the case for circum-Columbian orogenesis: Precambrian Research, v. 224, p. 512-528.

Gabrielse, H., 1967, Tectonic evolution of the northern Canadian Cordillera: Canadian Journal of Earth Sciences, v. 4, p. 271-298.

Gabrielse, H., Blusson, S.L., and Roddick, J.A., 1973, Flat River, Glacier Lake, and Wrigley Lake map-areas (95E, L, M), District of Mackenzie and Yukon Territory: Geological Survey of Canada, Memoir 366, 153 p.

Galán, E., and Pozo, M., 2011, Palygorskite and sepiolite deposits in continental environments: Description, genetic patterns, and sedimentary settings, *in* Galán, E., and Singer, A., editors, Developments in Palygorskite-Sepiolite Research: A new outlook on these nanomaterials: Developments in Clay Science, Amsterdam, Elsevier, p. 125-174.

Gat, J.R., and Bowser, C., 1991, The heavy isotope enrichment of water in coupled evaporative systems, *in* Taylor, H.P., O'Neil, J.R., Kaplan, I.R., editors, Stable Isotope Geochemistry: A Tribute to Samuel Epstein: Geochemical Society Special Publication, v. 3, p. 159–168.

Gawthorpe, R.L., Fraser, A.J., and Collier, R.E.L.L., 1994, Sequence stratigraphy in active extensional basins: implications for the interpretation of ancient basin-fills: Marine and Petroleum Geology, v. 11, p. 642-658.

Gawthorpe, R.L., and Leeder, M.R., 2000, Tectono-sedimentary evolution of active extensional basins: Basin Research, v. 12, no. 3-4, p. 195–218, doi: 10.1111/j.1365-2117.2000.00121.x.

Godderis, Y., Donnadieu, Y., Nedelec, A., Dupre, B., Dessert, C., Grard, A., Ramstein, G., and Francois, L., 2003, The Sturtian "snowball" glaciation: fire and ice: Earth And Planetary Science Letters, v. 211, no. 1-2, p. 1–12.

Goodfellow, W., Cecile, M., and Leybourne, M., 1995, Geochemistry, petrogenesis, and tectonic wetting of Lower Paleozoic alkalic and potassic volcanic rocks, northern Canadian Cordilleran miogeocline: Canadian Journal of Earth Sciences, v. 32, no. 8, p. 1236–1254.

Gordey, S.P., and Anderson, R.G., 1993, Evolution of the Cordilleran miogeocline, Nahanni map area (105I), Yukon and Northwest Territories: Geological Survey of Canada, Memoir 428, 214 p.

Gorjan, P., Veevers, J.J., and Walter, M.R., 2000, Neoproterozoic sulfur-isotope variation in Australia and global implications: Precambrian Research, v. 100, p. 151-179.

Green, L.H., 1972, Geology of Nash Creek, Larsen Creek, and Dawson Creek map areas, Yukon Territory, Geological Society of Canada, Memoir 364, 157 p.

Grotzinger, J.P., 1986, Evolution of Early Proterozoic passive margin carbonate platform, Rocknest Formation, Wopmay Orogen, Northwest Territories, Canada: Journal of Sedimentary Petrology, v. 56, no. 6, p. 831–847.

Grotzinger, J.P., 1989, Facies and evolution of Precambrian carbonate depositional systems: Emergence of the modern platform archetype, *in* Crevello, P.D., Wilson, J.L., Sarg, J.F., and Read, J.F., editors, Controls on Carbonate Platform and Basin Development: Society for Sedimentary Geology (SEPM) Special Publication, v. 44, p. 79-106.

Grotzinger, J.P., and James, N.P., 2000, Precambrian carbonates: Evolution of understanding, *in* Grotzinger, J.P., and James, N.P., editors, Carbonate Sedimentation and Diagenesis in the Evolving Precambrian World: Society for Sedimentary Geology (SEPM) Special Publication, v. 67, p. 1-20.

Halverson, G.P., 2006, A Neoproterzoic chronology, *in* Xiao, S., and Kaufman, A.J., editors, Neoproterozoic Geobiology and Paleobiology: Topics in Geobiology, Springer, New York, v. 27, p. 231-271.

Halverson, G.P., and Hurtgen, M.T., 2007, Ediacaran growth of the marine sulfate reservoir: Earth and Planetary Science Letters, v. 263, p. 32-44.

Halverson, G.P., Maloof, A.C., and Hoffman, P.F., 2004, The Marinoan glaciation (Neoproterozoic) in Svalbard: Basin Research, v. 16, p. 297-324.

Halverson, G.P., Hoffman, P.F., Schrag, D.P., Maloof, A.C., and Rice, A., 2005, Toward a Neoproterozoic composite carbon isotope record: Geological Society of America Bulletin, v. 117, p. 1181–1207.

Halverson, G.P., Wade, B.P., Hurtgen, M.T., and Barovich, K.M., 2010, Neoproterozoic Chemostratigraphy: Precambrian Research, v. 182, no. 4, p. 337-350.

Halverson, G.P., Macdonald, F.A., Strauss, J.V., Smith, E.F., Cox, G.M., and Hubert-Theou, L., 2012, Updated definition and correlation of the lower Fifteenmile Group in the central and eastern Ogilvie Mountains, *in* MacFarlane, K.E., and Sack, P.J., editors, Yukon Exploration and Geology 2011: Yukon Geological Survey, p. 75-90.

Halverson, G.P., Cox, G.C., Hurtgen, M.T., Sansjofre, P., Kunzmann, M., Strauss, J.V., and Macdonald, F.A., 2014, A continental flood basalt driver for Neoproterozoic climate and oxygenation: Geological Society of America Abstracts with Programs, p. 256–256.

Hansen, V.L., Goodge, J.W., Keep, M., and Oliver, D.H., 1993, Asymmetric rift interpretation of the western North American margin: Geology, v. 21, p. 1067-1070.

Harlan, S., Heaman, L., LeCheminant, A., and Premo, W., 2003, Gunbarrel mafic magmatic event: A key 780 Ma time marker for Rodinia plate reconstructions: Geology, v. 31, no. 12, p. 1053–1056.

Hartnett, H.E., Keil, R.G., Hedges, J.I., Devol, A.H., 1998, Influence of oxygen exposure time on organic carbon preservation in continental margin sediments: Nature, v. 391, p. 572-574.

Harwood, C.L., and Sumner, D.Y., 2011, Microbialites of the Neoproterozoic Beck Spring Dolomite, Southern California: Sedimentology, v. 58, no. 6, p. 1648–1673, doi: 10.1111/j.1365-3091.2011.01228.x.

Harwood, C.L., and Sumner, D.Y., 2012, Origins of microbial microstructures in the Neoproterozoic Beck Spring Dolomite: variations in microbial community and timing of lithification: Journal of Sedimentary Research, v. 82, no. 9, p. 709–722, doi: 10.2110/jsr.2012.65.

Heaman, L., LeCheminant, A., and Rainbird, R., 1992, Nature and timing of Franklin Igneous Events, Canada: implications for a Late Proterozoic mantle plume and the break-up of Laurentia: Earth And Planetary Science Letters, v. 109, p. 117–131.

Hedges, J.I., Hu, F.S., Devol, A.H., Hartnett, H.E., Tsamakis, E., and Keil, R.G., 1999, Sedimentary organic matter preservation: an assessment and speculative synthesis: American Journal of Science, v. 299, p. 529-555.

Helmstaedt, H., Eisbacher, G.H,, and McGregor, J.A., 1979, Copper mineralization near an intra-Rapitan unconformity, Nite copper prospect, Mackenzie Mountains, Northwest Territories, Canada: Canadian Journal of Earth Sciences, v. 16, p. 50-59.

Higgins, J.A., and Schrag, D.P., 2006, Beyond methane: Towards a theory for the Paleocene-Eocene Thermal Maximum: Earth and Planetary Science Letters, v. 245, p. 523-537.

Hoffman, P.F., 1989, Precambrian geology and tectonic history of North America, *in* Bally, A.W., and Palmer, A.R., editors, The geology of North America – an overview: Geological Society of America, The Geology of North America, v. A, p. 447-512.

Hoffman, P.F., 1991, Did the breakout of Laurentia turn Gondwanaland inside-out?: Science, v. 252, no. 5011, p. 1409–1412.

Hoffman, P.F., Kaufman, A.J., Halverson, G.P., and Schrag, D.P., 1998, A Neoproterozoic snowball earth: Science, v. 281, p. 1342–1346.

Hoffman, P.F., and Schrag, D.P., 2002, The snowball Earth hypothesis: testing the limits of global change: Terra Nova, v. 14, no. 3, p. 129–155.

Hoffman, P.F., Halverson, G.P., Domack, E., Maloof, A.C., Swanson-Hysell, N., and Cox, G.M., 2012, Cryogenian glaciations on the southern tropical paleomargin of Laurentia (NE Svalbard and East Greenland), and a primary origin for the upper Russøya (Islay) carbon isotope excursion: Precambrian Research, v. 206-207, p. 137-158.

Horodyski, R.J., and Knauth, P.L., 1994, Life on land in the Precambrian: Science, v. 263, no. 5146, p. 494-498.

Hover, V.C., Walter, L.M., Peacor, D.R., and Martini, A.M., 1999, Mg-smectite authigenesis in a marine evaporative environment, Salina Ometepec, Baja California: Clays and Clay Minerals, v. 47, no. 3, p. 252-268.

Hughes, G.W., Abdine, S., and Girgis, M.H., 1992, Miocene biofacies development and geological history of the Gulf of Suez, Egypt: Marine and Petroleum Geology, v. 9, p. 2-28.

Hurtgen, M.T., Arthur, M.A., Suits, N.S., and Kaufman, A.J., 2002, the sulfur isotopic composition of Neoproterozoic seawater sulfate: Implications for a snowball Earth?: Earth and Planetary Science Letters, v. 203, p. 413-430.

Jackson, J.A., and White, N.J., 1989, Normal faulting in the upper continental crust: observations from regions of active extension: Journal of Structural Geology, v. 11, p. 15-36.

Jackson, M.P.A., Warin, O.N., Woad, G.M., and Hudec, M.R., 2003, Neoproterozoic allochthonous salt tectonics during the Lufilian orogeny in the Katangan Copperbelt, central Africa: Geological Society of America Bulletin, v. 115, p. 314-330.

Jacobsen, S.B., and Kaufman, A.J., 1999, The Sr, C, and O isotopic evolution of Neoproterozoic seawater: Chemical Geology, v. 161, p. 37-57.

Jaffrés, J.B.D., Shields, G.A., and Wallman, K., 2007, The oxygen isotope evolution of seawater: A critical review of a long-standing controversy and an improved geological water cycle model for the past 3.4 billion years: Earth Science Reviews, v. 83, p. 83-122.

James, N., Narbonne, G., and Kyser, T., 2001, Late Neoproterozoic cap carbonates: Mackenzie Mountains, northwestern Canada: precipitation and global glacial meltdown: Canadian Journal of Earth Sciences, v. 38, no. 8, p. 1229–1262.

Jefferson, C.W., ms, 1983, The Upper Proterozoic Redstone Copper Belt, Mackenzie Mountains, N.W.T.: Ph.D. thesis, The University of Western Ontario, London, 445 p.

Jefferson, C.W., 1985, Uppermost Shaler Group and its contact with the Natkusiak basalts, Victoria Island, District of Franklin, Current Research Part A: Geological Survey of Canada, Paper 85-1A, p. 103-110.

Jefferson, C.W., and Ruelle, J.C.L., 1986, The Late Proterozoic Redstone Copper Belt, Mackenzie Mountains, N.W.T., *in* Morin, J.A., editor, Mineral Deposits of the Northern Cordillera: Canadian Institute of Mining and Metallurgy, Special Volume 37, p. 154-168.

Jefferson, C.W., and Parrish, R.R., 1989. Late Proterozoic stratigraphy, U–Pb zircon ages, and rift tectonics, Mackenzie Mountains, northwestern Canada: Canadian Journal of Earth Science, v. 26, p. 1784–1801.

Jeletsky, J.A., 1962, Pre-Cretaceous Richardson Mountains Trough – its place in the tectonic framework of Arctic Canada and its bearing on some geosynclinals concepts: Transactions of the Royal Society of Canada, v. 56, p. 55-84.

Johnson, J.G., Murphy, M.A., 1984, Time-rock model for Siluro-Devonian continental shelf, western United States: Geological Society of America Bulletin, v. 95, p. 1349-1359.

Johnson, J.G., Klapper, G., and Sandberg, C.A., 1985, Devonian eustatic fluctuations in Euramerica: Geological Society of America Bulletin, v. 96, p. 567-587.

Jones, D.S., Maloof, A.C., Hurtgen, M.T., Rainbird, R.H., and Schrag, D.P., 2010, Regional and global chemostratigraphic correlation of the early Neoproterozoic Shaler Supergroup, Arctic Canada: Precambrian Research, v. 181, p. 43-63.

Jones, D.S., Creel, R.C., Rios, B., and Santiago Ramos, D.P., 2015, Chemostratigraphy of an Ordovician–Silurian carbonate platform: $\delta^{13}$C records below glacioeustatic exposure surfaces: Geology, v. 43, no. 1, p. 59-62.

Kah, L.C., Sherman, A.G., Narbonne, G.M., Knoll, A.H., and Kaufman, A.J., 1999, $\delta^{13}$C stratigraphy of the Proterozoic Bylot Supergroup, Baffin Island, Canada: implications for regional lithostratigraphic correlation: Canadian Journal of Earth Science, v. 36, p. 313-332.

Kah, L.C., 2000, Depositional $\delta^{18}$O signatures in Proterozoic dolostones: constraints on seawater chemistry and early diagenesis, *in* Grotzinger, J.P., and James, N.P., editors, Carbonate Sedimentation and Diagenesis in the Evolving Precambrian World: Society for Sedimentary Geology (SEPM) Special Publication, v. 67, p. 345-360.

Karlstrom, K.E., Bowring, S.A., Dehler, C.M., Knoll, A.H., Porter, S.M., Des Marais, D.J., Weil, A.B., Sharp, Z.D., Geissman, J.W., Elrick, M.B., Timmons, J.M., Crossey, L.J., and Davidek, K.L., 2000, Chuar Group of the Grand Canyon: Record of breakup of Rodinia, associated change in the global carbon cycle, and ecosystem expansion by 740 Ma: Geology, v. 28, no. 7, p. 619–622.

Kaufman, A.J., Knoll, A.H., and Narbonne, G., 1997, Isotopes, ice ages, and terminal Proterozoic earth history: Proceedings of the National Academy of Sciences, v. 94, no. 13, p. 6600–6605.

Kaufman, A.J., Williams, B.P., Johnston, D.T., Farquhar, J., Knoll, A.H., Butterfield, N.J., and Rainbird, R.H., 2007, Environmental change in the prelude to a Neoproterozoic ice age:

Sulfur isotope evidence from the Shaler Supergroup, Northwest Territories, Canada: American Geophysical Union, Fall Meeting 2007, Abstract #V42A-01.

Kendall, A.C., 2001, Late diagenetic calcitization of anhydrite from the Mississippian of Saskatchewan, western Canada: Sedimentology, v. 48, p. 29-55.

Kendall, C.G.St.C., and Warren, J., 1987, A review of the origin and setting of tepees and their associated fabrics: Sedimentology, v. 34, p. 1007–1027.

Kingsbury-Stewart, E.M., Osterhout, S.L., Link, P.K., and Dehler, C.M., 2013, Sequence stratigraphy and formaliztion of the Middle Uinta Mountain Group (Neoproterozoic), central Uinta Mountains, Utah: A closer look at the western Laurentian Seaway at ca. 750 Ma: Precambrian Research, v. 236, p. 65–84, doi: 10.1016/j.precamres.2013.06.015.

Kirkham, A., 1997, Shoreline evolution, aeolian deflation and anhydrite distribution of the Holocene, Abu Dhabi: GeoArabia, v. 2, p. 403-416.

Kirshvink, J.L., 1992, Late Proterozoic low-latitude global glaciation: the snowball earth, *in* Klein, C., and Schopf, J.W., editors, The Proterozoic Biosphere: London, Cambridge University Press, p. 51-52.

Knauth, L.P., and Kennedy, M.J., 2009, The late Precambrian greening of the Earth: Nature, v. 460, no. 7256, p. 728–732, doi: 10.1038/nature08213.

Knoll, A.H., Hayes, J.M., Kaufman, A.J., Swett, K., and Lambert, I.B., 1986, Secular variation in carbon isotope ratios from Upper Proterozoic successions of Svalbard and East Greenland: Nature, v. 321, no. 6073, p. 832–838, doi: 10.1038/321832a0.

Krapez, B., 1996, Sequence stratigraphic concepts applied to the identification of basin-filling rhythms in Precambrian successions: Australian Journal of Earth Sciences, v. 43, no. 4, p. 355-380.

Kump, L.R., 1991, Interpreting carbon-isotope excursions: Strangelove oceans: Geology, v. 19, p. 299-302.

Kump, L.R., Arthur, M.A., Patzkowsky, M.E., Gibbs, M.T., Pinkus, D.S., and Sheehan, P.M., 1999, A weathering hypothesis for glaciation at high atmospheric *p*CO2 during the Late Ordovician: Palaeogeography, Palaeoclimatology, Palaeoecology, v. 152, p. 173-187.

Kunzmann, M., Halverson, G.P., Macdonald, F.A., Hodgskiss, M., Sansjofre, P.D., Schumann, D., and Rainbird, R.H., 2014, The early Neoproterozoic Chandindu Formation of the Fifteenmile Group in the Ogilvie Mountains, *in* MacFarlane, K.E., Nordling, M.G., and Sack, P.J., editors, Yukon Exploration and Geology 2013: Yukon Geological Survey, p. 93-107.

Land, L.S., 1983, The application of stable isotopes to studies of the origin of dolomite and to problems of diagenesis of clastic sediments, *in* Arthur, M.A., and Anderson, T.F., editors, Stable Isotopes in Sedimentary Geology: Society of Economic and Paleontologists Mineralogical (SEPM) Short Course No. 10, 4.1-4.22.

LeCheminant, A.N., and Heaman, L.M., 1989, Mackenzie igneous events, Canada: Middle

Proterozoic hotspot magmatism associated with ocean opening: Earth And Planetary Science Letters, v. 96, p. 38-48.

Leeder, M.R., and Gawthorpe, R.L., 1987, Sedimentary models for extensional tilt-block/half-graben basins, *in* Coward, M.P., Dewey, J.F., and Hancock, P.L., editors, Continental Extensional Tectonics: Geological Society of London Special Publication, v. 28, p. 139-152.

Lenz, A.C., 1972, Ordovician to Devonian history of northern Yukon and adjacent District of Mackenzie: Bulletin of Canadian Society of Petroleum Geologists, v. 20, no. 2, p. 321-361.

Levy, M., and Christie-Blick, N., 1991, Tectonic Subsidence of the Early Paleozoic Passive Continental-Margin in Eastern California and Southern Nevada: Geological Society of America Bulletin, v. 103, no. 12, p. 1590–1606.

Li, Z.-X., Bogdanova, S.V., Collins, A.S., Davidson, A., De Waele, B., Ernst, R.E., Fitzsimmons, I.C.W., Fuck, R.A., Gladkochub, D.P., Jacobs, J., Karlstrom, K.E., Lu, S., Natapov, L.M., Pease, V., Pisarevsky, S.A., Thrane, K., Vernikovsky, V., 2008, Assembly, configuration, and break-up history of Rodinia: A synthesis: Precambrian Research, v. 160, no. 1-2, p. 179–210, doi: 10.1016/j.precamres.2007.04.021.

Li, Z.-X., Kinny, P.D., and Wang, J., 1999, The breakup of Rodinia: did it start with a mantle plume beneath South China?: Earth And Planetary Science Letters, v. 173, p. 171-181.

Li, Z.-X., Evans, D.A.D., Halverson, G.P., 2013, Neoproterzoic glaciations in a revised global palaeogeography from the breakup of Rodinia to the assembly of Gondwanaland: Sedimentary Geology, v. 294, p. 219-232.

Lindsay, J.F., 2002, Supersequences, superbasins, supercontinents – evidence from the Neoproterozoic–Early Palaeozoic basins of central Australia: Basin Research, v. 14, p. 207-223.

Long, D.G.F., Rainbird, R.H., Turner, E.C., and MacNaughton, R.B., 2008, Early Neoproterozoic strata (Sequence B) of mainland northern Canada and Victoria and Banks Islands: a contribution to the Geological Atlas of the Northern Canadian Mainland Sedimentary Basin: Geological Survey of Canada, Open File 5700, 24 p.

Long, D.G.F., and Turner, E.C., 2012, Formal definition of the Neoproterozoic Mackenzie Moutains Supergroup (Northwest Territories), and formal stratigraphic nomenclature for terriginous clastic units of the Katherine Group: Geological Survey of Canada, Open File 7112, 40 p.

Lund, K., 2008, Geometry of the Neoproterozoic and Paleozoic rift margin of western Laurentia: implications for mineral deposit settings: Geosphere, v. 4, p. 429-444.

Lund, K., Aleinikoff, J.N., Evans, K.V., duBray, E.A., Dewitt, E.H., and Unruh, D.M., 2010, SHRIMP U-Pb dating of recurrent Cryogenian and Late Cambrian-Early Ordovician alkalic magmatism in central Idaho: Implications for Rodinian rift tectonics: Bulletin of the Geological Society of America, v. 122, no. 3-4, p. 430.

Lloyd, M.R., 1964, Variations in the oxygen and carbon isotope ratios of Florida Bay mollusks and their environmental significance: Journal of Geology, v. 72, p. 84-111.

Macdonald, F.A., and Roots, C.F., 2010, Upper Fifteenmile Group in the Ogilvie Mountains and correlations of early Neoproterozoic strata in the northern Cordillera, *in* McFarlane, K.E., Weston, L.H., and Blackburn, L.R., editors, Yukon Exploration and Geology 2009: Yukon Geological Survey, p. 237-252.

Macdonald, F.A., Schmitz, M.D., Crowley, J.L., Roots, C.F., Jones, D.S., Maloof, A.C., Strauss, J.V., Cohen, P.A., Johnston, D.T., and Schrag, D.P., 2010, Calibrating the Cryogenian: Science, v. 327, no. 5970, p. 1241–1243, doi: 10.1126/science.1183325.

Macdonald, F.A., Smith, E.F., Strauss, J.V., Cox, G.M, Halverson, G.P. and Roots, C.F., 2011, Neoproterozoic and early Paleozoic correlations in the western Ogilvie Mountains, Yukon, *in* MacFarlane, K.E., Weston, L.H., and Relf C., editors, Yukon Exploration and Geology 2010: Yukon Geological Survey, p. 161-182

Macdonald, F.A., Halverson, G.P., Strauss, J.V., Smith, E.F., Cox, G.M., Sperling, E.A., and Roots, C.F., 2012, Early Neoproterozoic basin formation in Yukon, Canada: Implications for the make-up and break-up of Rodinia: Geoscience Canada, v. 39, p. 77-99.

Macdonald, F.A., Strauss, J.V., Sperling, E.A., Halverson, G.P., Narbonne, G.M., Johnston, D.T., Kunzmann, M., Schrag, D.P., and Higgins, J.A., 2013a, The stratigraphic relationship between the Shuram carbon isotope excursion, the oxygenation of Neoproterozoic oceans, and the first appearance of the Ediacara bioto and bilaterian trace fossils in northwestern Canada: Chemical Geology, v. 362, p. 250-272, doi: 10.1016/j.chemgeo.2013.05.032.

Macdonald, F., Prave, A., Petterson, R., Smith, E., Pruss, S., Oates, K., Waechter, F., Trotzuk, D., and Fallick, A., 2013b, The Laurentian record of Neoproterozoic glaciation, tectonism, and eukaryotic evolution in Death Valley, California: Geological Society of America Bulletin, v. 125, no. 7-8, p. 1203–1223.

Mahon, R.C., Dehler, C.M., Link, P.K., Karlstrom, K.E., and Gehrels, G.E., 2014, Geochronologic and stratigraphic constraints on the Mesoproterozoic and Neoproterozoic Pahrump Group, Death Valley, California: A record of the assembly, stability, and breakup of Rodinia: Geological Society of America Bulletin, v. 126, no. 5-6, p. 652–664, doi: 10.1130/B30956.1.

Mann, P., Hempton, M.R., Bradley, D.C., and Burke, K., 1983, Development of pull-apart basins: Journal of Geology, v. 91, p. 529-554.

McCay, G.A., Prave, A.R., Alsop, G.I., Fallick, A.E., 2006, Glacial trinity: Neoproterozoic Earth history within the British-Irish Caledonides: Geology, v. 34, p. 909-912.

McDonough, M.R., and Parrish, R.R., 1991, Proterozoic gneisses of the Malton Complex, near Valemount, British Columbia: U-Pb ages and Nd isotopic signatures: Canadian Journal of Earth Sciences, v. 28, p. 1202-1216.

McKenzie, J.A., 1981, Holocene dolomitization of calcium carbonate sediments from the coastal sabkhas of Abu Dhabi, UAE: a stable isotope study: Journal of Geology, v. 89, p. 185–198.

Medig, K.P., Thorkelson, D.J., and Dunlop, R.L., 2010, The Proterozoic Pinguicula Group: stratigraphy, contact relationships, and possible correlations, *in* MacFarlane, K.E., Weston, L.H., and Blackburn, L.R., editors, Yukon Exploration and Geology 2009: Yukon Geological Survey, p. 265-278.

Medig, K.P.R., Thorkelson, D.J., Davis, W.J., Rainbird, R.H., Gibson, H.D., Turner, E.C., and Marshall, D.D., 2014, Pinning northeastern Australia to northwestern Laurentia in the Mesoproterozoic: Precambrian Research, v. 249, p. 88–99, doi: 10.1016/j.precamres.2014.04.018.

Mercier, E., 1989, Evenéments tectoniques d'origine compressive dans le Protérozoique du nord de la Cordillere canadienne (montagnes Ogilvie, Yukon): Canadian Journal of Earth Sciences, v. 26, p. 199-205.

Milliken, K.L., 1979, The silicified evaporite syndrome – two aspects of silicification history of former evaporite nodules from southern Kentucky and northern Tennessee: Journal of Sedimentary Research, v. 49, p. 245–256. doi: 10.1306/212F7707-2B24-11D7-8648000102C1865D.

Millot, G., 1970, Geology of Clays: London, Springer–Verlag, Chapman and Hall, 429 p.

Milton, J.E., Hickey, K.A., and Gleeson, S.A., 2014, New U-Pb constraints on Gunbarrel volcanism and the break-up of Rodinia: The 775 Ma Little Dal basalts: Geological Society of America Abstracts with Programs, v. 46, n. 6, p. 828.

Monger, J., and Price, R., 2002, The Canadian Cordillera: Geology and Tectonic Evolution: Canadian Society for Economic Geologists Recorder, p. 17-36.

Montenat, C., Orszag-Sperber, F., Plaziat, J.-C., and Purser, B.H., 1998, The sedimentary record of the initial stages of Oligo-Miocene rifting in the Gulf of Suez and the northern Red Sea, *in* Purser, B.H., and Bosence, D.W.J., editors, Sedimentation and Tectonics of Rift Basins: Red Sea–Gulf of Aden: Chapman and Hall, London, p. 146-xxx.

Moodley, L., Middelburg, J.J., Herman, P.M.J., and de Lange, G.J., 2005, Oxygenation and organic-matter preservation in marine sediments: direct experimental evidence from ancient organic carbon-rich deposits: Geology, v. 33, p. 889-892.

Morgan, W.J., 1981, Hot spot tracks and the opening of the Atlantic and Indian Oceans: The oceanic lithosphere, *in* Emiliani, C., editor, The Sea – Ideas and Observations on Progress in the Study of the Seas: New York, Wiley Interscience, v. 7, p. 443-487.

Morrow, D.W., 1999, Lower Paleozoic stratigraphy of northern Yukon Territory and northwestern District of Mackenzie: Geological Survey of Canada, Bulletin 538, 202 p.

Moynihan, D., 2014, Bedrock geology of NTS 106B/04, Eastern Rackla Belt, *in* MacFarlane, K.E., Nordling, M.G., and Sack, P.J., editors, Yukon Exploration and Geology 2013: Yukon Geological Survey, p. 147-167.

Mustard, P.S., ms, 1990, Sedimentology and Tectonic Evolution of the Upper Proterozoic Mount Harper Group Sedimentary Rocks, Yukon Territory: Ph.D. thesis, Carleton University, Ottawa, 330 p.

Mustard, P.S., 1991, Normal faulting and alluvial fan deposition, basal Windermere Tectonic

Assemblage, Yukon, Canada: Geological Society of America Bulletin, v. 103, no. 10, p. 1346–1364.

Mustard, P.S., and Donaldson, J.A., 1990, Paleokarst breccias, calcretes, silcretes and fault talus breccias at the base of Upper Proterozoic “Windermere” strata, northern Canadian Cordillera: Journal of Sedimentary Petrology, v. 60, no. 4, p. 525–539.

Mustard, P.S., and Roots, C.F., 1997, Rift-related volcanism, sedimentation, and tectonic setting of the Mount Harper Group, Ogilvie Mountains, Yukon Territory: Geological Survey of Canada, Bulletin 492, 92 p.

Naehr, T.H., Eichhubl, P., Orphan, V.J., Hovland, M., Paull, C.K., Ussler III, W., Lorenson, T.D., and Greene, H.G., 2007, Authigenic carbonate formation at hydrocarbon seeps in continental margin sediments: A comparative study: Deep Sea Research Part II: Tropical Studies in Oceanography, v. 54, no. 11-13, p. 1268-1291.

Narbonne, G.M., and Aitken, J., 1995, Neoproterozoic of the Mackenzie Mountains, Northwestern Canada: Precambrian Research, v. 73, p. 101–121.

Narbonne, G.M., Kaufman, A.J., and Knoll, A.H., 1994, Integrated chemostratigraphy and biostratigraphy of the Windermere Supergroup, northwestern Canada: Implications for Neoproterozoic correlations and the early evolution of animals: Geological Society of America Bulletin, v. 106, p. 1281–1292.

Norris, D.K., 1982, Snake River: Geological Survey of Canada, Map 1529A, scale 1:250,000.

Norris, D.K., 1997, Geology and mineral and hydrocarbon potential of northern Yukon Territory and northwestern District of Mackenzie: Geological Survey of Canada, Bulletin 422, 397 p.

Ootes, L., Sandeman, H., Lemieux, Y., and Leslie, C., 2008, The 780 Ma Tsezotene sills, Mackenzie Mountains: a field, petrographical, and geochemical study: Northwest Territories Geoscience Office, NWT Open File Report 2008-011, 21 p.

Orszag-Sperber, F., Harwood, G., Kendall, A., and Purser, B.H., 1998, A review of the evaporites of the Red Sea-Gulf of Suez rift, *in* Purser, B.H., and Bosence, D.W.J., editors, Sedimentation and Tectonics of Rift Basins: Red Sea–Gulf of Aden: London, Chapman and Hall, p. 409-426.

Park, J.K., Roots, C.F., and Brunet, N., 1992, Paleomagnetic evidence for rotation in the Neoproterozoic Mount Harper volcanic complex, Ogilvie Mountains, Yukon Territory: Current Research, Part E. Geological Survey of Canada Paper, p. 1–10.

Park, J., Buchan, K., and Harlan, S., 1995, A proposed giant radiating dyke swarm fragmented by the separation of Laurentia and Australia based on paleomagnetism of ca. 780 Ma mafic intrusions in western North America: Earth And Planetary Science Letters, v. 132, p. 129-139.

Parrish, R.R., and Scammell, R.J., 1988, The age of the Mount Copeland syenite gneiss and its metamorphic zircons, Monashee Complex, southeastern British Columbia: radiogenic age and isotopic studies, report 2: Geological Survey of Canada, Paper 88-2, p. 21-28.

Patterson, W.P., and Walter, L.M., 1994, Depletion of $^{13}C$ in seawater $\Sigma CO_2$ on modern carbonate platforms: Significance for carbon isotopic record of carbonates: Geology, v. 22, p. 885-888.

Pierre, C., and Rouchy, J.M., 1988, Carbonate replacements after sulphate evaporites in the Middle Miocene of Egypt: Journal of Sedimentary Petrology, v. 58, p. 446-456.

Pope, M.C., and Grotzinger, J.P., 2003, Paleoproterozoic Stark Formation, Athapuscow Basin, Northwest Canada: Record of cratonic-scale salinity crisis: Journal of Sedimentary Research, v. 73, no. 2, p. 280-295.

Pope, M.C., Grotzinger, J.P., and Schreiber, B.C., 2000, Evaporitic subtidal stromatolites produced by *in situ* precitipation: textures, facies associations, and temporal significance: Journal of Sedimentary Research, v. 70, no. 5, p. 1139-1151.

Porter, S., and Knoll, A., 2000, Testate amoebae in the Neoproterozoic Era: evidence from vase-shaped microfossils in the Chuar Group, Grand Canyon: Paleobiology, v. 26, no. 3, p. 360–385.

Posamentier, H.W., and Allen, G.P., 1999, Siliciclastic sequence stratigraphy: concepts and applications: Society of Economic Paleontologists and Mineralogists, Concepts in Sedimentology and Paleontology Number 7, 210 p.

Pratt, B., 2010, Peritidal Carbonates, *in* James, N.P., and Dalrymple, R.W., editors, Facies Models 4: Geological Association of Canada GEOtext 6, p. 401-420.

Prave, A., 1999, Two diamictites, two cap carbonates, two $\delta^{13}C$ excursions, two rifts: The Neoproterozoic Kingston Peak Formation, Death Valley, California: Geology, v. 27, no. 4, p. 339–342.

Prave, A., Fallick, A., Thomas, C.W., and Graham, C.M., 2009, A composite C-isotope profile for the Neoproterozoic Dalradian Supergroup of Scotland and Ireland: Journal Of The Geological Society of London, v. 166, p. 129–135.

Prince, J.K.G., ms, 2014, Sequence stratigraphic, lithostratigraphic, and stable isotope analysis of the Minto Inlet Formation and Kilian Formation of the Shaler Supergroup, Northwest Territories: MSc Thesis, Carleton University, 139 p.

Prokoph, A., Shields, G.A., and Veizer, J., 2008, Compilation and time-series analysis of a marine carbonate $\delta^{18}0$, $\delta^{13}C$, $^{87}Sr/^{86}Sr$ and $\delta^{34}S$ database through Earth history: Earth-Science Reviews, v. 87, p. 113-133.

Purser, B.H., 1973, The Persian Gulf: Holocene Carbonate Sedimentation and Diagenesis in a Shallow Epicontinental Sea: Berlin, Springer-Verlag, 471 p.

Pyle, L.J., and Barnes, C.R., 2003, Lower Paleozoic stratigraphic and biostratigraphic correlations in the Canadian Cordillera: implications for the tectonic evolution of the Laurentian margin: Canadian Journal of Earth Sciences, v. 40, no. 12, p. 1739-1753.

Rainbird, R.H., ms, 1991, Stratigraphy, sedimentology, and tectonic setting of the upper Shaler Group, Victoria Island, Northwest Territories: Ph.D. thesis, University of Western Ontario, London, 257 p.

Rainbird, R.H., 1992, Anatomy of a large-scale braidplain quartz-arenite from the Neoproterozoic Shaler Group, Victoria Island, NWT, Canada: Canadian Journal of Earth Sciences, v. 29, p. 2537-2550.

Rainbird, R.H., 1993, The sedimentary record of mantle plume uplift preceding eruption of the Neoproterozoic Natkusiak flood basalt: The Journal of Geology, v. 101, no. 3, p. 305-318.

Rayner, N., and Rainbird, R.H., 2013, U-Pb geochronology of the Shaler Supergroup, Victoria Island, northwest Canada: 2009-2013: Geological Survey of Canada, Open File 7419, 62 p.

Rainbird, R., Jefferson, C., and Young, G., 1996, The early Neoproterozoic sedimentary succession B of northwestern Laurentia: Correlations and paleogeographic significance: Geological Society of America Bulletin, v. 108, no. 4, p. 454–470.

Rainbird, R., Jefferson, C.W., Halverson, G.P., and Thomson, D., 2014, Features of Rodinia break-up in the Minto Inlier with comparisions to the northern Cordillera: Geological Society of America Abstracts with Programs, v. 46, n. 6, p. 828.

Read, J.F., 1982, Carbonate platforms of passive (extensional) continental margins: Types, characteristics and evolution: Tectonophysics, v. 81, no. 3-4, p. 195–212.

Reading, H.G., 1980, Characteristics and recognition of strike-slip fault systems, *in* Balance, P.F., and Reading, H.G., editors, Sedimentation in Oblique-Slip Mobile Zones: International Association of Sedimentologists Special Publication No. 4, p. 7-26.

Reimers, C.E., Ruttenberg, K.C., Canfield, D.E., Christiansen, M.B., and Martin, J.B., 1996, Porewater pH and authigenic phases formed in the uppermost sediments of the Santa Barbara Basin: Geochimica et Cosmochimica Acta, v. 60, p. 4037-4057.

Riboulleau, A., Baudin, F., Deconinck, J.-F., Derenne, S., Largeau, C., and Tribovillard, N., 2003, Depositional conditions and organic matter preservation pathways in an epicontinental environment: the Upper Jurassic Kashpir Oil Shales (Volga Basin, Russia): Palaeogeography, Palaeoclimatology, and Palaeoecology, p. 1-27.

Richardson, M., and Arthur, M.A., 1988, The Gulf of Suez–northern Red Sea Neogene rift: a quantitative basin analysis: Marine and Petroleum Geology, v. 5, p. 247-270.

Rooney, A.D., Macdonald, F.A., Strauss, J.V., Dudás, F.O., Hallmann, C., and Selby, D., 2014, Re-Os geochronology and coupled Os-Sr isotope constraints on the Sturtian snowball: Proceedings of the National Academy of Sciences, v. 111, p. 51-56.

Rooney, A.D., Strauss, J.V., Brandon, A.D., and Macdonald, F.A., 2015, A Cryogenian chronology: Two long-lasting, synchronous Neoproterozoic glaciations: Geology, v. 43, n. 5, p. 459–462.

Roots, C.F., ms, 1987, Regional tectonic setting and evolution of the Late Proterozoic Mount Harper volcanic complex, Ogilvie Mountains, Yukon: Ph.D. thesis, Carleton University, Ottawa, 180 p.

Roots, C.F., and Thompson, R.I., 1992, Long-lived basement weak zones and their role in extensional magmatism in the Ogilvie Mountains, Yukon Territory, *in* Bartholomew, M.J., Hyndman, D.W., Mogk, D.W., and Mason, R., editors, Basement Tectonics and Characterization of Ancient and Mesozoic Continental Margins – Proceedings of the 8th International Conference in Basement Tectonics: Dordrecht, Kluwer Academic Publishers, p. 359-372.

Ross, G., 1991, Tectonic Setting of the Windermere Supergroup Revisited: Geology, v. 19, no. 11, p. 1125–1128.

Sandeman, H.A., Ootes, L., Cousens, B., and Kilian, T., 2014, Petrogenesis of Gunbarrel magmatic rocks: Homogeneous continental tholeiites associated with extension and rifting of Neoproterozoic Laurentia: Precambrian Research, v. 252, p. 166-179.

Saunders, A.D., Jones, S.M., Morgan, L.A., Pierce, K.L., Widdowson, M., and Xu, Y.G., 2007, Regional uplift associated with continental large igneous provinces: The roles of mantle plumes and the lithosphere: Chemical Geology, v. 241, p. 282-318.

Schrag, D.P., Berner, R.A., Hoffman, P.F., and Halverson, G.P., 2002, On the initiation of a snowball Earth: Geochemistry, Geophysics, Geosystems, v. 3, no. 6, p. 1-21.

Schrag, D.P., Higgins, J.A., Macdonald, F.A., and Johnston, D.T., 2013, Authigenic carbonate and the history of the global carbon cycle: Science, v. 339, no. 6119, p. 540–543, doi: 10.1126/science.1229578.

Schreiber, B.C., Tucker, M.E., and Till, R., 1986, Arid shorelines and evaporites, *in* Reading, H.G., editor, Sedimentary Environments and Facies: Oxford, Blackwell, p. 189–228.

Schreiber, B.C., and El Tabakh, M., 2000, Deposition and early alteration of evaporites: Sedimentology, v. 47, p. 215-238.

Schwab, D.L., Thorkelson, D.J., Mortensen, J.K., Creaser, R.A., and Abbott, J.G., 2004, The Bear River dykes (1265–1269 Ma): westward continuations of the Mackenzie dyke swarm into Yukon, Canada: Precambrian Research, v. 133, p. 175-186.

Selley, D., Broughton, D, Scott, R.J., Hizman, M., Bull, S.W., Large, R.R., McGoldrick, P.J., Croaker, M and Pollington, N., 2005, A new look at the geology of the Zambian Copperbelt: Society of Economic Geologists, v. 100, p. 965-1000

Sharp, I.R., Gawthorpe, R.L., Armstrong, B., and Underhill, J.R., 2000, Fault-propagation folding in extensional settings: Examples of structural style and syn-rift sedimentary response from the Suez Rift, Sinai, Egypt: Geologial Society of America Bulletin, v. 112, p. 1877-1899.

Shearman, D.J., 1978, Evaporites of coastal sabkhas, *in* Dean, W.E., and Schreiber, B.C., editors, Marine Evaporites: Society of Economic Paleontologists and Mineralogists (SEPM) Short Course 4, p. 6–42.

Slingerland, R., Kump, L.R., Arthur, M.A., Fawcett, P.J., Sageman, B.B., and Barron, E.J., 1996, Estuarine circulation in the Turonian Western Interior seaway of North America: Geological Society of America Bulletin, v. 108, p. 941-952.

Smith, E.F., Macdonald, F.A., Crowley, J.L., Hodgin, E.B., and Schrag, D.P., 2015, Tectono-stratigraphic evolution of the c. 780-730 Ma Beck Spring Dolomite: Basin formation in the core of Rodinia, *in* Li, Z.X., Evans, D.A.D., and Murphy, J.B., editors, Supercontinent Cycles Through Earth History: Geological Society of London, Special Publications, v. 424, p. xx.

Stewart, J.H., 1972, Initial deposits in the Cordilleran Geosyncline: Evidence of a late Precambrian (<850 m.y.) continental separation: Geological Society of America Bulletin, v. 83, no. 5, p. 1345-1360.

Stoessell, R.K., and Hay, R.L., 1978, The geochemical origin of sepiolite and kerolite at Amboseli, Kenya: Contributions to Mineralogy and Petrology, v. 65, no. 3, p. 255–267.

Strauss, J.V., Rooney, A.D., Macdonald, F.A., Brandon, A.D., and Knoll, A.H., 2014a, 740 Ma vase-shaped microfossils from Yukon, Canada: Implications for Neoproterozoic chronology and biostratigraphy: Geology, v. 42, no. 8, p. 659-662.

Strauss, J.V., Roots, C.F., Macdonald, F.A., Halverson, G.P., Eyster, A., and Colpron, M., 2014b, Geological map of the Coal Creek inlier, Ogilvie Mountains (NTS 116B/10-15 and 116C/9, 16): Yukon Geological Survey, Open File 2014-15, 1:100,000.

Sun, X., and Turchyn, A.V., 2014, Significant contribution of authigenic carbonate to marine carbon burial: Nature Geoscience, v. 7, p. 201-204.

Swart, P.K., and Kennedy, M.J., 2012, Does the global stratigraphic reproducibility of $\delta^{13}C$ in Neoproterozoic carbonates require a marine origin? A Pliocene-Pleistocene comparison: Geology, v. 40, no. 1, p. 87–90.

Swett, K., and Knoll, A.H., 1989, Marine pisolites from Upper Proterozoic carbonates of East Greenland and Spitsbergen: Sedimentology, v. 36, p. 75-93.

Thomas, W.A., 1990, Controls on the location of transverse zones in thrust belts: Eclogae Geologicae Helvetiae, v. 83, p. 727-744.

Thomson, D., Rainbird, R.H., and Dix, G., 2014, Architecture of a Neoproterozoic intracratonic carbonate ramp succession: Wynniatt Formation, Amundsen Basin, Arctic Canada: Sedimentary Geology, v. 299, p. 119-138.

Thomson, D., Rainbird, R.H., and Krapez, B., 2015a, Sequence and tectonostratigraphy of the Neoproterozoic (Tonian-Cryogenian) Amundsen Basin prior to supercontinent (Rodinia) break-up: Precambrian Research, v. 263, p. 246–259.

Thomson, D., Rainbird, R.H., Planavsky, N., Lyons, T.W., and Bekker, A., 2015b, Chemostratigraphy of the Shaler Supergroup, Victoria Island, NW Canada: A record of ocean composition prior to the Cryogenian glaciations: Precambrian Research, v. 263, p. 232–245.

Thompson, R.I., and Roots, C.F., 1992, Ogilvie Mountains project, Yukon: A new regional mapping program: Current Research, Part A, Geological Survey of Canada, Paper 82-1A, p. 403-411.

Thompson, R.I., Mercier, B., and Roots, C.F., 1987, Extension and its influence on Canadian Cordilleran passive-margin evolution, *in* Coward, M.P., Dewey, J.F., and Hancock, P.L., editors, Continental Extensional Tectonics: London, Geological Society Special Publication, v. 28, p. 409-417.

Thompson, R.I., Roots, C.F., and Mustard, P.S., 1994, Geology of Dawson map area (116B, C, northeast of Tintina Trench): Geological Survey of Canada, Open File 2849.

Thorkelson, D.J., 2000, Geology and mineral occurrences of the Slats Creek, Fairchild Lake, and “Dolores Creek” areas, Wernecke Mountains, Yukon Territory (106D/16, 106C/13, 106C/14): Exploration and Geological Services Division, Yukon Region, Indian and Northern Affairs Canada, Bulletin 10, 80 p.

Thorkelson, D., Abbott, J., Mortensen, J., Creaser, R., Villeneuve, M., McNicoll, V., and Layer, P., 2005, Early and Middle Proterozoic evolution of Yukon, Canada: Canadian Journal of Earth Sciences, v. 42, no. 6, p. 1045–1071, doi: 10.1139/E05-075.

Thorsteinsson, R., and Tozer, E.T., 1962, Banks, Victoria, and Sefansson Islands, Arctic Archipelago: Geological Survey of Canada, Memoir 330, 85 p.

Tosca, N.J., 2015, Geochemical pathways for Mg-silicate formation, *in* Pozo, M., ed., Magnesian Clays: Characterization, origins and applications: Association Internationale pour l’Etude des Argiles Special Publication, v. 2, 1-48.

Tosca, N.J. and Wright, V.P., 2015, Diagenetic pathways linked to labile Mg-clays in lacustrine carbonate reservoirs: A model for the origin of secondary porosity in the Cretaceous Pre-Salt Barra Velha Formation, offshore Brazil: Geological Society of London, Special Publication xxx, p. xxx.

Tosca, N.J., Macdonald, F.A., Strauss, J.V., Johnston, D.T., and Knoll, A.H., 2011, Sedimentary talc in Neoproterozoic carbonate successions: Earth And Planetary Science Letters, v. 306, no. 1-2, p. 11–22, doi: 10.1016/j.epsl.2011.03.041.

Tucker, M.E., 1982, Precambrian dolomites: petrographic and isotopic evidence that they differ from Phanerozoic dolomites: Geology, v. 10, p. 7–12.

Tucker, M.E., 1985, Shallow-marine carbonate facies and facies models, *in* Brenchley, P.J., and Williams, B.P.J., editors, Sedimentology: Recent Developments and Applied Aspects: Special Publications of the Geological Society of London, v. 18, p. 139–161.

Turner, E.C., 2011, Stratigraphy of the Mackenzie Mountains Supergroup in the Wernecke Mountains, Yukon, *in* MacFarlane, K.E., Weston, L.H., and Relf, C., editors, Yukon Exploration and Geology 2010: Yukon Geological Survey, p. 207-231.

Turner, E.C., Roots, C.F., MacNaughton, R.B., Long, D.G.F., Fischer, B.J., Gordey, S.P., Martel, E., and Pope, M.C., 2011, Chapter Three: Stratigraphy, *in* Martel, E., Turner, E.C., and Fischer, B.J., editors, Geology of the central Mackenzie Mountains of the northern Canadian

Cordillera, Sewki Mountain (105P), Mount Eduni (106A), and northwestern Wrigley Lake (95M) map-areas, Northwest Territories, NWT Special Volume 1, NWT Geoscience Office, p. 31-193.

Turner, E.C., and Long, D.G.F., 2008, Basin architecture and syndepositional fault activity during deposition of the Neoproterozoic Mackenzie Mountains supergroup, Northwest Territories, Canada: Canadian Journal of Earth Sciences, v. 45, p. 1159-1184.

Turner, E.C., and Long, D.G.F., 2012, Formal definition of the Neoproterozoic Mackenzie Mountains Supergroup (Northwest Territories), and formal stratigraphic nomenclature for its carbonate and evaporite formations: Geological Survey of Canada, Open File 7112, 57 p.

Tziperman, E., Halevy, I., Johnston, D.T., Knoll, A.H., and Schrag, D.P., 2011, Biologically induced initiation of Neoproterozoic snowball-Earth events: Proceedings of the National Academy of Sciences, v. 108, no. 37, p. 15091–15096.

Ulmer-Scholle, D.S., and Scholle, P.A., 1994, Replacement of evaporites within the Permian Park City Formation, Bighorn Basin, Wyoming, USA: Sedimentology, v. 41, p. 1203-1222.

Ulmer-Scholle, D.S., Scholle, P.A., and Brady, P.V., 1993, Silicification of evaporites in Permian (Guadalupian) back-reef carbonates of the Delaware Basin, West Texas and New Mexico: Journal of Sedimentary Research, v. 63, p. 955-965.

van Acken, D., Thomson, D., Rainbird, R.H., and Creaser, R.A., 2013, Constraining the depositional history of the Neoproterozoic Shaler Supergroup, Amundsen Basin, NW Canada: Rhenium-osmium dating of black shales from the Wynniatt and Boot Inlet formations: Precambrian Research, v. 236, p. 124–131.

van Straaten, L.M.J.U., 1954, Composition and structure of Recent marine sediments in the Netherlands: Leidsche Geologische Mededeelingen, v. 19, p. 1-110.

Villeneuve, M.E., Theriault, R.J., and Ross, G.M., 1991, U-Pb ages and Sm-Nd signature of two subsurface granites from the Fort Simpson magnetic high, northwest Canada: Canadian Journal of Earth Science, v. 28, p. 1003-1008.

Vogl, J.J., Min, K., Carmenate, A., Foster, D.A., and Marsellos, A., 2014, Miocene regional hotspot-related uplift, exhumation, and extension north of the Snake River Plain: Evidence from apatite (U-Th)/He thermochronology: Lithosphere, v. 6, no. 2, p. 108-123.

Walter, M.R., Veevers, J.J., Calver, C.R., and Grey, K., 1995, Neoproterozoic stratigraphy of the Centralian Superbasin, Australia: Precambrian Research, v. 73, p. 173–195.

Warren, J.K., 1989, Evaporite Sedimentology: Importance in Hydrocarbon Accumulation: Prentice Hall, Englewood Cliffs, N.J., 285 p.

Warren, J.K., 2006, Evaporites: Sediments, Resources, and Hydrocarbons: Berlin, Springer, 1035 p.

Weaver, C., and Beck, K., 1977, Miocene of the SE United States – A model for chemical sedimentation in a peri-marine environment: Sedimentary Geology, v. 17, p. 1-234.

Wheeler, J.P., 1954, A geological reconnaissance of the northern Selwyn Mountains region, Yukon and Northwest Territories: Geological Survey of Canada, Paper 53-7.

Wheeler, J.O., and McFeeley, P., 1991, Tectonic assemblage map of the Canadian Cordillera and adjacent parts of the United States of America: Geological Survey of Canada Map 1712A.

Wilson, J.P., Fischer, W.W., Johnston, D.J., Knoll, A.H., Grotzinger, J.P., Walter, M.R., McNaughton, N.J., Simon, M., Abelson, J., Schrag, D.P., Summons, R., Allwood, A., Andres, M., Gammon, C., Garvin, J., Rashby, S., Schweizer, M., and Watters, W.A., 2010, Geobiology of the late Paleoproterozoic Duck Creek Formation, Western Australia: Precambrian Research, v. 179, p. 135-149.

Wortmann, U.G., and Paytan, A., 2012, Rapid variability of seawater chemistry over the past 130 million years: Science, v. 337, p. 334-336.

Yan, J., Munnecke, A., Steuber, T., Carlson, E.H., and Xiao, Y., 2005, Marine sepiolite in Middle Permian carbonates of South China: Implications for secular variation of Phanerozoic seawater chemistry: Journal of Sedimentary Research, v. 75, no. 3, p. 328–338, doi: 10.2110/jsr.2005.026.

Yonkee, W.A., Dehler, C.D., Link, P.K., Balgord, E.A., Keeley, J.A., Hayes, D.S., Wells, M.L., Fanning, C.M., and Johnston, S.M., 2014, Tectono-stratigraphic framework of Neoproterozoic to Cambrian strata, west-central U.S.: Protracted rifting, glaciation, and evolution of the North American Cordilleran margin: Earth Science Reviews, v. 136, no. C, p. 59–95, doi: 10.1016/j.earscirev.2014.05.004.

Young, G.M. 1981, The Amundsen embayment, Northwest Territories: relevance to the upper Proterozoic evolution of North America, *in* Campbell, F.H.A., editor, Proterozoic basins of Canada: Geological Survey of Canada Paper 81-10, p. 203-211.

Young, G.M., Jefferson, C.W., Delaney, G.D., and Yeo, G.M., 1979. Middle and Upper Proterozoic evolution of the northern Canadian Cordillera and Shield; Geology, v. 7, p.125– 128.

## FIGURE CAPTIONS

Fig. 1. Simplified location maps of Proterozoic inliers in northwestern Canada adapted from Young and others (1979), Eisbacher (1981), Wheeler and McFeeley (1991), Rainbird and others (1996), and Abbott (1997). The blue boxes outline the location of detailed geological maps presented in figures 3 and 4. This map does not display Windermere Supergroup strata of the Hyland Group in the Selwyn Basin. NWT–Northwest Territories; YT–Yukon Territory; SG–Supergroup.

Fig. 2. Schematic lithostratigraphic correlation of Windermere Supergroup strata in northwestern Canada. The gray box outlines the proposed correlation of the Mount Harper Group with equivalent strata of the Windermere Supergroup throughout Yukon and Northwest Territories (NWT). Inset map depicts the rough location of each region and is adapted from Thomson and others (2014). All italicized names in the stratigraphic columns lack formalization. ORR–organic-rich-rock; Gp–Group; Fm–Formation; FMG–Fifteenmile Group; Chan.–Chandindu Formation; Ck.–Creek; Hem. Ck.–Hematite Creek Group; LD–Little Dal Group; Rav.–Ravensthroat formation; JB–June Beds; GT.–Gametrail Formation; Mt.–Mount; conglom.–conglomerate; Ft. Co.–Fort Collinson Formation; Pt.–Point; Hd.–Head.

Fig. 3. Geology of the Hart River Inlier, central Ogilvie Mountains, Yukon. Mapping based on previous work by Green (1972) and Abbott (1993; 1997) with updates from the authors over the summers of 2009–2012. Stratigraphic sections plotted on figure 7 and discussed in the text are depicted as red lines with accompanying section numbers.

Fig. 4. Geology of the Coal Creek Inlier, western Ogilvie Mountains, Yukon, after Strauss and others (2014b) and references therein. Stratigraphic sections discussed in the text and plotted on figure 6 are depicted as red lines with accompanying section numbers.

Fig. 5. Photographs of key selected localities from the Coal Creek and Hart River inliers with solid red lines outlining the trace of measured stratigraphic sections shown in figures

6 and 7. A) Image looking west at the prominent angular unconformity beneath the Callison Lake Formation in the headwaters of Mark Creek, Hart River inlier (fig. 3). The distinct erosional unconformity of Rapitan Group strata over the Callison Lake Formation is also evident. B) Looking west in the NW portion of the Coal Creek inlier at the profound angular unconformity between the Craggy dolostone (Fifteenmile Group) and Callison Lake Formation. One can also see the erosional unconformity with the Eagle Creek Formation (Rapitan Group) cutting down into the Ramp member. C) Impressive m-scale relief (solid white line) associated with a paleokarst unconformity at the base of the Callison Lake Formation in the eastern Hart River inlier (section J1223, figs. 3, 7). Geologist for scale. D) Typical outcrop style of the Callison Lake Formation in the Coal Creek inlier. Note the discontinuous yellow-orange stromatolitic bioherms in the Heterolithic member and the prominent black, talc-rich shale interbedded with light gray dolostone of the Talc member. Tent circled for scale. E) The Harper Fault in the Coal Creek inlier (fig. 4) as depicted in Mustard and Roots (1997). Largest outlined clast is on the order of ~50 m tall. F) Looking west in the Coal Creek inlier at the type section of the Callison Lake Formation (Mount Harper East, J1301) with Mount Harper in the background. G) Typical outcrop pattern of the Heterolithic member with lenticular bodies of amalgamated sandstone outlined by dashed white lines. H) Base of the Callison Lake Fm type section with a decameter-thick stromatolitic “reef” shown above the circled geologist. The 752.7 ± 5.5 Ma Re-Os age of Rooney and others (2015) is from just above this stromatolitic unit.

Fig. 6. Detailed measured sections and carbon isotope stratigraphy of the Callison Lake Formation in the Coal Creek inlier. The inset map in the upper left depicts the location of each measured section (GPS coordinates provided in AJS online supplementary data file[1] table DR1). Note the reproducible Islay carbon isotope excursion (ICIE) in the upper Transitional member. The thinning of strata to the NW is a function of the primary accommodation space and secondary erosional truncation during basin-scale uplift in Transitional member and Seela Pass time (see text for an explanation). Strom.–stromatolite; sh/slt–shale/siltstone; sst–sandstone; cglm–conglomerate; dlmud–dolomudstone; dlgrnstn–dolograinstone; dlbdstn–doloboundstone; rxtal–recrystallized.

Fig. 7. Detailed measured sections and carbon isotope stratigraphy of the Callison Lake Formation in the Hart River inlier. The inset map in the upper right depicts the location of each measured section (GPS coordinates in AJS online supplementary data file[1] table DR1). Note the lack of Transitional member strata due to post-Callison Lake erosional truncation beneath the Rapitan Group.

Fig. 8. Selected photographs from Heterolithic member strata in the Hart River and Coal Creek inliers (facies descriptions in table 3). A) Thick-bedded quartz- and chert-pebble conglomerate (Facies, F1) from a basal transgressive lag in the Hart River inlier. Note the abundant jaspillitic chert clasts and yellow-brown oxidized hematitic halos after pyrite. B) Interbedded fine- to medium-grained quartz and chert arenite and gray-green shale and siltstone (F2 and F3). Hammer circled for scale is 27.94 cm tall. C) Mudcracks in green siltstone filled by maroon sandstone (top to left) in the *variegated shale and siltstone*

facies (F3). Canadian coin is 2.39 cm in diameter. D) Dashed white line outlines an ornately branching stromatolite in the *stromatolitic bioherm and biostrome* facies (F7). Canadian coin is 2.65 cm in diameter. E) Distinct yellow-orange stromatolitic bioherms (top outlined with dashed white line) interbedded with gray-green silicified and slightly cleaved shale and siltstone (F3, 7). Meter stick for scale. F) Domal stromatolites in the *stromatolitic bioherm and biostrome* facies (F7). Canadian coin is 2.65 cm in diameter. G) Photomicrograph of disseminated organic matter and dolomite-replaced microbial sheaths from stromatolitic laminae at Mount Gibben East (section J1019, fig. 6). Scale bar is 200 μm. H) Dolomite-replaced vase-shaped microfossils (VSMs) in the same photomicrograph of (G). Scale bar is 150 μm.

Fig. 9. Detailed stratigraphic section of the Talc member, Callison Lake Formation, Coal Creek inlier (Mine Camp, section J1302). Letters next to the stratigraphic column relate to the location of accompanying photographs. A) Distinct black, vitreous luster of talc-rich black shale (Facies, F5; table 1). Canadian coin is 2.65 cm in diameter. B) Subrounded to rounded talc-rich shale-chip clasts floating in a dolomudstone matrix (F10). Canadian coin is 2.39 cm in diameter. C) Plan view of large domal stromatolite (F8) with black, talc-rich shale drapes in individual laminae. Hammer is 27.94 cm tall. D) Chaotic stromatolitic rudstone with clasts floating in a talc-rich shale matrix. Canadian coin is 2.39 cm in diameter. E) Ptygmatically-folded microbialite and isopachus laminite. Hammer is 27.94 cm tall. F) Nodular dolomite-replacement fabric after chickenwire anhydrite. Canadian coin is 2.65 cm in diameter. G) Microbial dolostone (microbialite)

interbedded with black, talc-rich shale. Canadian coin is 2.39 cm in diameter. Deform.–deformation; strom.–stromatolite.

Fig. 10. Selected photographs from Ramp member strata in the Hart River and Coal Creek inliers. A) Trough cross-bedded oolitic dolograinstone (Facies, F11; table 1). Canadian coin is 2.65 cm in diameter. B) Planar-laminated dolomudstone and dolosiltite with ferruginous clay partings and abundant black chert nodules (F12) marking a prominent flooding surface at the base of the Ramp member. Hammer is 31.75 cm tall. C) Massive and clotty fabric that is reminiscent of microbial fabrics described in Harwood and Sumner (2011; 2012) from the Beck Spring Dolomite. Canadian coin is 2.65 cm in diameter. D) Cm-scale oncolites with distinct pendant cements (black arrows with geopetal features indicating top to the left) floating in a dolosiltite matrix. Canadian coin is 2.65 cm in diameter. E) High-inheritance domal stromatolites truncated by a distinct erosional surface (white dashed line) and capped by dolowackestone with abundant stromatolite clasts (F10). Lens cap is 5.2 cm in diameter. F) Large, m-scale domal stromatolite buildups (F8). Geologist for scale is 1.75 m tall. G) Partially-silicified microbialite (F9) characterized by synsedimentary deformation and ptygmatic folding. Canadian coin is 2.65 cm in diameter. H) Massive silicified dolostone breccia (F14) characteristic of many paleokarst horizons in the Ramp member. Hammer is 31.75 cm tall.

Fig. 11. Field photographs of Transitional member strata in the Coal Creek inlier. A) Digitate stromatolites in the basal transitional member doloboundstone. Canadian coin is

2.65 cm in diameter. B) Irregular, low-inheritance stromatolites with a distinct, healed synsedimentary normal fault (shown with white dashed line and arrow depicting hangingwall). Canadian coin is 2.65 cm in diameter. C) Photomicrograph of abundant vase-shaped microfossils in silicified black shale from Gibben East (section J1204, Strauss and others, 2014a). Scale bar is 100 μm. D) Partially silicified massive dolostone breccia with distinct microbialite clasts from the upper Ramp member. Canadian coin is 2.65 cm in diameter.

Fig. 12. Callison Lake Formation sequence stratigraphic interpretation based on a reference section from the Coal Creek inlier (Gibben East, composite sections J1018-J1019; fig. 6). Transgressive-Regressive (T-R) cycles are built upon the sequence stratigraphic architecture developed by Thomson and others (2015a) in the upper Shaler Supergroup of Victoria Island and conform to the priciples and terminology outlined in Johnson and Murphy (1984), Johnson and others (1985), Embry and Johannesson (1992), Embry (2009), and Catuneanu and others (2009; 2011). Lithofacies symbols are the same as depicted in legends from figures 6 and 7. Ages are from Re-Os geochronology published in Strauss and others (2014a) and Rooney and others (2015). SU–subaerial unconformity; MRS–maximum regressive surface; MFS–maximum flooding surface; Trans.–transgression; Regr.–regression; Fm.–Formation; dolomudstn–dolomudstone; dologrnstn–dolograinstone; dolobdstn–doloboundstone; rxtal.–recrystallized.

Fig. 13. $\delta^{13}C_{carb}$–$\delta^{18}O_{carb}$ cross-plots for individual members of the Callison Lake Formation.

Fig. 14. Cartoon depositional reconstruction and schematic tectono-stratigraphic evolutionary model for the Callison Lake Formation. Note that only a small portion of these hypothetical basins are exposed in the Coal Creek and Hart River inliers. A) Initiation of Callison Lake sedimentation is recorded in syn-rift mixed siliciclastic, evaporite, and carbonate deposits of the Heterolithic and Talc members, which were deposited in marginal marine embayments associated with an ancestral basin-bounding extensional fault system. B) Ramp member deposition records a shift to pure carbonate sedimentation and the development of a hangingwall dip-slope ramp. Detailed inset depicts a hypothetical reconstruction of the inner ramp setting with characteristic depositional environments for specific Ramp member facies (table 3). Modified from Harwood and Sumner (2011). C) Transitional member sedimentation records a change in Mount Harper Group basin dynamics and the onset of renewed extensional tectonism. This is evidenced by coeval subaerial exposure and marine sedimentation associated with rotation of the Callison Lake hangingwall depocenter, the northward propogation of basin-bounding structures accompanied by segmentation of the original Callison Lake basin, and the eventual progradation of fault-related siliciclastic deposits of the Seela Pass Formation. This event may also record the onset of strike-slip tectonism throughout the Ogilvie and Mackenzie Mountains as depicted by the activation of the Dawson Fault.

Fig. 15. Preliminary lithostratigraphic, chemostratigraphic, and sequence stratigraphic correlations among basal Windermere Supergroup strata in northwestern Canada adapted from Strauss and others (2014a). Note that the Islay carbon isotope excursion (ICIE) is

consistently present in the third Transgressive-Regressive (T-R) cycle (T-R8). Schematic stratigraphy, chemostratigraphy, and geochronology of each column are from the following sources: Ogilvie Mountains (Macdonald and others, 2010; Strauss and others, 2014a; Rooney and others, 2015); Mackenzie Mountains (Jefferson, ms, 1983; Jefferson and Parrish, 1989; Rooney and others, 2014; Milton and others, 2015); Victoria Island (Rainbird, 1993; Long and others, 2008; Jones and others, 2010; Macdonald and others, 2010; van Acken and others, 2013; Prince, ms, 2014; Thomson and others, 2015b). RAP.–Rapitan Group; Mtns–Mountains; MHV–Mount Harper Volcanics; 15 Mi.–Fifteenmile Group; NWT–Northwest Territories; Fm.–Formation; LDB–Little Dal basalt; Natkus.–Natkusiak Formation; W–Wynniatt Formation.

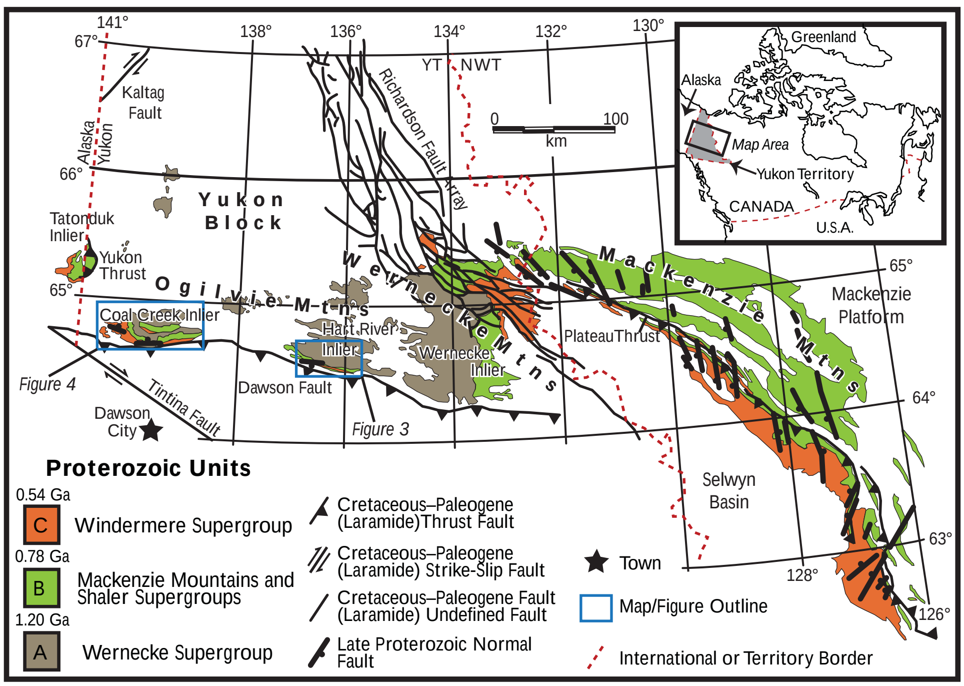

141°
67°
138°
136°
134°
132°
130°
YT
NWT
Kaltag Fault
Richardson Fault Array
0
100
km
Alaska
Yukon
66°
Yukon Block
Tatonduk Inlier
Yukon Thrust
65°
Ogilvie Mtns
Wernecke Mtns
Mackenzie Mtns
Mackenzie Platform
Coal Creek Inlier
Hart River Inlier
Wernecke Inlier
Plateau Thrust
Figure 4
Dawson Fault
Tintina Fault
Dawson City
Figure 3
64°
Selwyn Basin
63°
128°
126°
Greenland
Alaska
Map Area
Yukon Territory
CANADA
U.S.A.
Proterozoic Units
0.54 Ga
C
Windermere Supergroup
0.78 Ga
B
Mackenzie Mountains and Shaler Supergroups
1.20 Ga
A
Wernecke Supergroup
Cretaceous–Paleogene (Laramide) Thrust Fault
Cretaceous–Paleogene (Laramide) Strike-Slip Fault
Cretaceous–Paleogene Fault (Laramide) Undefined Fault
Late Proterozoic Normal Fault
Town
Map/Figure Outline
International or Territory Border

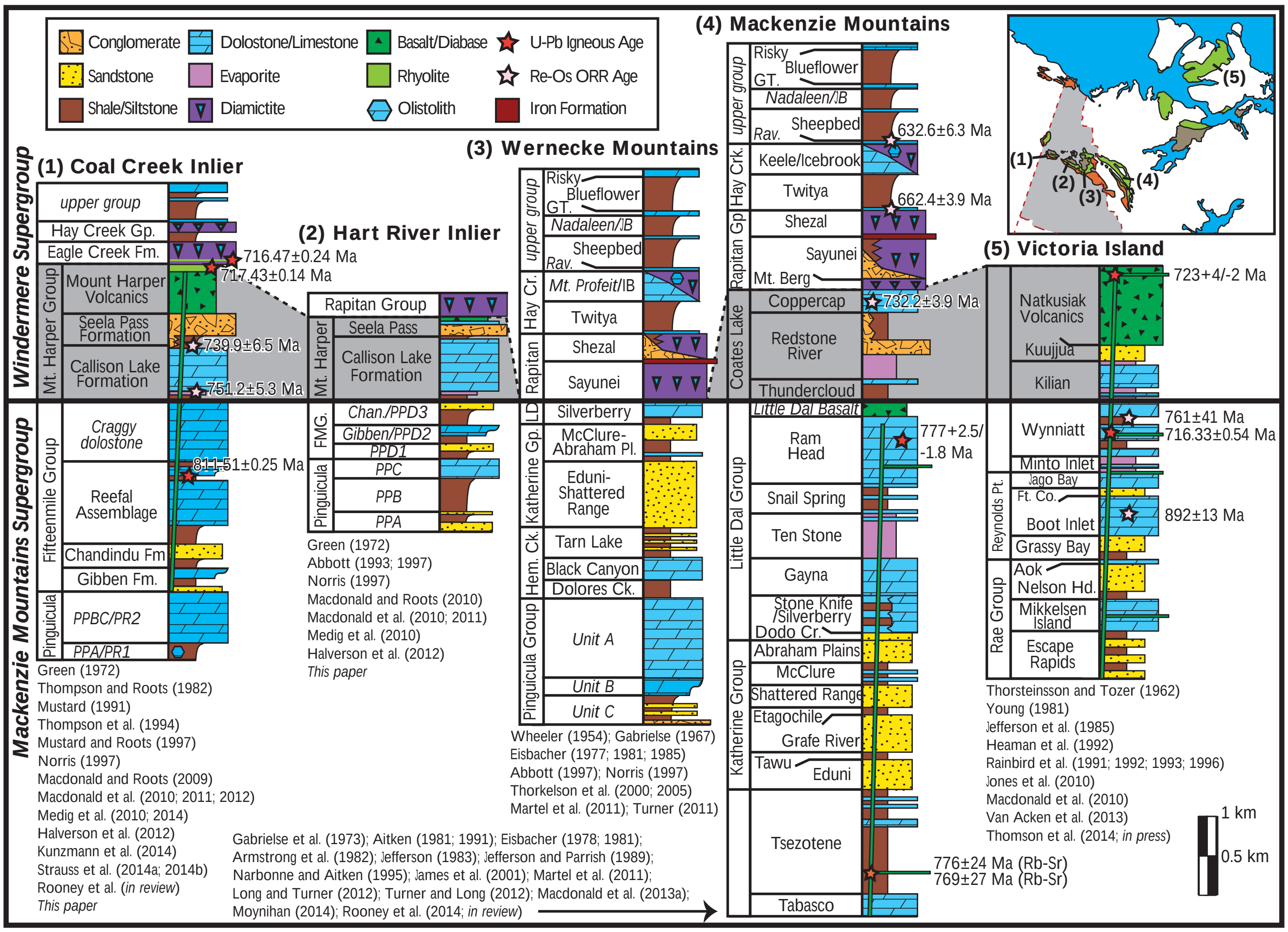

Conglomerate
Sandstone
Shale/Siltstone
Dolostone/Limestone
Evaporite
Diamictite
Basalt/Diabase
Rhyolite
Olistolith
U-Pb Igneous Age
Re-Os ORR Age
Iron Formation
Windermere Supergroup
Mackenzie Mountains Supergroup
(1) Coal Creek Inlier
upper group
Hay Creek Gp.
Eagle Creek Fm.
Mt. Harper Group
Mount Harper Volcanics
Seela Pass Formation
Callison Lake Formation
716.47±0.24 Ma
717.43±0.14 Ma
739.9±6.5 Ma
751.2±5.3 Ma
Fifteenmile Group
Craggy dolostone
Reefal Assemblage
811.51±0.25 Ma
Chandindu Fm
Gibben Fm.
Pinguicula
PPBC/PR2
PPA/PR1
Green (1972)
Thompson and Roots (1982)
Mustard (1991)
Thompson et al. (1994)
Mustard and Roots (1997)
Norris (1997)
Macdonald and Roots (2009)
Macdonald et al. (2010; 2011; 2012)
Medig et al. (2010; 2014)
Halverson et al. (2012)
Kunzmann et al. (2014)
Strauss et al. (2014a; 2014b)
Rooney et al. (in review)
This paper
(2) Hart River Inlier
Rapitan Group
Mt. Harper
Seela Pass
Callison Lake Formation
FMG.
Chan./PPD3
Gibben/PPD2
PPD1
Pinguicula
PPC
PPB
PPA
Green (1972)
Abbott (1993; 1997)
Norris (1997)
Macdonald and Roots (2010)
Macdonald et al. (2010; 2011)
Medig et al. (2010)
Halverson et al. (2012)
This paper
(3) Wernecke Mountains
upper group
Risky
Blueflower
GT.
Nadaleen/IB
Sheepbed
Rav.
Hay Cr.
Mt. Profeit/IB
Twitya
Rapitan
Shezal
Sayunei
LD
Silverberry
Katherine Gp.
McClure-Abraham Pl.
Eduni-Shattered Range
Hem. Ck
Tarn Lake
Black Canyon
Dolores Ck.
Pinguicula Group
Unit A
Unit B
Unit C
Wheeler (1954); Gabrielse (1967)
Eisbacher (1977; 1981; 1985)
Abbott (1997); Norris (1997)
Thorkelson et al. (2000; 2005)
Martel et al. (2011); Turner (2011)
Gabrielse et al. (1973); Aitken (1981; 1991); Eisbacher (1978; 1981);
Armstrong et al. (1982); Jefferson (1983); Jefferson and Parrish (1989);
Narbonne and Aitken (1995); James et al. (2001); Martel et al. (2011);
Long and Turner (2012); Turner and Long (2012); Macdonald et al. (2013a);
Moynihan (2014); Rooney et al. (2014; in review)
(4) Mackenzie Mountains
upper group
Risky
Blueflower
GT.
Nadaleen/IB
Sheepbed
Rav.
Hay Crk.
Keele/Icebrook
632.6±6.3 Ma
Twitya
662.4±3.9 Ma
Rapitan Gp
Shezal
Sayunei
Mt. Berg
Coates Lake
Coppercap
732.2±3.9 Ma
Redstone River
Thundercloud
Little Dal Basalt
Little Dal Group
Ram Head
777+2.5/-1.8 Ma
Snail Spring
Ten Stone
Gayna
Stone Knife /Silverberry
Dodo Cr.
Katherine Group
Abraham Plains
McClure
Shattered Range
Etagochile
Grafe River
Tawu
Eduni
Tsezotene
776±24 Ma (Rb-Sr)
769±27 Ma (Rb-Sr)
Tabasco
(1)
(2)
(3)
(4)
(5)
(5) Victoria Island
Natkusiak Volcanics
723+4/-2 Ma
Kuujjua
Kilian
Wynniatt
761±41 Ma
716.33±0.54 Ma
Minto Inlet
Jago Bay
Reynolds Pt.
Ft. Co.
Boot Inlet
892±13 Ma
Grassy Bay
Rae Group
Aok
Nelson Hd.
Mikkelsen Island
Escape Rapids
Thorsteinsson and Tozer (1962)
Young (1981)
Jefferson et al. (1985)
Heaman et al. (1992)
Rainbird et al. (1991; 1992; 1993; 1996)
Jones et al. (2010)
Macdonald et al. (2010)
Van Acken et al. (2013)
Thomson et al. (2014; in press)
1 km
0.5 km

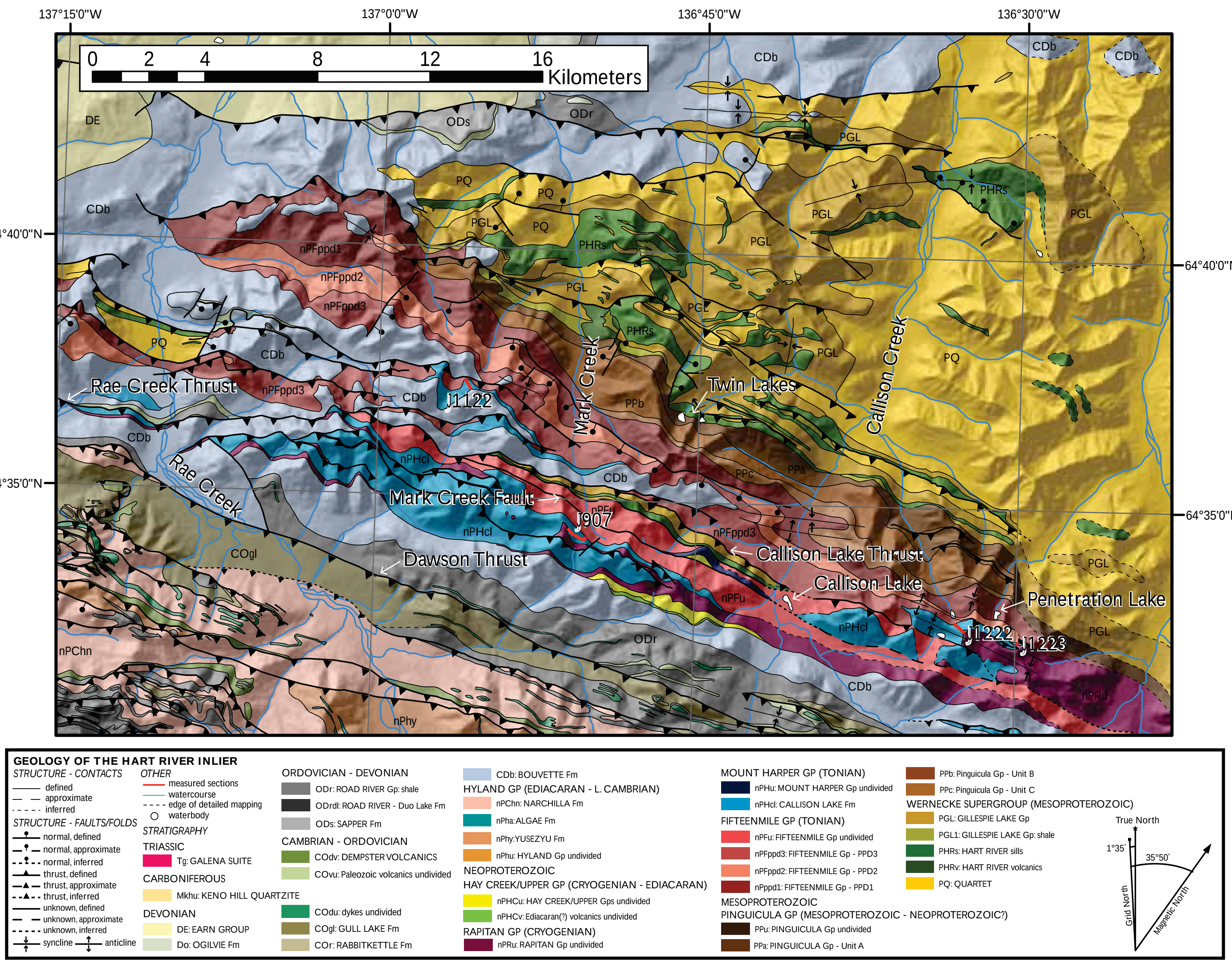

137°15'0"W
137°0'0"W
136°45'0"W
136°30'0"W
64°40'0"N
64°35'0"N
0 2 4 8 12 16 Kilometers
Rae Creek Thrust
Rae Creek
Mark Creek
Mark Creek Fault
Dawson Thrust
Twin Lakes
Callison Creek
Callison Lake Thrust
Callison Lake
Penetration Lake
J1122
J907
J1222
J1223
DE
CDb
ODs
ODr
PQ
PGL
PHRs
nPFppd1
nPFppd2
nPFppd3
nPHcl
nPFu
PPb
PPc
PPa
COgl
nPChn
nPhy
nPRu
GEOLOGY OF THE HART RIVER INLIER
STRUCTURE - CONTACTS
defined
approximate
inferred
STRUCTURE - FAULTS/FOLDS
normal, defined
normal, approximate
normal, inferred
thrust, defined
thrust, approximate
thrust, inferred
unknown, defined
unknown, approximate
unknown, inferred
syncline
anticline
OTHER
measured sections
watercourse
edge of detailed mapping
waterbody
STRATIGRAPHY
TRIASSIC
Tg: GALENA SUITE
CARBONIFEROUS
Mkhu: KENO HILL QUARTZITE
DEVONIAN
DE: EARN GROUP
Do: OGILVIE Fm
ORDOVICIAN - DEVONIAN
ODr: ROAD RIVER Gp: shale
ODrdl: ROAD RIVER - Duo Lake Fm
ODs: SAPPER Fm
CAMBRIAN - ORDOVICIAN
COdv: DEMPSTER VOLCANICS
COvu: Paleozoic volcanics undivided
COdu: dykes undivided
COgl: GULL LAKE Fm
COr: RABBITKETTLE Fm
CDb: BOUVETTE Fm
HYLAND GP (EDIACARAN - L. CAMBRIAN)
nPChn: NARCHILLA Fm
nPha: ALGAE Fm
nPhy: YUSEZYU Fm
nPhu: HYLAND Gp undivided
NEOPROTEROZOIC
HAY CREEK/UPPER GP (CRYOGENIAN - EDIACARAN)
nPHCu: HAY CREEK/UPPER Gps undivided
nPHCv: Ediacaran(?) volcanics undivided
RAPITAN GP (CRYOGENIAN)
nPRu: RAPITAN Gp undivided
MOUNT HARPER GP (TONIAN)
nPHu: MOUNT HARPER Gp undivided
nPHcl: CALLISON LAKE Fm
FIFTEENMILE GP (TONIAN)
nPFu: FIFTEENMILE Gp undivided
nPFppd3: FIFTEENMILE Gp - PPD3
nPFppd2: FIFTEENMILE Gp - PPD2
nPppd1: FIFTEENMILE Gp - PPD1
MESOPROTEROZOIC
PINGUICULA GP (MESOPROTEROZOIC - NEOPROTEROZOIC?)
PPu: PINGUICULA Gp undivided
PPa: PINGUICULA Gp - Unit A
PPb: Pinguicula Gp - Unit B
PPc: Pinguicula Gp - Unit C
WERNECKE SUPERGROUP (MESOPROTEROZOIC)
PGL: GILLESPIE LAKE Gp
PGL1: GILLESPIE LAKE Gp: shale
PHRs: HART RIVER sills
PHRv: HART RIVER volcanics
PQ: QUARTET
True North
Grid North
Magnetic North
1°35'
35°50'

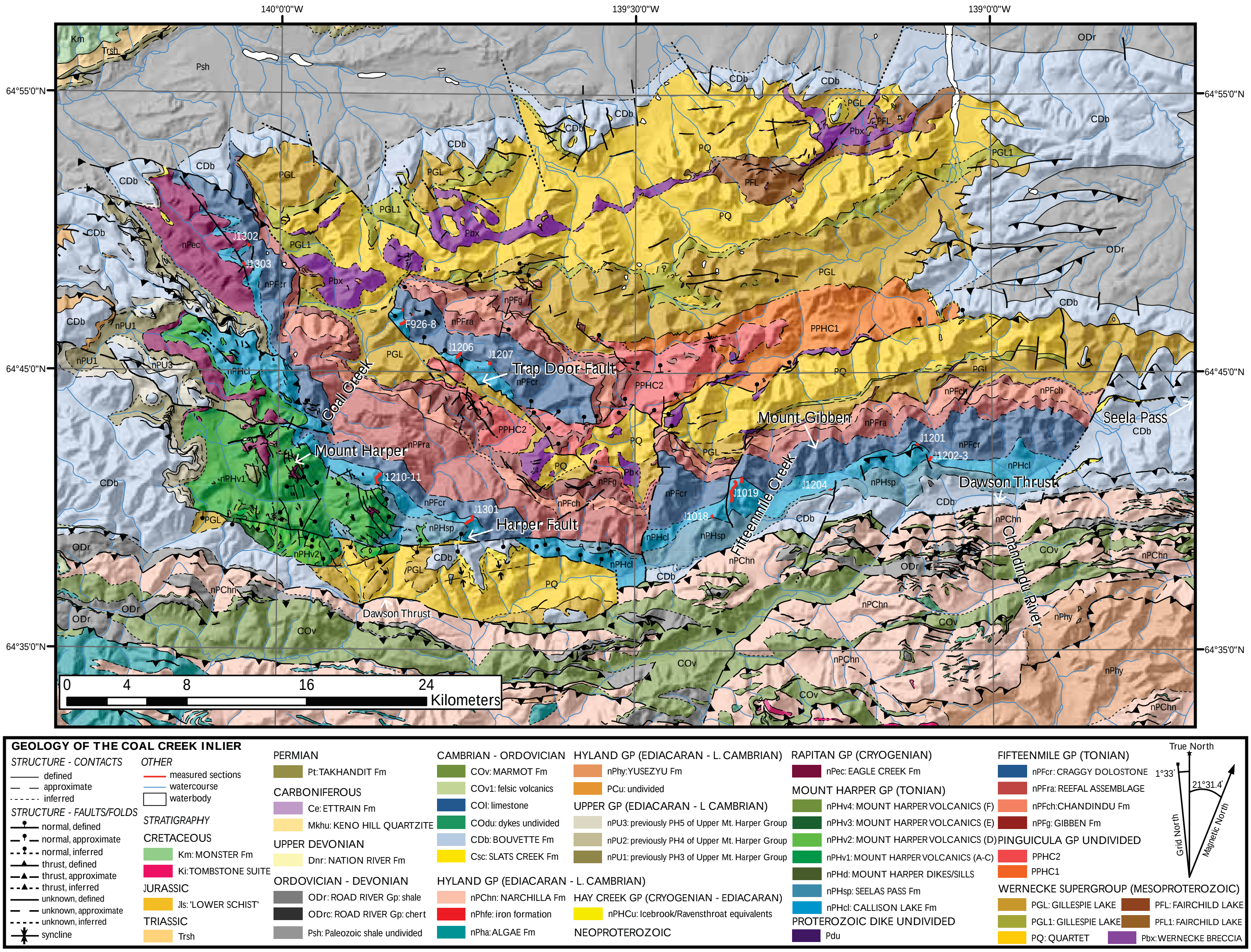
140°0'0"W
139°30'0"W
139°0'0"W
64°55'0"N
64°45'0"N
64°35'0"N
Coal Creek
Trap Door Fault
Mount Harper
Harper Fault
Mount Gibben
Fifteenmile Creek
Seela Pass
Dawson Thrust
Chandindu River
J1302
J1303
F926-8
J1206
J1207
J1210-11
J1301
J1019
J1018
J1204
J1201
J1202-3
0 4 8 16 24
Kilometers
GEOLOGY OF THE COAL CREEK INLIER
STRUCTURE - CONTACTS
defined
approximate
inferred
STRUCTURE - FAULTS/FOLDS
normal, defined
normal, approximate
normal, inferred
thrust, defined
thrust, approximate
thrust, inferred
unknown, defined
unknown, approximate
unknown, inferred
syncline
OTHER
measured sections
watercourse
waterbody
STRATIGRAPHY
CRETACEOUS
Km: MONSTER Fm
Ki:TOMBSTONE SUITE
JURASSIC
Jls: 'LOWER SCHIST'
TRIASSIC
Trsh
PERMIAN
Pt: TAKHANDIT Fm
CARBONIFEROUS
Ce: ETTRAIN Fm
Mkhu: KENO HILL QUARTZITE
UPPER DEVONIAN
Dnr: NATION RIVER Fm
ORDOVICIAN - DEVONIAN
ODr: ROAD RIVER Gp: shale
ODrc: ROAD RIVER Gp: chert
Psh: Paleozoic shale undivided
CAMBRIAN - ORDOVICIAN
COv: MARMOT Fm
COv1: felsic volcanics
COl: limestone
COdu: dykes undivided
CDb: BOUVETTE Fm
Csc: SLATS CREEK Fm
HYLAND GP (EDIACARAN - L. CAMBRIAN)
nPChn: NARCHILLA Fm
nPhfe: iron formation
nPha: ALGAE Fm
HYLAND GP (EDIACARAN - L. CAMBRIAN)
nPhy: YUSEZYU Fm
PCu: undivided
UPPER GP (EDIACARAN - L CAMBRIAN)
nPU3: previously PH5 of Upper Mt. Harper Group
nPU2: previously PH4 of Upper Mt. Harper Group
nPU1: previously PH3 of Upper Mt. Harper Group
HAY CREEK GP (CRYOGENIAN - EDIACARAN)
nPHCu: Icebrook/Ravensthroat equivalents
NEOPROTEROZOIC
RAPITAN GP (CRYOGENIAN)
nPec: EAGLE CREEK Fm
MOUNT HARPER GP (TONIAN)
nPHv4: MOUNT HARPER VOLCANICS (F)
nPHv3: MOUNT HARPER VOLCANICS (E)
nPHv2: MOUNT HARPER VOLCANICS (D)
nPHv1: MOUNT HARPER VOLCANICS (A-C)
nPHd: MOUNT HARPER DIKES/SILLS
nPHsp: SEELAS PASS Fm
nPHcl: CALLISON LAKE Fm
PROTEROZOIC DIKE UNDIVIDED
Pdu
FIFTEENMILE GP (TONIAN)
nPFcr: CRAGGY DOLOSTONE
nPFra: REEFAL ASSEMBLAGE
nPFch: CHANDINDU Fm
nPFg: GIBBEN Fm
PINGUICULA GP UNDIVIDED
PPHC2
PPHC1
WERNECKE SUPERGROUP (MESOPROTEROZOIC)
PGL: GILLESPIE LAKE
PGL1: GILLESPIE LAKE
PQ: QUARTET
PFL: FAIRCHILD LAKE
PFL1: FAIRCHILD LAKE
Pbx: WERNECKE BRECCIA
True North
Grid North
Magnetic North
1°33'
21°31.4'

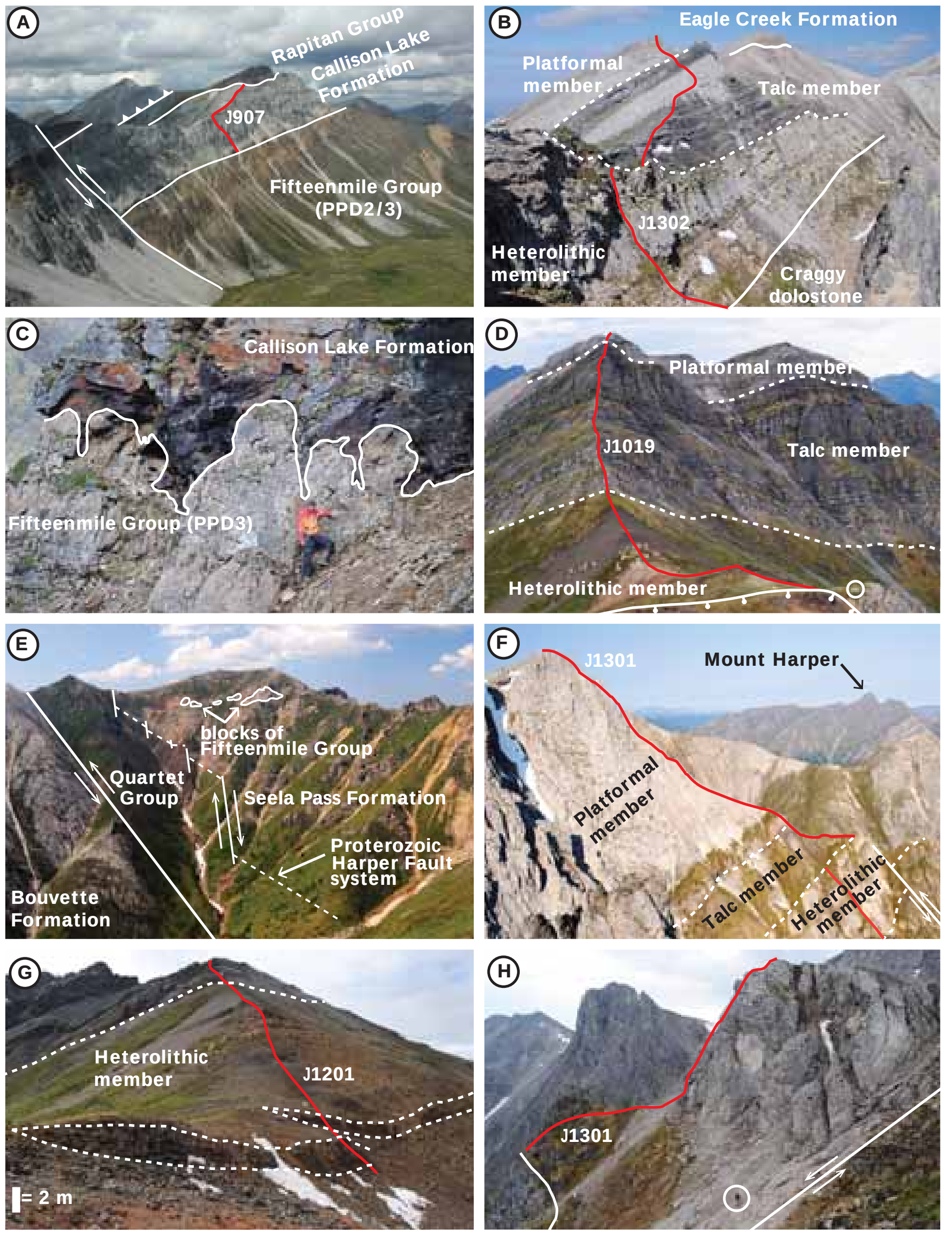
A
Rapitan Group
Callison Lake Formation
J907
Fifteenmile Group (PPD2/3)
B
Eagle Creek Formation
Platformal member
Talc member
J1302
Heterolithic member
Craggy dolostone
C
Callison Lake Formation
Fifteenmile Group (PPD3)
D
Platformal member
J1019
Talc member
Heterolithic member
E
blocks of Fifteenmile Group
Quartet Group
Seela Pass Formation
Proterozoic Harper Fault system
Bouvette Formation
F
J1301
Mount Harper
Platformal member
Talc member
Heterolithic member
G
Heterolithic member
J1201
= 2 m
H
J1301

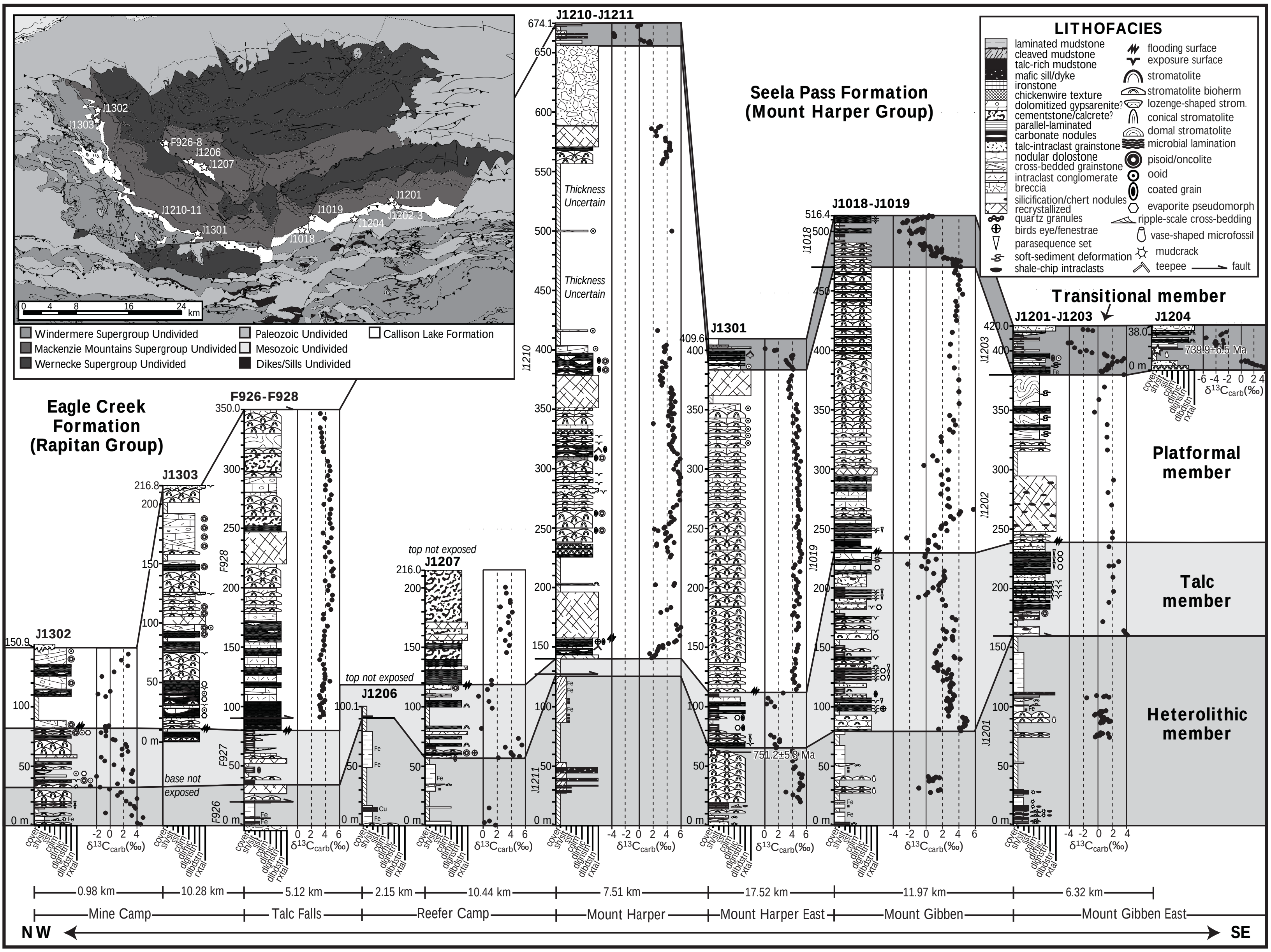

Seela Pass Formation (Mount Harper Group)
Eagle Creek Formation (Rapitan Group)
LITHOFACIES
laminated mudstone
cleaved mudstone
talc-rich mudstone
mafic sill/dyke
ironstone
chickenwire texture
dolomitized gypsarenite?
cementstone/calcrete?
parallel-laminated
carbonate nodules
talc-intraclast grainstone
nodular dolostone
cross-bedded grainstone
intraclast conglomerate
breccia
silicification/chert nodules
recrystallized
quartz granules
birds eye/fenestrae
parasequence set
soft-sediment deformation
shale-chip intraclasts
flooding surface
exposure surface
stromatolite
stromatolite bioherm
lozenge-shaped strom.
conical stromatolite
domal stromatolite
microbial lamination
pisoid/oncolite
ooid
coated grain
evaporite pseudomorph
ripple-scale cross-bedding
vase-shaped microfossil
mudcrack
teepee
fault
Windermere Supergroup Undivided
Mackenzie Mountains Supergroup Undivided
Wernecke Supergroup Undivided
Paleozoic Undivided
Mesozoic Undivided
Dikes/Sills Undivided
Callison Lake Formation
J1302
J1303
F926-F928
J1206
J1207
J1210-J1211
J1301
J1018-J1019
J1201-J1203
J1204
Transitional member
Platformal member
Talc member
Heterolithic member
Thickness Uncertain
top not exposed
base not exposed
751.2±5.3 Ma
739.9±6.5 Ma
$\delta^{13}C_{carb}$(‰)
0.98 km
10.28 km
5.12 km
2.15 km
10.44 km
7.51 km
17.52 km
11.97 km
6.32 km
Mine Camp
Talc Falls
Reefer Camp
Mount Harper
Mount Harper East
Mount Gibben
Mount Gibben East
NW
SE

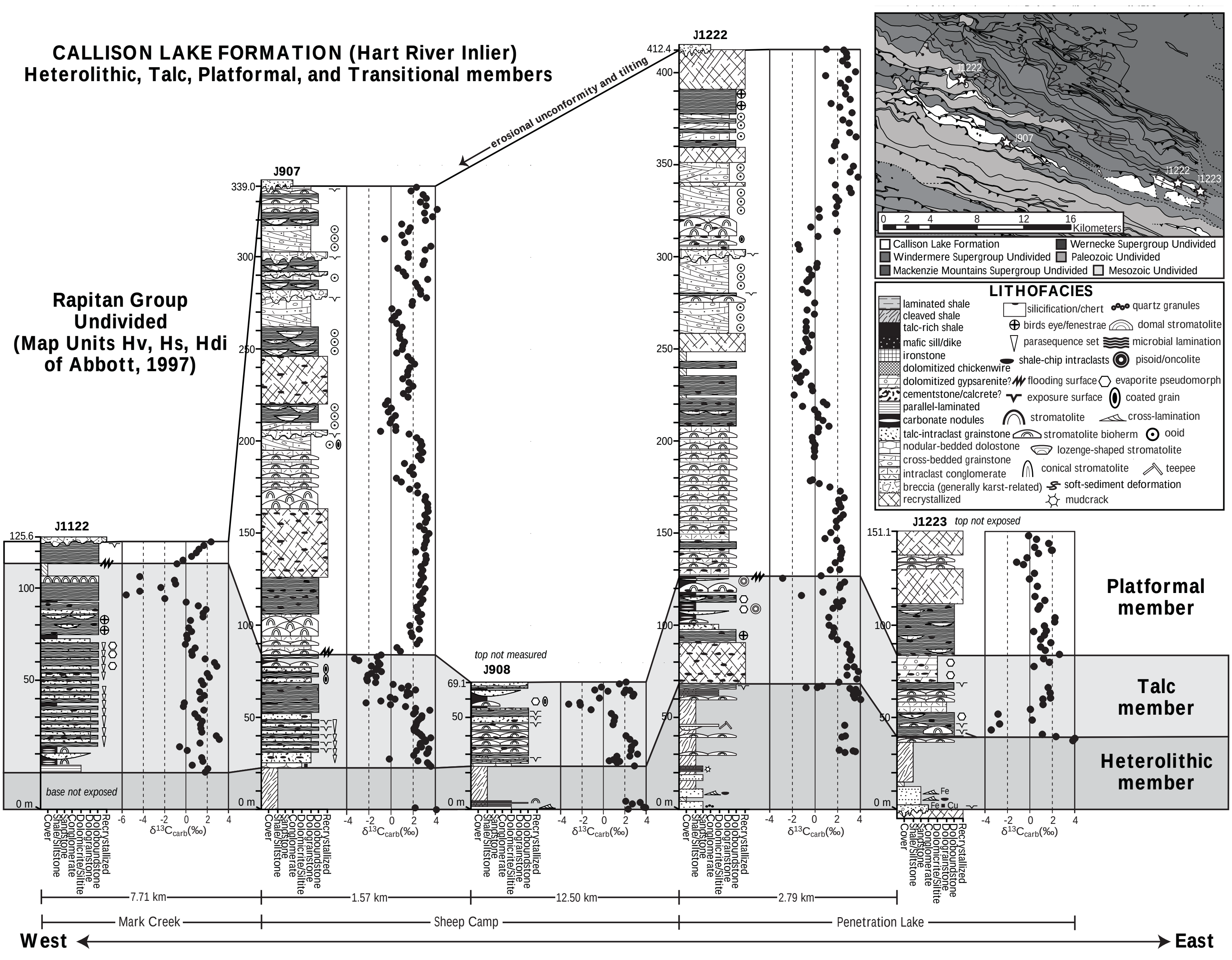

CALLISON LAKE FORMATION (Hart River Inlier)
Heterolithic, Talc, Platformal, and Transitional members
Rapitan Group Undivided (Map Units Hv, Hs, Hdi of Abbott, 1997)
erosional unconformity and tilting
J1122
J907
J908
J1222
J1223
top not measured
top not exposed
base not exposed
Platformal member
Talc member
Heterolithic member
Callison Lake Formation
Wernecke Supergroup Undivided
Windermere Supergroup Undivided
Paleozoic Undivided
Mackenzie Mountains Supergroup Undivided
Mesozoic Undivided
Kilometers
LITHOFACIES
laminated shale
cleaved shale
talc-rich shale
mafic sill/dike
ironstone
dolomitized chickenwire
dolomitized gypsarenite?
cementstone/calcrete?
parallel-laminated
carbonate nodules
talc-intraclast grainstone
nodular-bedded dolostone
cross-bedded grainstone
intraclast conglomerate
breccia (generally karst-related)
recrystallized
silicification/chert
quartz granules
birds eye/fenestrae
domal stromatolite
parasequence set
microbial lamination
shale-chip intraclasts
pisoid/oncolite
flooding surface
evaporite pseudomorph
exposure surface
coated grain
stromatolite
cross-lamination
stromatolite bioherm
ooid
lozenge-shaped stromatolite
conical stromatolite
teepee
soft-sediment deformation
mudcrack
Cover
Shale/Siltstone
Sandstone
Conglomerate
Dolomicrite/Siltite
Dolograinstone
Doloboundstone
Recrystallized
δ13Ccarb(‰)
7.71 km
1.57 km
12.50 km
2.79 km
Mark Creek
Sheep Camp
Penetration Lake
West
East

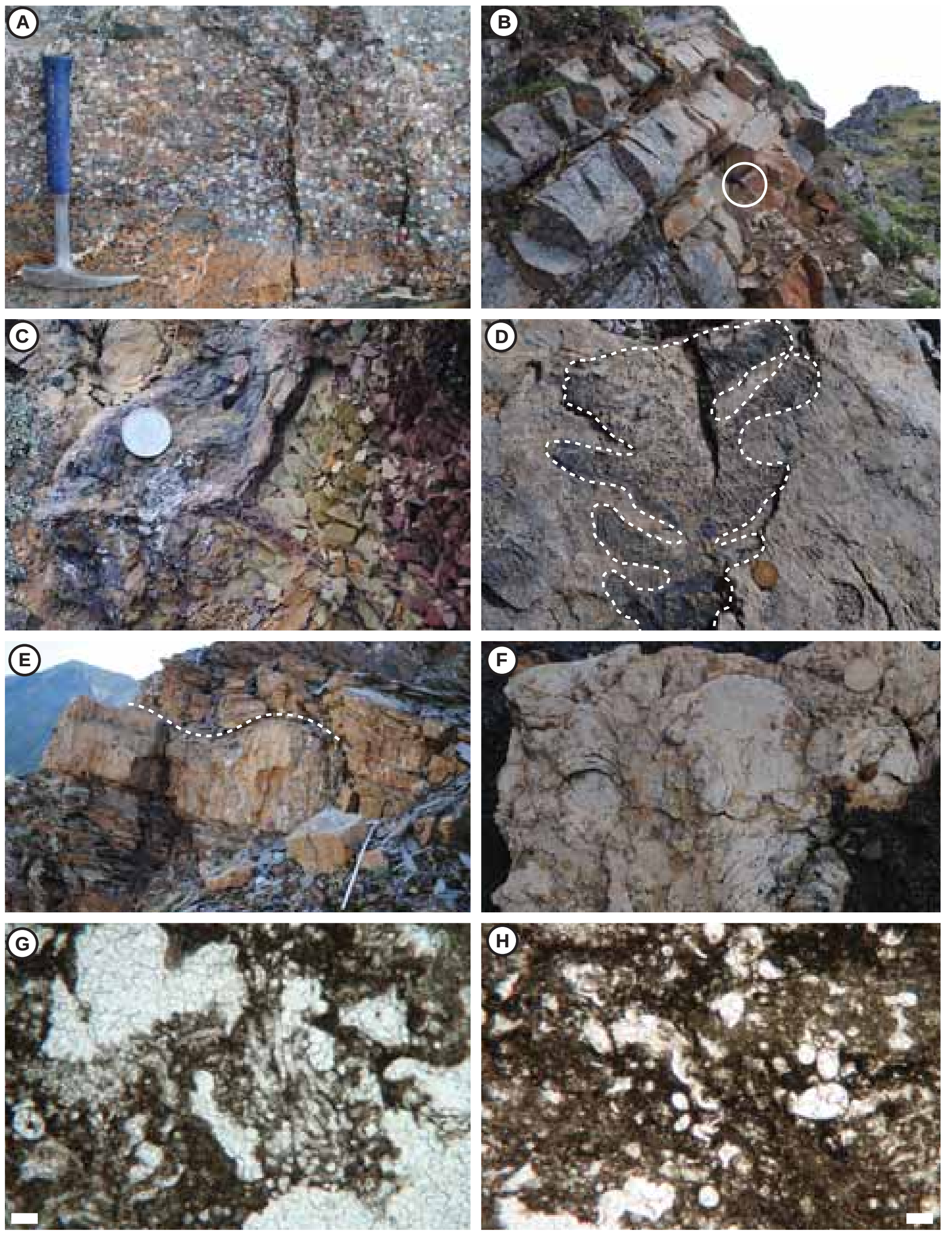
A
B
C
D
E
F
G
H

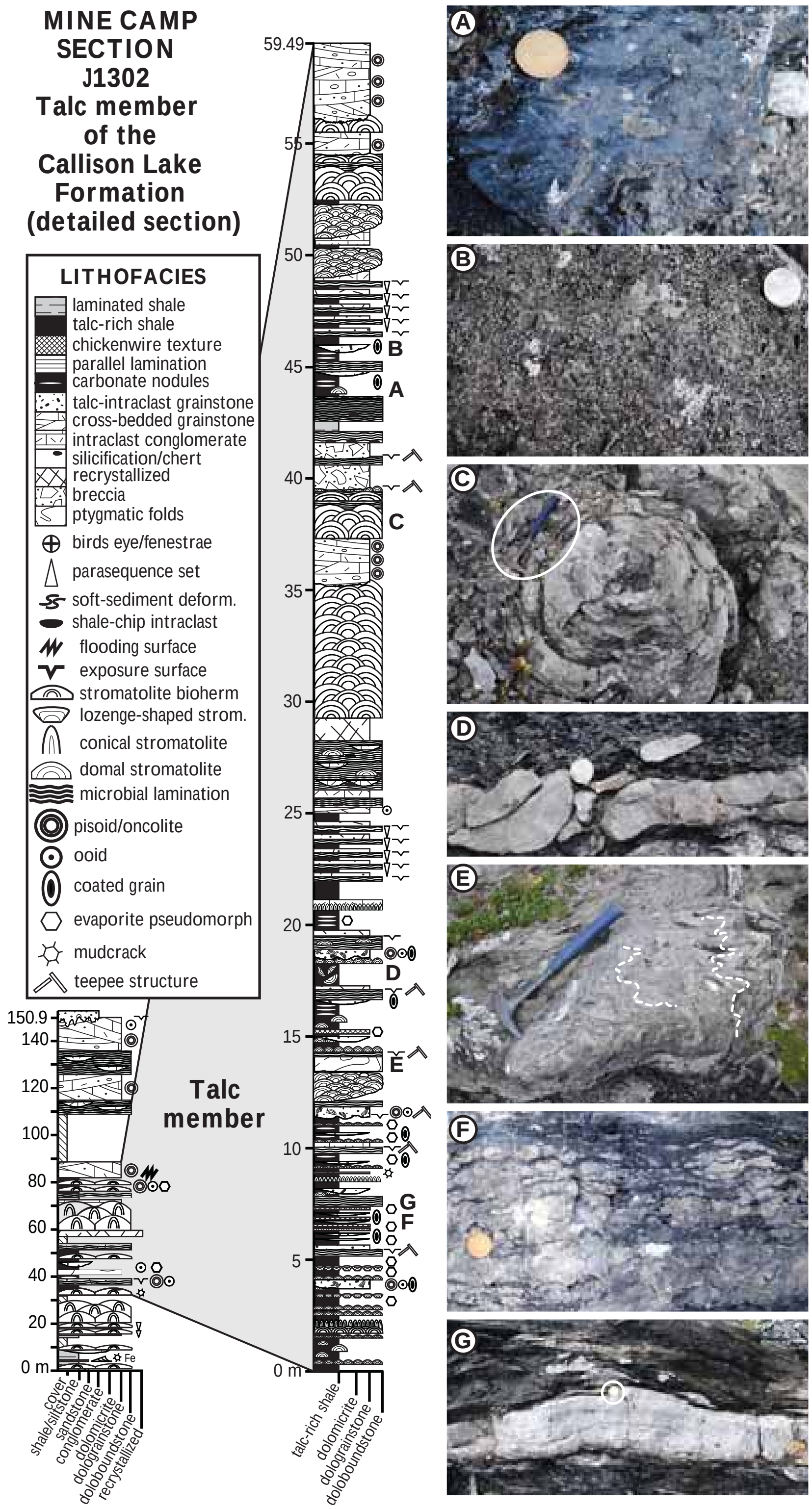
MINE CAMP SECTION J1302 Talc member of the Callison Lake Formation (detailed section)
LITHOFACIES
laminated shale
talc-rich shale
chickenwire texture
parallel lamination
carbonate nodules
talc-intraclast grainstone
cross-bedded grainstone
intraclast conglomerate
silicification/chert
recrystallized
breccia
ptygmatic folds
birds eye/fenestrae
parasequence set
soft-sediment deform.
shale-chip intraclast
flooding surface
exposure surface
stromatolite bioherm
lozenge-shaped strom.
conical stromatolite
domal stromatolite
microbial lamination
pisoid/oncolite
ooid
coated grain
evaporite pseudomorph
mudcrack
teepee structure
Talc member
150.9
140
120
100
80
60
40
20
0 m
Fe
cover
shale/siltstone
sandstone
conglomerate
dolomicrite
dolograinstone
doloboundstone
recrystallized
59.49
55
50
45
40
35
30
25
20
15
10
5
0 m
talc-rich shale
dolomicrite
dolograinstone
doloboundstone
A
B
C
D
E
F
G

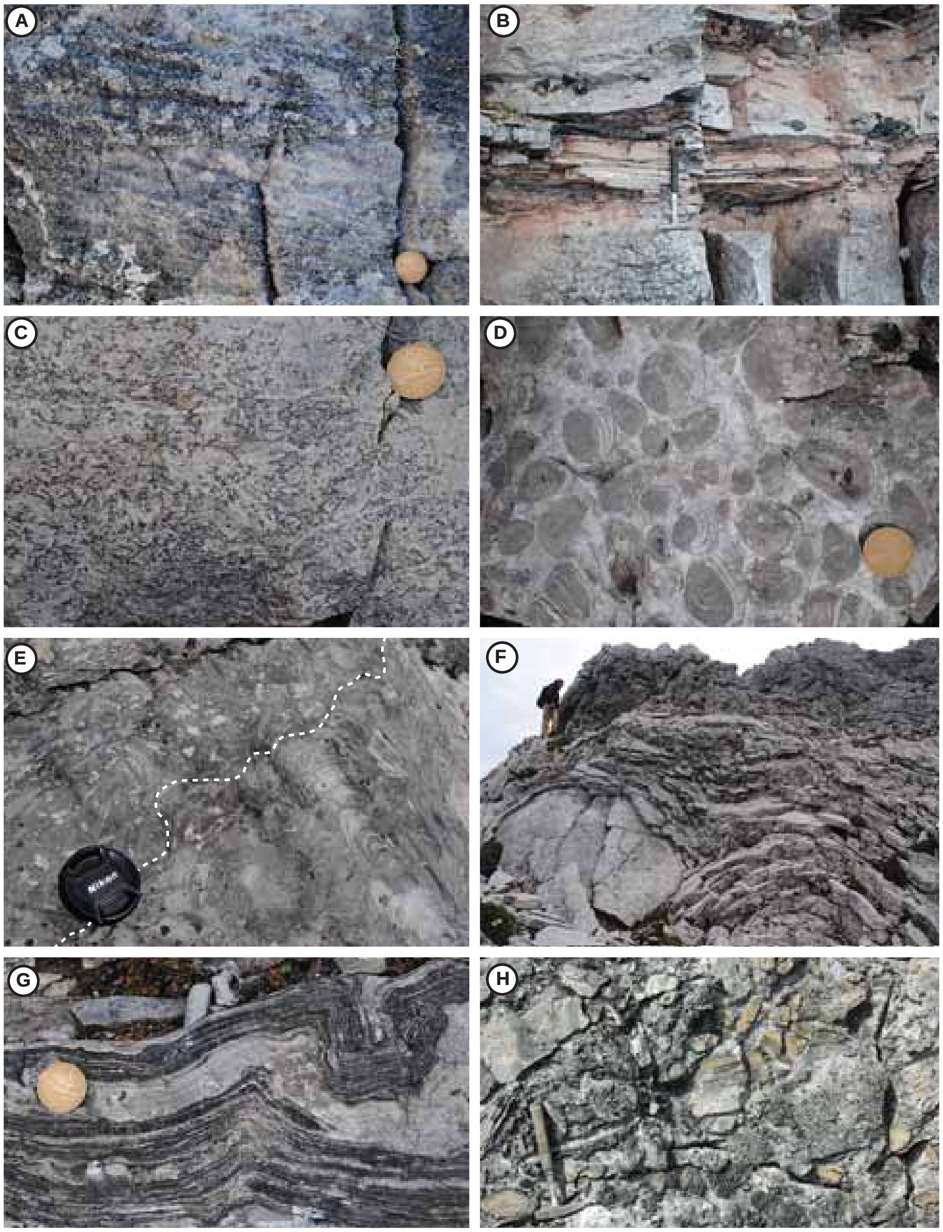
A
B
C
D
E
F
G
H

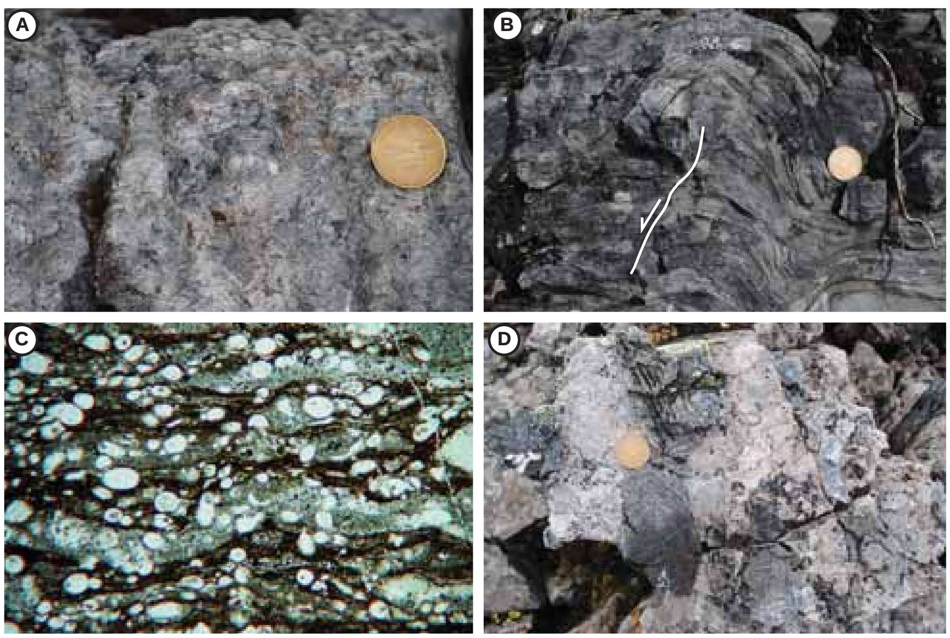
A
B
C
D

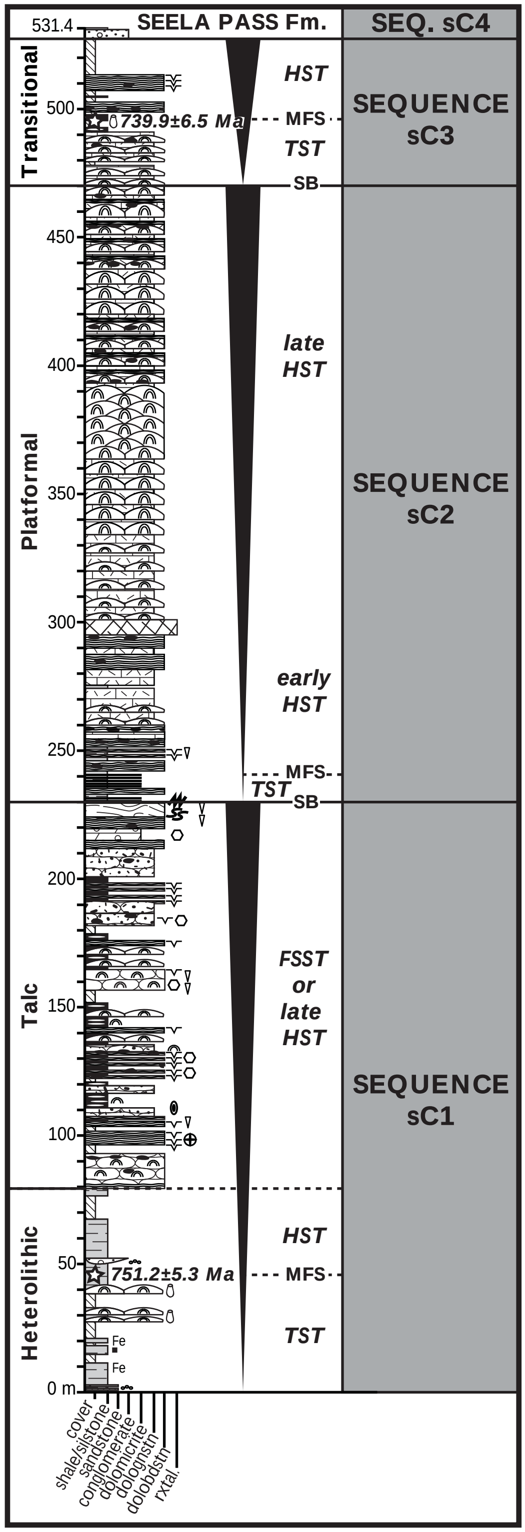

531.4
SEELA PASS Fm.
SEQ. sC4
Transitional
HST
500
739.9±6.5 Ma
MFS
TST
SB
SEQUENCE
sC3
Platformal
450
400
late
HST
350
SEQUENCE
sC2
300
early
HST
250
MFS
TST
SB
Talc
200
FSST
or
late
HST
150
100
SEQUENCE
sC1
Heterolithic
HST
50
751.2±5.3 Ma
MFS
TST
Fe
Fe
0 m
cover
shale/siltstone
sandstone
conglomerate
dolomicrite
dolognstn
dolobdstn
rxtal.

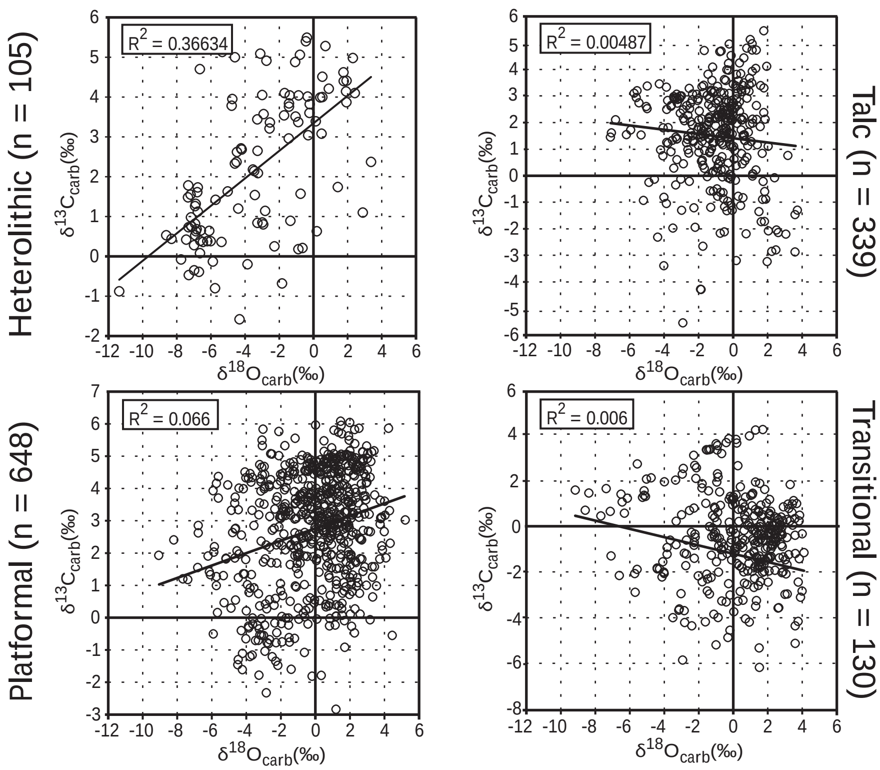

Heterolithic (n = 105)
$R^2$ = 0.36634
Talc (n = 339)
$R^2$ = 0.00487
Platformal (n = 648)
$R^2$ = 0.066
Transitional (n = 130)
$R^2$ = 0.006
$\delta^{13}C_{carb}$(‰)
$\delta^{18}O_{carb}$(‰)

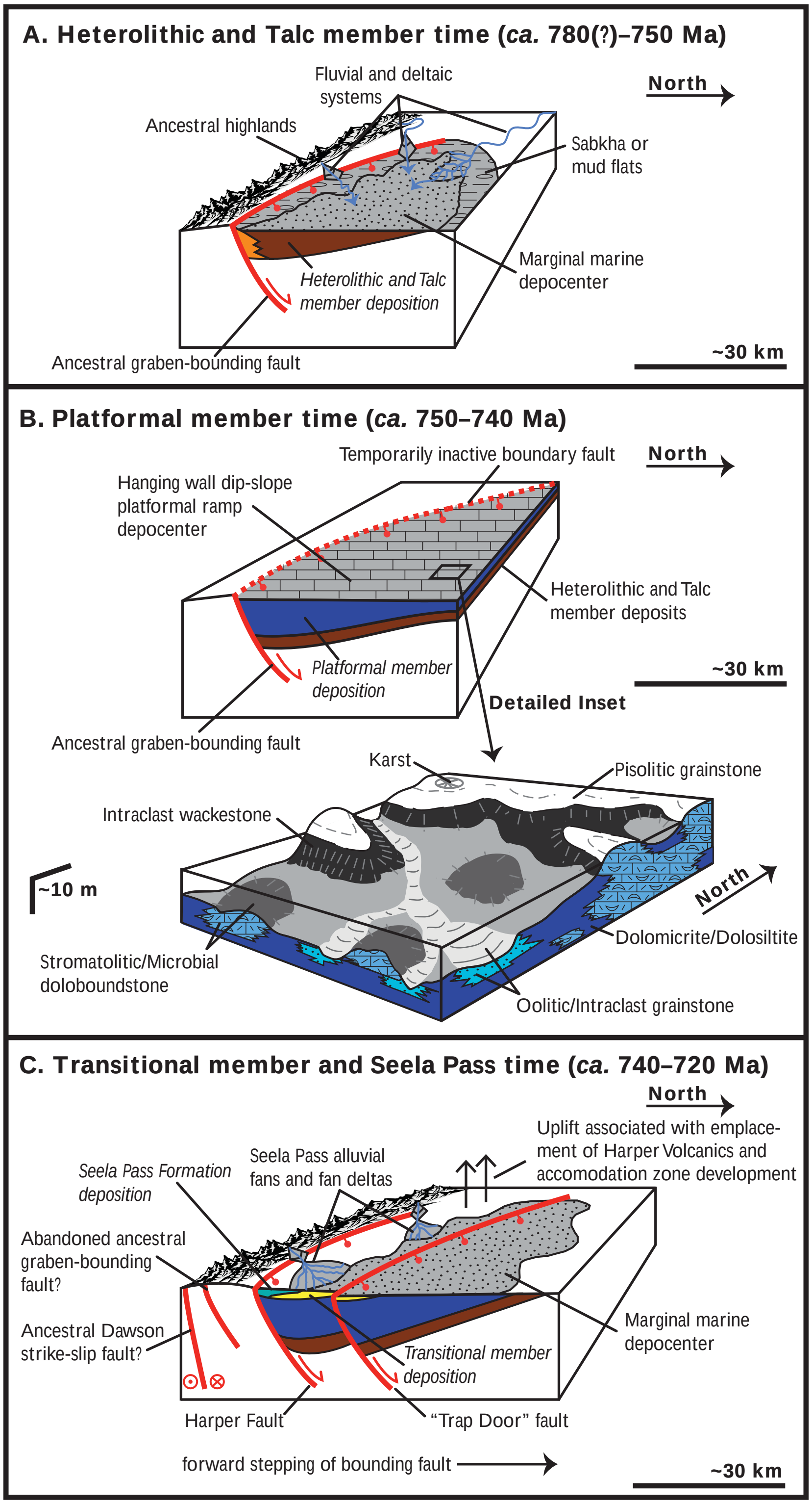
A. Heterolithic and Talc member time (ca. 780(?)–750 Ma)
Fluvial and deltaic systems
North
Ancestral highlands
Sabkha or mud flats
Marginal marine depocenter
Heterolithic and Talc member deposition
Ancestral graben-bounding fault
~30 km
B. Platformal member time (ca. 750–740 Ma)
Temporarily inactive boundary fault
North
Hanging wall dip-slope platformal ramp depocenter
Heterolithic and Talc member deposits
Platformal member deposition
~30 km
Detailed Inset
Ancestral graben-bounding fault
Karst
Pisolitic grainstone
Intraclast wackestone
~10 m
North
Dolomicrite/Dolosiltite
Stromatolitic/Microbial doloboundstone
Oolitic/Intraclast grainstone
C. Transitional member and Seela Pass time (ca. 740–720 Ma)
North
Uplift associated with emplacement of Harper Volcanics and accomodation zone development
Seela Pass Formation deposition
Seela Pass alluvial fans and fan deltas
Abandoned ancestral graben-bounding fault?
Ancestral Dawson strike-slip fault?
Marginal marine depocenter
Transitional member deposition
Harper Fault
"Trap Door" fault
forward stepping of bounding fault
~30 km

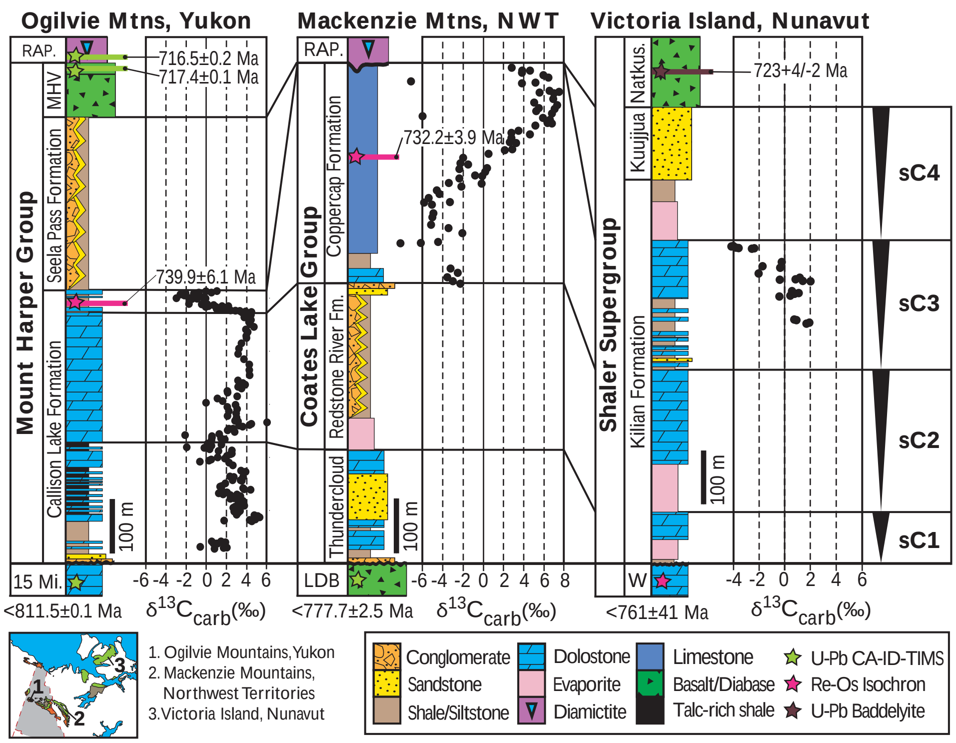

Ogilvie Mtns, Yukon
Mackenzie Mtns, NWT
Victoria Island, Nunavut
Mount Harper Group
RAP.
MHV
Seela Pass Formation
Callison Lake Formation
15 Mi.
716.5±0.2 Ma
717.4±0.1 Ma
739.9±6.1 Ma
100 m
<811.5±0.1 Ma
-6 -4 -2 0 2 4 6
δ13Ccarb(‰)
Coates Lake Group
RAP.
Coppercap Formation
Redstone River Fm.
Thundercloud
LDB
732.2±3.9 Ma
100 m
<777.7±2.5 Ma
-6 -4 -2 0 2 4 6 8
δ13Ccarb(‰)
Shaler Supergroup
Natkus.
Kuujjua
Kilian Formation
W
723+4/-2 Ma
100 m
<761±41 Ma
-4 -2 0 2 4 6
δ13Ccarb(‰)
sC4
sC3
sC2
sC1
1. Ogilvie Mountains, Yukon
2. Mackenzie Mountains, Northwest Territories
3. Victoria Island, Nunavut
Conglomerate
Sandstone
Shale/Siltstone
Dolostone
Evaporite
Diamictite
Limestone
Basalt/Diabase
Talc-rich shale
U-Pb CA-ID-TIMS
Re-Os Isochron
U-Pb Baddelyite

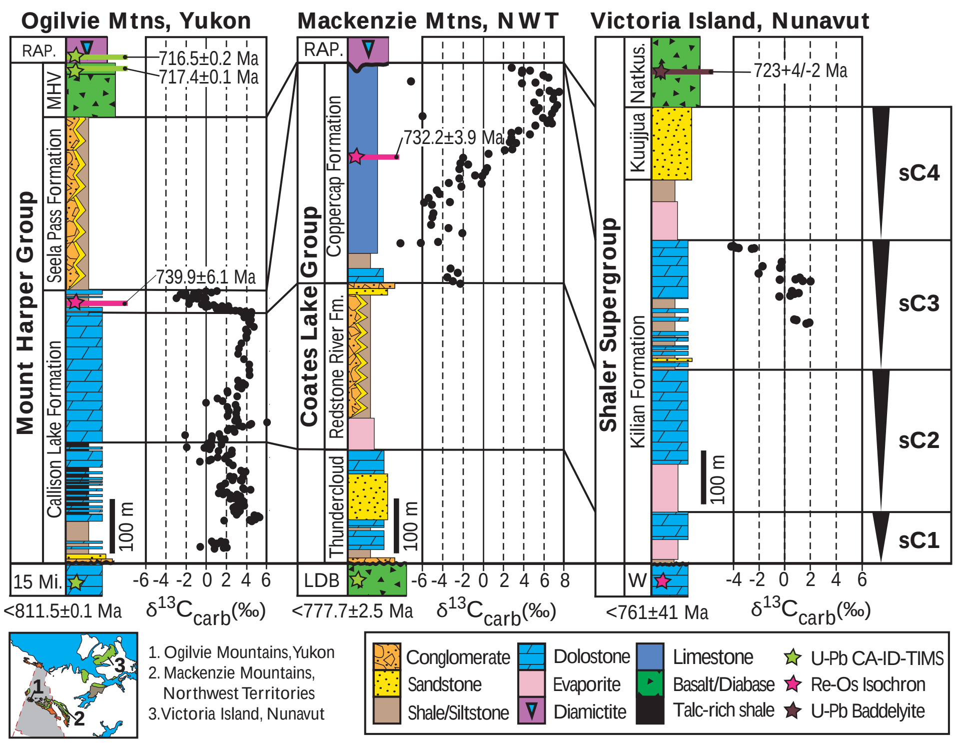

Ogilvie Mtns, Yukon
Mackenzie Mtns, NWT
Victoria Island, Nunavut
RAP.
MHV
Seela Pass Formation
Callison Lake Formation
Mount Harper Group
15 Mi.
716.5±0.2 Ma
717.4±0.1 Ma
739.9±6.1 Ma
100 m
<811.5±0.1 Ma
δ13Ccarb(‰)
Coppercap Formation
Redstone River Fm.
Thundercloud
Coates Lake Group
LDB
732.2±3.9 Ma
<777.7±2.5 Ma
Natkus.
Kuujjua
Kilian Formation
Shaler Supergroup
W
723+4/-2 Ma
<761±41 Ma
sC4
sC3
sC2
sC1
1. Ogilvie Mountains, Yukon
2. Mackenzie Mountains, Northwest Territories
3. Victoria Island, Nunavut
Conglomerate
Sandstone
Shale/Siltstone
Dolostone
Evaporite
Diamictite
Limestone
Basalt/Diabase
Talc-rich shale
U-Pb CA-ID-TIMS
Re-Os Isochron
U-Pb Baddelyite

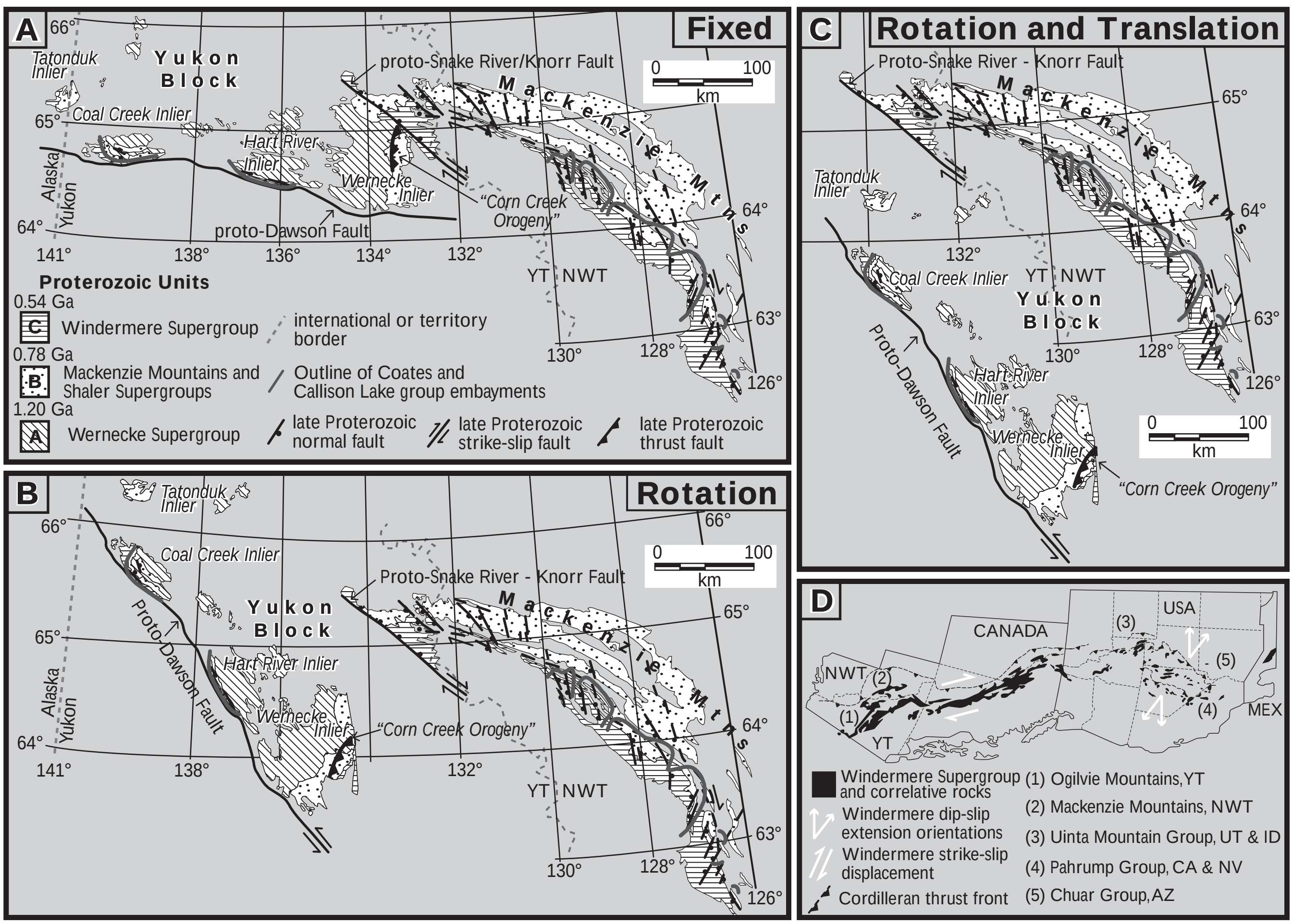

A
Fixed
Yukon Block
Tatonduk Inlier
Coal Creek Inlier
Hart River Inlier
Wernecke Inlier
proto-Snake River/Knorr Fault
proto-Dawson Fault
"Corn Creek Orogeny"
Mackenzie Mtns
Alaska
Yukon
YT NWT
66°
65°
64°
63°
141°
138°
136°
134°
132°
130°
128°
126°
0 100 km
Proterozoic Units
0.54 Ga
C Windermere Supergroup
0.78 Ga
B Mackenzie Mountains and Shaler Supergroups
1.20 Ga
A Wernecke Supergroup
international or territory border
Outline of Coates and Callison Lake group embayments
late Proterozoic normal fault
late Proterozoic strike-slip fault
late Proterozoic thrust fault
B
Rotation
Proto-Snake River - Knorr Fault
Proto-Dawson Fault
C
Rotation and Translation
D
CANADA
USA
MEX
NWT
YT
Windermere Supergroup and correlative rocks
Windermere dip-slip extension orientations
Windermere strike-slip displacement
Cordilleran thrust front
(1) Ogilvie Mountains, YT
(2) Mackenzie Mountains, NWT
(3) Uinta Mountain Group, UT & ID
(4) Pahrump Group, CA & NV
(5) Chuar Group, AZ

TABLE 1. SUMMARY OF CALLISON LAKE FORMATION LITHOFACIES (PAGE 1)

| Lithofacies | Composition | Bedding Style/Structures | Depositional Environment | Distribution |
|---|---|---|---|---|
| **Siliciclastic Facies:** | | | | |
| F1: Pebble to granule conglomerate | Clast- to matrix-supported conglomerate; light grey to brown; dominated by quartz and chert with occasional lithics; well-rounded to subangular; moderate sorting; hematite and silica cement | Thin- to thick-bedded; occasionally forming distinct transgressive lags; faint ripple- to dune-scale trough and tabular cross-bedding up to 20 cm thick; erosional base, lenticular geometry, and fining-up packages common; associated with F2 and F3 | Braided fluvial channels. Tidal/Estuarine? Amalgamated channel deposits with abrupt lateral facies change; difficult to discern distinct point-bar or lateral accretion geometries; locally reworking underlying strata; transgressive lag | Restricted to HM |
| F2: Sandstone | Quartz and chert arenite and wacke; very fine- to coarse-grained with occasional granules; moderate sorting; well-rounded to subangular; abundant hematite staining; tan yellow to brown; silica cement | Thin- to medium-bedded; commonly with unidirectional and symmetrical ripple cross-bedding and parallel lamination; occasionally amalgamated; mud chip intraclasts common; interbedded with F3 and forming fining-up packages with F1 | Coastal plain/Estuarine. Maybe local shoreface? Evidence for floodplain or tidal flat deposition with clear tidal influence in the form of distinct tidal ravinement surfaces and fining-up packages | Restricted to HM |
| F3: Variegated siltstone and shale | Variegated shale (red, yellow, green, and purple) interbedded with siltstone; locally contains diagenetic dolostone lenses and iron formation; heavily silicified in certain horizons; occasional very-fine sand sized particles | Locally abundant mudcracks and scours; mostly planar-laminated and associated with F1 and F2; occasional coarsening-upward packages with ripple cross lamination; flaser-bedding and ball and pillows locally | Floodplain or peritidal mud flat/lagoon. Generally associated with transition into marginal marine inner ramp to lagoonal deposits; interbedded sandstone units could represent crevasse splays in a fluvial setting | Restricted to HM |
| F4: Black shale | Black to dark grey shale; TOC to 3.5 wt. %; occasionally silicified with abundant chert nodules; locally contains vase-shaped microfossils; minor silt and very-fine sand; Fe-oxides, pyrite, sphalerite, ankerite(?) locally | Planar-laminated and fissile; occasionally silicified and more resistant; locally interbedded with various lithofacies and no evidence for wave or storm activity; poor sorting with coarser grained horizons | Outer–inner ramp subtidal or lagoonal. Suspension depositon in a low-energy setting; elevated TOC tied to episodic restriction? | HM, TRM |
| **Evaporite/Talc Facies:** | | | | |
| F5: Talc-rich shale | Black talc-rich shale; commonly silicified with abundant chert nodules; organic-rich with TOC up to 4 wt% | Planar-laminated to nodular bedded; abundant diagenetic chert; occasional soft-sediment deformation; intimate association with F6 | Restricted lagoonal to sahbka. Playa lake? Suspension deposition in a low-energy setting; evidence for seismic or storm-generated disruption | TM, TRM? |
| F6: Interbedded talc and dolostone | Black talc-rich shale interbedded with microbial and sucrosic light to dark dolostone; commonly silicified with chert nodules | Nodular- to planar-bedded with microbial lamination; teepees structures, mudcracks, and evaporite pseudomorphs after anhydrite and gypsum common; horizons of talc-shale chip intraclast conglomerate common; local overturned stromatolites and seismites | Sahbka to peritidal mud flat. Evidence for intertidal to peritidal deposition; episodic restriction with sulfate deposition; wave-, storm-, and seismically-generated structures common; complex paragenetic history with multiple Mg-silicate and evaporite transformations | Restricted to TM |
| **Carbonate Facies:** | | | | |
| F7: Stromatolitic bioherm/biostrome | Orange-yellow to dark grey (fresh) stromatolitic doloboundstone; minor terriginous silt and frosted quartz grains; occasional vase-shaped microfossils in disseminated organic matter; microbial sheaths after cyanobacteria | Meter- to decimeter-thick stromatolitic biohermal/biostromal buildups interbedded with F3,4; stromatolites range from domal to columnar with both low- and high-inheritance forms; micritic, oolitic, and intraclastic fill; isolated to laterally linked forms | Middle- to inner-ramp subtidal or lagoonal. Isolated to linked stromatolitic patch reefs or buildups associated with a subtidal depositional setting; possibly lagoonal with no evidence for exposure or wave activity | HM, TRM |

HM – Heterolithic member, TM – Talc member, PM – Platformal member, TRM – Transitional member

TABLE 1. SUMMARY OF CALLISON LAKE FORMATION LITHOFACIES (PAGE 2)

| Lithofacies | Composition | Bedding Style/Structures | Depositional Environment | Distribution |
|---|---|---|---|---|
| F8: Stromatolitic doloboundstone | Light to dark grey stromatolitic doloboundstone; occasional black chert and ferruginous clay-rich laminae; close association with stromatolite-rich intraclast wackestone and grainstone | Centimeter- to meter-thick stromatolitic structures; forms range from laterally-linked, low relief, and domal to high-inheritance columnar structures; intercolumnal fill micritic, oolitic, pisolitic, and intraclasts; scours and corrosive structures common | Middle-Inner ramp subtidal. Heterogeneous assemblage of stromatolitic morphologies; common wave-generated scours and association with F9 and F10; meter-scale high relief domes suggest occasional deeper water setting | All members. |
| F9: Microbialite | Light to dark grey microbial doloboundstone; occasional black chert nodules, terriginous silt, fine- to medium-sized frosted quartz grains; distinguished from F8 by flat, crinkly lamination | Centimeter- to meter-thick microbialite; mm-scale undulatory and wavy lamination; locally containing fenestrae (birds' eye), teepee structures, and mudcracks; occasional seismically-disrupted and folded laminae; discrete intervals of intraclast conglomerate | Inner ramp intertidal to peritidal. Intertidal deposition evidenced by intimate association with F8 and wave- or storm-generated intraclasts; exposure surfaces common; discrete parasequences with F6,8, and 10 | All members. |
| F10: Intraclast grainstone/wackestone | Light to dark grey dolomitic intraclast grainstone and wackestone; almost exclusively composed of clasts from F8 and F9; minor rudstone | Thin- to thick-bedded, tabular to subrounded, sand- to cobble-sized intraclastic grainstone and wackestone matrix-supported with scoured and erosive bases, occasional crude lamination, and faint grading; commonly randomly oriented | Inner ramp subtidal. Subtidal deposits associated with high-energy storm- or wave-generated events that scour and rework material from F9 and F10; no evidence for subaerial exposure | PM, TRM |
| F11: Dolograinstone | Light to dark grey dolograinstone composed of ooids, peloids, pisoids, and/or oncoids; minor terriginous silt component | Thin- to thick-bedded and massive to finely laminated; occasional trough cross-bedding and planar laminated but generally quite massive and crudely stratified; intimately associated with F8, F9, and F10; occasional low-angle cross-bedding | Inner ramp subtidal to intertidal bar or shoal complex. High-energy subtidal deposition associated with tidal sand bars and/or migrating barrier complex; 3D morphology not worked out but commonly interbedded with diverse lithofacies | Restricted to PM |
| F12: Thin-bedded dolomicrite/siltite | Dark grey to black dolomicrite and dolosiltite; commonly composed of microcrystalline and neomorphosed dolospar and dolomicrite; occasional hints of peloidal precuser allochems; ferruginous clay drapes and black chert common | Thin-bedded and laminated with mm-scale parallel lamination; occasional erosional base; black chert commonly late diagenetic and fabric destructive; no evidence for grading or turbidite deposition; commonly resemble Phanerozoic ribbon-bedded limestone | Mid-outer ramp subtidal. Generally constrained to transgressive horizons associated with relatively low-energy deposition; ferruginous drapes could indicate hardground conditions or suspension rainout during highstand; occasionally deformed during seismic activity | PM, TRM |
| **Diagenetic Facies:** | | | | |
| F13: Recrystallized dolostone | Light grey to white sucrosic dolostone with fabric-destructive diagenetic recrystallization; occasional oolitic ghosts | Medium- to thick-bedded and massive; crude stratification and commonly impossible to tell precursor lithology; abundant secondary isopachus, drusy, and botryoidal cements; veins common; locally contains clotty secondary fabric that resembles "thrombolitic" texture | Unclear but commonly associated with subaerial exposure surfaces and coarser-grained lithofacies. | All members |
| F14: Breccia | Grey to white dolostone breccia; commonly silicified with angular clasts of dolostone; matrix composed of both terriginous silt, secondary dolomite spar, and dolosiltite; clasts range from sand- to boulder-sized; local well-rounded quartz sand within cavity fill | Massive and generally thick-bedded; crude stratification with clear horizons indicating subaerial exposure and karst development; clasts composed exclusively of underlying strata in puzzle-fitting fabric; local grykes and irregular cavities filled with terriginous silt and sand | Inner ramp intertidal to peritidal. Clearly associated with subaerial exposure and karst development in dolostone lithologies; possibly associated with uplift and fault breccia in certain localities | PM, TRM |

HM – Heterolithic member, TM – Talc member, PM – Platformal member, TRM – Transitional member

**STRAUSS AND OTHERS (XXX) SUPPLEMENTARY DATA FILE XXX**

Table DR1. Formalization of the Seela Pass Formation.

| | |
|---|---|
| **Name** | Seela Pass Formation |
| **Name Derivation** | Type area located west of Seela Pass, western Ogilvie Mountains, Yukon Territory, Canada; Dawson Quadrangle (NTS 116BC) |
| **Category and Rank** | lithostratigraphic Formation |
| **Type Area** | Situated broadly between Eagle Creek and Chandindu River, western Ogilvie Mountains, Yukon Territory, Canada |
| **Unit Type Section** | Composite stratigraphic sections 10 and 12 of Mustard (1991) |
| | Located on prominent N-S trending ridgeline ~8.7 km ENE of Mount Harper (N64°39.539' W139°44.405') |
| | Lower boundary: gradational transition from Transitional member of Callison Lake Formation |
| | Upper boundary: covered, sharp transition into Mount Harper Volcanics |
| **Unit Description** | Mustard (1990; 1991) documented five main facies in the Seela Pass Formation including *fault-adjacent breccias*, *coarse conglomerate*, *conglomerate-sandstone*, and *mudstone-sandstone*. The type section consists of ~1100 m of mostly thick-bedded, sheet-like, poorly sorted and disorganized massive conglomerate. The conglomerate consists of clast-supported, pebble- to boulder-sized clasts of dolostone and sandstone (with minor chert) in a dolowacke matrix with minor matrix-supported lenses and sandstone. Grading is poorly developed and clasts are typically subangular to subrounded. Near the Harper Fault, there are distinct lenses of clast-supported dolostone megaboulders > 20 m across. Further to the east, the Seela Pass Formation generally becomes finer-grained and displays a distinct gradational transition in bedding thickness and grain-size into the other characteristic facies of the unit. The other reference section (section 20 of Mustard, 1991) is dominated by maroon dolomitic mudstone and siltsone with mudcracks that coarsen-upwards into thicker deposits of sandstone and minor conglomerate. Overall, Mustard (1991) interpreted the Seela Pass Formation as a distint progradational alluvial fan and fan delta succession. |
| **Unit Reference Sections** | Stratigraphic section 20 of Mustard (1991) |
| | Located in a small N-facing gully ~18 km from Seela Pass (N64°40.946 W139°13.982) |
| **Dimensions** | ~1100 m thick in composite section at type section (Mustard, 1991) |
| | ~605 m at reference section (Mustard, 1991) |
| **Geologic Age** | Neoproterozoic (<739.9±6.1 Ma, >717.43±0.14 Ma, Macdonald et al., 2010; Strauss et al., 2014a) |
| **Regional Correlations** | unnamed equivalent in Hart River inlier; Coates Lake Group, Mackenzie Mountains; Kuujjua Formation, Shaler Supergroup |

Table DR2. Formalization of the Callison Lake Formation.

| | |
|---|---|
| **Name** | Callison Lake Formation |
| **Name Derivation** | Type area located in the Coal Creek inlier, Ogilvie Mountains, Yukon Territory, Canada; Dawson Quadrangle (NTS 116BC) |
| **Category and Rank** | lithostratigraphic Formation |
| **Type Area** | Situated broadly between Eagle Creek and Chandindu River, western Ogilvie Mountains, Yukon Territory, Canada |
| **Unit Type Section** | Mount Harper East, section J1301 (Figure 6; *this paper*)<br>Located on prominent N-S trending ridgeline ~10 km ENE of Mount Harper<br>Lower boundary: sharp contact on silicified karst of Craggy dolostone, Fifteenmile Group (N64.6644833°, W-139.73135°)<br>Upper boundary: gradational transition into Seela Pass Formation (N64.6599667°, W-139.73685°) |
| **Unit Description** | Divided into four informal members: (1) **Heterolithic member**: heterogeneous siliciclastic-dominated package of interbedded conglomerate, sandstone, siltstone, and shale with minor stromatolitic and microbial dolostone. Conglomerate is both clast- and matrix-supported and dominated by pebble- to cobble-size clasts of quartz, chert, and occasional lithics. Sandstone units are characterized by subangular to subrounded quartz and chert arenite with minor wacke. Coarse lithologies tend to be thick- to medium-bedded and host trough- and tabular-crossbedding, soft sediment deformation, and erosional scours. Shale and siltstone units are generally variegated, locally contain mudcracks and synaeresis cracks, and locally become organic-rich. Yellow-brown stromatolitic dolostone units generally form prominent biostromes or bioherms and are laterally discontinuous. Lower contact is sharp and erosive on paleokarst intervals of upper Craggy dolostone and upper contact is sharp with overlying strata of Talc member: (2) **Talc member**: interbedded black, talc-rich shale and grey-white dolostone. Talc-rich shale displays a vitreous luster, is locally finely laminated and pure, but also drapes microbial dolostone units and is commonly interbedded with nodular dolostone. Dolostone units are characterized by stromatolitic and microbial doloboundstone with intevals of wackestone, grainstone, and rudstone. Common sedimentary structures include evaporitive pseudomorphs, mudcracks, teepees, crudley laminated intraclast rip-ups, and occasional erosional scours. Upper contact is sharp with the overlying Platformal member dolostone. (3) **Platformal member**: dominated by light- to dark-grey, medium-thick-bedded dolograinstone, doloboundstone, dolowackestone, and dolorudstone. Allochems characterized by pisoids, ooids, peloids, oncoids, and distinct stromatolite clasts ("flakestone") and common sedimentary structures include dune-scale crossbedding, erosional scours within doloboundstone units, morphologically-diverse stromatolites and microbialite, occasional evaporite pseudomorphs, teepees, and massively recrystallized intervals. Upper contact either gradational into Transitional member deposits or marked by a profound subaerial exposure surface and paleokarst interval. (4) **Transitional member**: heterogeneous package of interbedded microbial and stromatolitic dolostone and black shale/siltstone. Dolostone units marked by morphologically-diverse stromatolites, healed synsedimentary faults, seismites subaerial exposure surfaces, teepees, and abundant detrital material. Siliciclastic intervals commonly fine-grained, organic-rich, silicified, and occasionally poorly sorted. Upper contact gradational into siliciclastic deposits of the overlying Seela Pass Formation. |
| **Unit Reference Sections** | 1. Mount Gibben, composite section J1018-1019 (Figure 6, *this paper*)<br>Located on a prominent N-S trending ridgeline with upper part of section exposed to SW (N64.6886°, W-139.3528167°)<br>2. Sheep Camp, section J907, Hart River inlier (Figure 7, *this paper*)<br>Located in a steep, N-facing gully and SW-trending ridgeline (64.572229°,-136.836461°) |
| **Dimensions** | 409.6 m thick at type section (Figure 6, *this paper*)<br>516.4 m thick at reference section (Figure 7, *this paper*) |
| **Geologic Age** | Neoproterozoic (<780 Ma, >717.43±0.14 Ma, Macdonald et al., 2010; Strauss et al., 2014a; *this paper*)<br>Two internal Re-Os depositional ages: 752.7±5.1 Ma (Heterolithic member), 739.9±6.1 Ma (Transitional member)<br>(Strauss et al., 2014a; Rooney et al., in review) |
| **Regional Correlations** | Thundercloud, Redstone River, and Coppercap formations of Coates Lake Group, Mackenzie Mountains; Kilian and Kuujjua formations, Shaler Supergroup |

Table DR3. Location of measured stratigraphic sections.

| **Section Name** | **Camp Name** | **Inlier** | **Latitude** | **Longitude** |
|---|---|---|---|---|
| F927 - base | Talc Falls | Coal Creek | 64.787756 | -139.825689 |
| F927 - top | Talc Falls | Coal Creek | 64.787531 | -139.828554 |
| F928 - base | Talc Falls | Coal Creek | 64.781026 | -139.822763 |
| F928 - top | Talc Falls | Coal Creek | 64.777922 | -139.836666 |
| J907 - base | Sheep Camp | Hart River | 64.572229 | -136.836461 |
| J907 - top | Sheep Camp | Hart River | 64.573667 | -136.849934 |
| J908 - base | Sheep Camp | Hart River | 64.569988 | -136.802585 |
| J908 - top | Sheep Camp | Hart River | 64.568602 | -136.803404 |
| J1018 - base | Mount Gibben | Coal Creek | 64.6631833 | -139.3974333 |
| J1018 - top | Mount Gibben | Coal Creek | 64.6627833 | -139.3969833 |
| J1019 - base | Mount Gibben | Coal Creek | 64.6886 | -139.35081 |
| J1019 - top | Mount Gibben | Coal Creek | 64.6725 | -139.3692667 |
| J1122 - base | Mark Creek | Hart River | 64.623077 | -136.930764 |
| J1122 - top | Mark Creek | Hart River | 64.620149 | -136.927846 |
| J1201 - base | Gibben East | Coal Creek | 64.70755 | -139.1039333 |
| J1201 - top | Gibben East | Coal Creek | 64.7064667 | -139.1080333 |
| J1202 - base | Gibben East | Coal Creek | 64.6986667 | -139.0937167 |
| J1202 - top | Gibben East | Coal Creek | 64.69785 | -139.09945 |
| J1203 - base | Gibben East | Coal Creek | 64.69685 | -139.0962333 |
| J1203 - top | Gibben East | Coal Creek | 64.69655 | -139.0963833 |
| J1204 - base | Gibben East | Coal Creek | 64.68155 | -139.2321 |
| J1206 - base | Reefer Camp | Coal Creek | 64.7568833 | -139.7067667 |
| J1206 - top | Reefer Camp | Coal Creek | 64.758063 | -139.752754 |
| J1207 - base | Reefer Camp | Coal Creek | 64.7617667 | -139.7470167 |
| J1207 - top | Reefer Camp | Coal Creek | 64.7587 | -139.7526 |
| J1210 - base | Mount Harper | Coal Creek | 64.6883333 | -139.85805 |
| J1210 - top | Mount Harper | Coal Creek | 64.6829333 | -139.8633667 |
| J1211 - base | Mount Harper | Coal Creek | 64.6920333 | -139.8670333 |
| J1211 - top | Mount Harper | Coal Creek | 64.6905833 | -139.867 |
| J1222 - base | Penetration Lake | Hart River | 64.54539 | -136.549296 |
| J1222 - top | Penetration Lake | Hart River | 64.542626 | -136.541623 |
| J1223 - base | Penetration Lake | Hart River | 64.544011 | -136.487438 |
| J1223 - top | Penetration Lake | Hart River | 64.543031 | -136.484123 |
| J1301 - base | Mount Harper East | Coal Creek | 64.6644833 | -139.731729 |
| J1301 - top | Mount Harper East | Coal Creek | 64.6599667 | -139.73685 |
| J1302 - base | Mine Camp | Coal Creek | 64.8242 | -140.0427333 |
| J1302 - top | Mine Camp | Coal Creek | 64.8276833 | -140.0504333 |
| J1303 - base | Mine Camp | Coal Creek | 64.8148333 | -140.0499 |
| J1303 - top | Mine Camp | Coal Creek | 64.8126667 | -140.0478333 |

Table DR4. Carbonate carbon and oxygen isotope data.

| Section | Stratigraphic Height | δ13C | δ18O | Section | Stratigraphic Height | δ13C | δ18O |
|---|---|---|---|---|---|---|---|
| **J1302** | 1.2 | 4.51 | 0.52 | **J1018** | 0.1 | 4.21 | 1.74 |
| **J1302** | 2.3 | 4.04 | -1.39 | **J1018** | 0.5 | 3.78 | 0.20 |
| **J1302** | 6.8 | 4.88 | -1.07 | **J1018** | 1 | 3.35 | -1.29 |
| **J1302** | 8.6 | 3.21 | -2.57 | **J1018** | 1.5 | 3.59 | -0.95 |
| **J1302** | 10.7 | -0.68 | -1.84 | **J1018** | 2 | 3.51 | -0.87 |
| **J1302** | 14.6 | 3.76 | -1.43 | **J1018** | 2.5 | 3.32 | -1.48 |
| **J1302** | 16.5 | 3.54 | -1.72 | **J1018** | 3 | 3.33 | -1.51 |
| **J1302** | 18.3 | 2.96 | -1.45 | **J1018** | 3.5 | 3.32 | -0.89 |
| **J1302** | 20.7 | 2.37 | 3.37 | **J1018** | 4.5 | 3.93 | 0.97 |
| **J1302** | 22.8 | 3.99 | 0.40 | **J1018** | 5 | 4.19 | 1.32 |
| **J1302** | 25.5 | 1.10 | 2.89 | **J1018** | 5.5 | 3.81 | -0.22 |
| **J1302** | 28.1 | 1.57 | -0.75 | **J1018** | 6 | 3.62 | 0.24 |
| **J1302** | 30.8 | -0.10 | 2.43 | **J1018** | 6.5 | 3.16 | -0.63 |
| **J1302** | 32.5 | -1.50 | 3.62 | **J1018** | 7 | 2.63 | 0.30 |
| **J1302** | 33.5 | -2.92 | 3.62 | **J1018** | 7.5 | 2.14 | -0.84 |
| **J1302** | 35.3 | 1.10 | 2.06 | **J1018** | 8 | 2.28 | -0.87 |
| **J1302** | 36.9 | 3.37 | -1.78 | **J1018** | 9.2 | 1.17 | -0.20 |
| **J1302** | 37.8 | 3.11 | -0.20 | **J1018** | 9.5 | 0.82 | -1.05 |
| **J1302** | 41.6 | -2.01 | -3.47 | **J1018** | 10 | 0.68 | -2.48 |
| **J1302** | 43.8 | 3.17 | -0.71 | **J1018** | 10.5 | 0.73 | 0.33 |
| **J1302** | 46.4 | 3.38 | -0.88 | **J1018** | 11 | 0.99 | 0.15 |
| **J1302** | 47.3 | 1.92 | -2.34 | **J1018** | 11.5 | 1.29 | -0.13 |
| **J1302** | 51.3 | 0.57 | -1.76 | **J1018** | 12 | 1.26 | 0.74 |
| **J1302** | 54.6 | -0.80 | 0.32 | **J1018** | 12.5 | 1.86 | 1.56 |
| **J1302** | 57.8 | -1.33 | 3.76 | **J1018** | 13 | 1.49 | -0.75 |
| **J1302** | 59.6 | 1.77 | -0.37 | **J1018** | 14 | 0.61 | 0.88 |
| **J1302** | 62.6 | 2.65 | 1.38 | **J1018** | 14.5 | -0.33 | 0.16 |
| **J1302** | 64.6 | 1.78 | -0.51 | **J1018** | 15 | 1.92 | 1.32 |
| **J1302** | 66.6 | 2.48 | -0.03 | **J1018** | 16 | 1.27 | 0.04 |
| **J1302** | 68.6 | 2.28 | -2.60 | **J1018** | 16.5 | 0.48 | 0.70 |
| **J1302** | 72.2 | 0.75 | 3.21 | **J1018** | 17 | 0.45 | 1.25 |
| **J1302** | 72.8 | 0.43 | 0.56 | **J1018** | 17.5 | -0.06 | 1.43 |
| **J1302** | 75.6 | -0.62 | 1.86 | **J1018** | 18 | -0.56 | 0.58 |
| **J1302** | 78.5 | -1.35 | -0.34 | **J1018** | 18.5 | -0.40 | 1.45 |
| **J1302** | 79.6 | -0.61 | -1.12 | **J1018** | 19 | -0.73 | -0.11 |
| **J1302** | 81.7 | -0.66 | -0.56 | **J1018** | 19.5 | -0.19 | 0.66 |
| **J1302** | 83.8 | -0.72 | -3.31 | **J1018** | 20 | -2.01 | -0.81 |
| **J1302** | 84.4 | -0.18 | -2.36 | **J1018** | 28 | -1.74 | 1.57 |
| **J1302** | 109 | -0.66 | -1.22 | **J1018** | 29 | -0.47 | -1.04 |
| **J1302** | 111.1 | -1.81 | 0.32 | **J1018** | 29.5 | -1.23 | -3.77 |
| **J1302** | 113.4 | 0.02 | -1.95 | **J1018** | 30 | -3.27 | -0.62 |
| **J1302** | 125.9 | -1.23 | -2.51 | **J1018** | 30.5 | -2.00 | 0.64 |
| **J1302** | 129.8 | 0.58 | -2.33 | **J1018** | 31 | -0.94 | 0.15 |
| **J1302** | 134.8 | 2.63 | -0.64 | **J1018** | 31.5 | -0.35 | -2.17 |
| **J1302** | 139.7 | 1.67 | -1.07 | **J1018** | 32 | -0.61 | -2.66 |
| **J1302** | 144.8 | 2.69 | 1.19 | **J1018** | 37.1 | -2.83 | -1.46 |
| | | | | **J1018** | 37.5 | -2.43 | -1.75 |
| **J1201** | 74.4 | 1.61 | -6.80 | **J1018** | 38.5 | -1.56 | -0.93 |
| **J1201** | 74.8 | -0.39 | -6.70 | **J1018** | 39 | -2.31 | -1.44 |
| **J1201** | 75.6 | -0.08 | -7.75 | **J1018** | 39.5 | -1.20 | -0.31 |
| **J1201** | 76.2 | 0.28 | -6.99 | **J1018** | 40 | -1.03 | -0.66 |
| **J1201** | 76.5 | -0.13 | -5.89 | **J1018** | 40.5 | -1.01 | -0.62 |
| **J1201** | 77.5 | 1.42 | -5.73 | **J1018** | 41 | -0.53 | -0.76 |
| **J1201** | 77.6 | 0.64 | -6.10 | **J1018** | 41.5 | 0.18 | -0.90 |
| **J1201** | 78 | 0.38 | -6.02 | **J1018** | 42 | -0.36 | -1.07 |

| | | | | | | | |
|---|---|---|---|---|---|---|---|
| **J1201** | 78.3 | 0.38 | -6.21 | **J1018** | 42.6 | 0.77 | -1.01 |
| **J1201** | 86.5 | 0.36 | -6.47 | **J1018** | 43 | 0.37 | -1.03 |
| **J1201** | 87.1 | 0.73 | -7.31 | | | | |
| **J1201** | 87.5 | 1.55 | -7.19 | **J1210** | 0.6 | 1.81 | -3.75 |
| **J1201** | 88 | 1.78 | -7.33 | **J1210** | 2.3 | 2.16 | -2.86 |
| **J1201** | 88.5 | 0.53 | -6.92 | **J1210** | 3.2 | 2.36 | -3.04 |
| **J1201** | 89 | 1.26 | -6.93 | **J1210** | 4.1 | 1.50 | -2.34 |
| **J1201** | 89.5 | 1.32 | -6.89 | **J1210** | 6.1 | 2.57 | -1.21 |
| **J1201** | 90 | 0.76 | -7.15 | **J1210** | 8.2 | 2.74 | -2.45 |
| **J1201** | 90.5 | 0.63 | -6.88 | **J1210** | 9.1 | 3.42 | -1.68 |
| **J1201** | 90.9 | 0.75 | -7.15 | **J1210** | 10.1 | 2.87 | -2.34 |
| **J1201** | 91.2 | 0.82 | -6.93 | **J1210** | 11.1 | 3.39 | -4.96 |
| **J1201** | 92.5 | 0.42 | -7.45 | **J1210** | 12.6 | 4.20 | -3.73 |
| **J1201** | 93 | -0.47 | -7.30 | **J1210** | 13.9 | 5.07 | -2.53 |
| **J1201** | 93.8 | -0.35 | -6.98 | **J1210** | 15 | 5.33 | -1.78 |
| **J1201** | 94.5 | 0.08 | -6.64 | **J1210** | 19.2 | 5.84 | -3.04 |
| **J1201** | 96 | 0.68 | -6.84 | **J1210** | 22.6 | 6.09 | 1.43 |
| **J1201** | 96.3 | 0.39 | -6.63 | **J1210** | 24.4 | 5.50 | -3.10 |
| **J1201** | 96.7 | 1.12 | -6.77 | **J1210** | 26.3 | 5.97 | -0.01 |
| **J1201** | 107.5 | -1.58 | -4.33 | **J1210** | 28.4 | 5.33 | -3.08 |
| **J1201** | 108.1 | 1.54 | -3.43 | **J1210** | 38.8 | 3.10 | -2.08 |
| **J1201** | 108.5 | 0.80 | -2.94 | **J1210** | 41 | 3.99 | -4.17 |
| **J1201** | 109.1 | 1.14 | -2.83 | **J1210** | 43 | 4.55 | -0.56 |
| **J1201** | 109.4 | -0.20 | -3.86 | **J1210** | 61.6 | 4.97 | 0.96 |
| | | | | **J1210** | 62.1 | 2.33 | 1.88 |
| **J1202** | 0.3 | 4.11 | -1.16 | **J1210** | 63.2 | 5.08 | -2.60 |
| **J1202** | 1.8 | 3.86 | 0.47 | **J1210** | 85.4 | 4.44 | -2.94 |
| **J1202** | 3.9 | 3.61 | -1.20 | **J1210** | 87.1 | 4.59 | 1.36 |
| **J1202** | 11.4 | 0.68 | 0.83 | **J1210** | 90.2 | 4.11 | -5.07 |
| **J1202** | 27.6 | 1.53 | -5.32 | **J1210** | 93.4 | 4.01 | -4.42 |
| **J1202** | 36.8 | 2.20 | -0.36 | **J1210** | 95.1 | 2.48 | -0.70 |
| **J1202** | 48.7 | 2.10 | -1.96 | **J1210** | 96.5 | 2.52 | 0.92 |
| **J1202** | 58.1 | 1.54 | -1.57 | **J1210** | 97.6 | 5.00 | 2.07 |
| **J1202** | 58.3 | 2.17 | 0.45 | **J1210** | 99.2 | 3.82 | 0.63 |
| **J1202** | 61.8 | 2.90 | 0.23 | **J1210** | 101.4 | 4.15 | 0.99 |
| **J1202** | 74.3 | 1.54 | -6.17 | **J1210** | 103.1 | 4.53 | 1.34 |
| **J1202** | 81.6 | 2.02 | -5.87 | **J1210** | 105 | 3.73 | -4.64 |
| **J1202** | 86.7 | 2.06 | -4.54 | **J1210** | 106.2 | 3.93 | -5.92 |
| **J1202** | 109.2 | 1.92 | -9.05 | **J1210** | 108.9 | 2.18 | -0.99 |
| **J1202** | 119.7 | 1.41 | -6.13 | **J1210** | 109.8 | 3.54 | -4.67 |
| **J1202** | 130.2 | 2.19 | -5.84 | **J1210** | 107.5 | 2.70 | -2.51 |
| **J1202** | 155.4 | 1.32 | -6.07 | **J1210** | 110.7 | 3.68 | -1.17 |
| **J1202** | 166.2 | 1.26 | -5.72 | **J1210** | 113.3 | 4.26 | 0.58 |
| **J1202** | 176.7 | 1.29 | -5.32 | **J1210** | 114.9 | 4.61 | 0.04 |
| **J1202** | 187.2 | -0.48 | -2.25 | **J1210** | 117.1 | 5.03 | 1.84 |
| **J1202** | 197.7 | 0.13 | -0.72 | **J1210** | 119.2 | 4.61 | 2.26 |
| **J1202** | 208.2 | 0.91 | -3.56 | **J1210** | 123.1 | 4.46 | 2.79 |
| **J1202** | 218.5 | 3.63 | -0.43 | **J1210** | 127.2 | 4.88 | 1.60 |
| | | | | **J1210** | 129.2 | 5.39 | 2.25 |
| **J1203** | 0.3 | 0.56 | -6.23 | **J1210** | 133.4 | 5.83 | 2.24 |
| **J1203** | 0.9 | 0.64 | -7.05 | **J1210** | 137.8 | 5.63 | 1.89 |
| **J1203** | 1.6 | 0.44 | -7.59 | **J1210** | 140.3 | 5.87 | 2.49 |
| **J1203** | 2.5 | 1.21 | -6.06 | **J1210** | 142.4 | 6.05 | 1.96 |
| **J1203** | 3.3 | 1.05 | -6.36 | **J1210** | 147.1 | 5.75 | 1.31 |
| **J1203** | 4.1 | 1.25 | -5.19 | **J1210** | 149.5 | 5.70 | 1.50 |
| **J1203** | 4.15 | 1.54 | -5.10 | **J1210** | 152.5 | 5.96 | 1.46 |
| **J1203** | 5 | 1.34 | -5.10 | **J1210** | 155.1 | 5.81 | 1.05 |
| **J1203** | 6.3 | 1.39 | -6.43 | **J1210** | 157.1 | 5.56 | -1.19 |

| | | | | | | | |
|---|---|---|---|---|---|---|---|
| **J1203** | 7 | 1.93 | -3.93 | **J1210** | 159.4 | 4.96 | 0.82 |
| **J1203** | 8.8 | 2.05 | -4.96 | **J1210** | 163 | 5.26 | 0.92 |
| **J1203** | 9.7 | 2.71 | -5.49 | **J1210** | 165.4 | 5.50 | 1.92 |
| **J1203** | 10.1 | 3.33 | -1.37 | **J1210** | 168.1 | 5.87 | 4.19 |
| **J1203** | 12.1 | 3.64 | -0.37 | **J1210** | 172.3 | 5.48 | 0.47 |
| **J1203** | 13.2 | 2.10 | -4.69 | **J1210** | 174.1 | 5.02 | -2.13 |
| **J1203** | 14.2 | 1.29 | -5.02 | **J1210** | 176 | 4.77 | 1.05 |
| **J1203** | 15.1 | 0.99 | -1.54 | **J1210** | 177.9 | 4.62 | 0.62 |
| **J1203** | 16 | 0.90 | -0.70 | **J1210** | 180.2 | 4.30 | -0.76 |
| **J1203** | 17 | -0.84 | -2.22 | **J1210** | 182.2 | 4.72 | 0.39 |
| **J1203** | 17.8 | -2.49 | 0.68 | **J1210** | 183.7 | 4.84 | 2.13 |
| **J1203** | 18.8 | -1.63 | 0.24 | **J1210** | 186.1 | 5.06 | 0.71 |
| **J1203** | 21.1 | -3.28 | 0.31 | **J1210** | 187.9 | 4.91 | 0.62 |
| **J1203** | 25.2 | -4.18 | -1.57 | **J1210** | 192.3 | 4.73 | -1.77 |
| **J1203** | 25.4 | -3.74 | 0.07 | **J1210** | 194.2 | 4.89 | -0.29 |
| **J1203** | 35.5 | -0.73 | -0.63 | **J1210** | 196.2 | 4.22 | 0.59 |
| **J1203** | 36.1 | -1.41 | -2.21 | **J1210** | 197.8 | 2.02 | 0.64 |
| **J1203** | 36.5 | -2.10 | -1.49 | **J1210** | 200.1 | 4.68 | -2.97 |
| | | | | **J1210** | 201.9 | 4.66 | -3.11 |
| **J1204** | 0.3 | 4.00 | -2.84 | **J1210** | 204.1 | 4.16 | -5.72 |
| **J1204** | 1 | 3.91 | -3.11 | **J1210** | 207.8 | 4.42 | -3.08 |
| **J1204** | 1.3 | 3.61 | -5.12 | **J1210** | 206.1 | 4.74 | -3.23 |
| **J1204** | 2 | 3.77 | -4.16 | **J1210** | 206.2 | 5.03 | -0.78 |
| **J1204** | 2.5 | 3.61 | -4.36 | **J1210** | 208.2 | 4.29 | -1.04 |
| **J1204** | 3 | 3.78 | -2.45 | **J1210** | 210.7 | 4.58 | 0.63 |
| **J1204** | 3.4 | 3.15 | -2.96 | **J1210** | 212.1 | 4.82 | -1.28 |
| **J1204** | 4.1 | 2.58 | 0.35 | **J1210** | 214.1 | 4.53 | 1.92 |
| **J1204** | 4.4 | 2.26 | -0.19 | **J1210** | 216.2 | 5.15 | 0.48 |
| **J1204** | 5 | 2.01 | -0.93 | **J1210** | 218 | 4.53 | -1.50 |
| **J1204** | 5.5 | 1.67 | 0.42 | **J1210** | 220.1 | 4.66 | -0.17 |
| **J1204** | 6.1 | 1.63 | 0.11 | **J1210** | 222.4 | 4.92 | -0.44 |
| **J1204** | 6.5 | 1.29 | -0.19 | **J1210** | 223.9 | 4.46 | -3.78 |
| **J1204** | 7 | 0.73 | 0.31 | **J1210** | 226.1 | 4.70 | -0.50 |
| **J1204** | 7.4 | 0.01 | 0.92 | **J1210** | 227.9 | 4.56 | -0.63 |
| **J1204** | 8 | 1.05 | 1.33 | **J1210** | 230.1 | 3.24 | 0.73 |
| **J1204** | 8.3 | 0.58 | 1.00 | **J1210** | 232.1 | 3.35 | -1.85 |
| **J1204** | 19.3 | -2.78 | -1.19 | **J1210** | 234.2 | 3.05 | -0.43 |
| **J1204** | 20 | -2.67 | -1.22 | **J1210** | 236.1 | 3.36 | -2.36 |
| **J1204** | 20.4 | -4.02 | -1.56 | **J1210** | 238.2 | 2.97 | 1.66 |
| **J1204** | 20.9 | -3.77 | -0.94 | **J1210** | 242.1 | 3.32 | -3.67 |
| **J1204** | 21.1 | -3.60 | -0.62 | **J1210** | 244.6 | 3.30 | -1.54 |
| **J1204** | 21.9 | -7.00 | -1.30 | **J1210** | 245.9 | 3.85 | 0.80 |
| **J1204** | 22.3 | -2.76 | -4.21 | **J1210** | 248.4 | 3.74 | -0.49 |
| **J1204** | 22.9 | -4.21 | -1.87 | **J1210** | 249.8 | 3.31 | 1.06 |
| **J1204** | 23.3 | -3.96 | -2.01 | **J1210** | 252.6 | 4.37 | 2.88 |
| **J1204** | 23.9 | -3.94 | -2.07 | **J1210** | 258.2 | 3.61 | 1.85 |
| **J1204** | 24.4 | -4.07 | -2.22 | **J1210** | 260.1 | 3.77 | 2.85 |
| **J1204** | 25.4 | -2.88 | -5.85 | **J1210** | 262.4 | 3.56 | 1.91 |
| **J1204** | 25.9 | -6.53 | -2.16 | **J1210** | 263.9 | 3.90 | -1.23 |
| **J1204** | 27.2 | -5.64 | -2.07 | **J1210** | 276.1 | 2.64 | 0.95 |
| **J1204** | 27.5 | -5.50 | -1.89 | **J1210** | 359.9 | 4.68 | 2.34 |
| **J1204** | 29.6 | -3.26 | -0.82 | **J1210** | 416.5 | 3.25 | 2.13 |
| **J1204** | 30.9 | -2.97 | -2.95 | **J1210** | 418.1 | 3.39 | 1.40 |
| **J1204** | 32.2 | -2.37 | -0.28 | **J1210** | 420.1 | 3.51 | -2.98 |
| | | | | **J1210** | 422.1 | 3.98 | 0.91 |
| **J1207** | 0.5 | 1.74 | 1.43 | **J1210** | 424.2 | 3.90 | 1.94 |
| **J1207** | 2.6 | 0.18 | -0.88 | **J1210** | 426.3 | 3.84 | -0.30 |
| **J1207** | 3.9 | 0.89 | -1.35 | **J1210** | 427.8 | 4.51 | -4.08 |

| | | | | | | | |
|---|---|---|---|---|---|---|---|
| **J1207** | 14.9 | 0.85 | -2.99 | **J1210** | 428.2 | 4.34 | -3.66 |
| **J1207** | 57.2 | 2.16 | -0.90 | **J1210** | 430.1 | 4.33 | -4.03 |
| **J1207** | 58.4 | 5.16 | 1.02 | **J1210** | 431.8 | 4.37 | -5.61 |
| **J1207** | 59.2 | 4.27 | 0.40 | **J1210** | 434 | 4.38 | -1.94 |
| **J1207** | 60.8 | 3.99 | -0.24 | **J1210** | 435.8 | 3.80 | -0.92 |
| **J1207** | 61.7 | 3.95 | 1.14 | **J1210** | 438.1 | 3.74 | -2.22 |
| **J1207** | 66.1 | 3.14 | -1.14 | **J1210** | 440.1 | 2.49 | -0.41 |
| **J1207** | 68 | 5.49 | 1.81 | **J1210** | 443.8 | 2.37 | -1.22 |
| **J1207** | 73.5 | 5.00 | 1.13 | **J1210** | 446.1 | 1.76 | 0.04 |
| **J1207** | 81.9 | -0.24 | 1.77 | **J1210** | 447 | 2.76 | -2.40 |
| **J1207** | 99 | 1.28 | 1.08 | **J1210** | 448.2 | 3.07 | -1.13 |
| **J1207** | 104.7 | 0.82 | 0.52 | **J1210** | 518 | 1.63 | -7.28 |
| **J1207** | 109.1 | -0.65 | -0.71 | **J1210** | 518.5 | 1.44 | -8.28 |
| **J1207** | 114.7 | 0.61 | 0.08 | **J1210** | 519 | 1.57 | -9.06 |
| **J1207** | 118.9 | 1.21 | -3.75 | **J1210** | 519.5 | 0.69 | -8.49 |
| **J1207** | 122.5 | 1.19 | -7.66 | **J1210** | 521.8 | 0.49 | -2.94 |
| **J1207** | 145.9 | 3.32 | -4.86 | **J1210** | 524.3 | -3.62 | -3.07 |
| **J1207** | 151.8 | 3.70 | -5.61 | **J1210** | 526.1 | -3.67 | -3.10 |
| **J1207** | 156.1 | 3.13 | -2.65 | **J1210** | 527.9 | -3.69 | -2.79 |
| **J1207** | 161.2 | 3.81 | -0.38 | **J1210** | 531 | -0.45 | -4.68 |
| **J1207** | 165.4 | 2.45 | 0.83 | **J1210** | 534 | 0.27 | -4.94 |
| **J1207** | 171.2 | 3.55 | -3.24 | | | | |
| **J1207** | 176.4 | 3.63 | -2.28 | **J1301** | 20 | 5.13 | -5.34 |
| **J1207** | 179.9 | 4.14 | 1.66 | **J1301** | 22 | 5.00 | -4.60 |
| **J1207** | 184.4 | 2.45 | -0.80 | **J1301** | 24 | 4.70 | -6.65 |
| **J1207** | 188 | 3.86 | 1.23 | **J1301** | 25.9 | 4.05 | -3.00 |
| **J1207** | 189.7 | 3.84 | -0.75 | **J1301** | 28.3 | 3.04 | -0.31 |
| **J1207** | 196 | 3.29 | -1.72 | **J1301** | 30.2 | 4.91 | -2.75 |
| **J1207** | 201 | 3.17 | -0.10 | **J1301** | 32.2 | 5.09 | -3.11 |
| | | | | **J1301** | 33.8 | 5.49 | -0.38 |
| **J907** | 0 | 4.10 | -1.69 | **J1301** | 36 | 5.06 | -0.79 |
| **J907** | 1 | 2.18 | -3.54 | **J1301** | 40.2 | 5.28 | 0.70 |
| **J907** | 23.5 | 3.60 | -0.40 | **J1301** | 42.9 | 5.40 | -0.44 |
| **J907** | 24.5 | 3.44 | 0.96 | **J1301** | 43.8 | 4.98 | 2.31 |
| **J907** | 25.5 | 3.29 | 0.22 | **J1301** | 48 | 4.14 | 1.91 |
| **J907** | 26.5 | 2.43 | 0.40 | **J1301** | 49.7 | 4.40 | 1.77 |
| **J907** | 27.5 | -0.15 | -4.55 | **J1301** | 54.5 | 4.00 | 0.52 |
| **J907** | 29.5 | 2.05 | -0.31 | **J1301** | 56.4 | 4.41 | 1.94 |
| **J907** | 30.5 | 3.23 | 0.77 | **J1301** | 58.1 | 4.21 | 0.90 |
| **J907** | 31 | 3.32 | 1.81 | **J1301** | 60.2 | 4.62 | 1.76 |
| **J907** | 32 | 2.30 | -0.81 | **J1301** | 62.6 | 4.10 | 2.42 |
| **J907** | 33 | 3.41 | 0.59 | **J1301** | 62.8 | 3.87 | 1.93 |
| **J907** | 34 | 2.75 | 0.05 | **J1301** | 65.6 | 1.61 | -7.04 |
| **J907** | 35 | 2.62 | -3.58 | **J1301** | 66.4 | 1.72 | -5.92 |
| **J907** | 36 | 2.66 | -3.56 | **J1301** | 68.6 | 1.45 | -7.10 |
| **J907** | 37 | 3.13 | -1.69 | **J1301** | 70.7 | 2.12 | 1.39 |
| **J907** | 38 | 3.04 | -1.47 | **J1301** | 72.6 | 2.13 | 1.89 |
| **J907** | 39 | 3.59 | 0.33 | **J1301** | 74.7 | 1.32 | 0.70 |
| **J907** | 40 | 2.79 | 0.39 | **J1301** | 76.4 | 0.83 | 1.72 |
| **J907** | 41 | 2.64 | 0.27 | **J1301** | 100.5 | 1.42 | -0.28 |
| **J907** | 42 | 2.40 | 0.03 | **J1301** | 102.7 | 0.27 | -3.42 |
| **J907** | 43 | 2.10 | 0.52 | **J1301** | 104.5 | 0.89 | -3.58 |
| **J907** | 44 | 2.08 | -0.27 | **J1301** | 107.6 | 0.46 | -0.26 |
| **J907** | 45 | 2.20 | 0.64 | **J1301** | 112 | 2.64 | -2.67 |
| **J907** | 46 | 2.27 | 0.03 | **J1301** | 115 | 4.52 | 0.14 |
| **J907** | 47 | 2.30 | -0.88 | **J1301** | 118 | 4.89 | -0.87 |
| **J907** | 48 | 2.39 | -0.57 | **J1301** | 120.8 | 4.32 | -3.88 |
| **J907** | 49 | 2.54 | 0.12 | **J1301** | 123.7 | 4.05 | -2.95 |

| | | | | | | | |
|---|---|---|---|---|---|---|---|
| **J907** | 50 | 2.77 | -0.40 | **J1301** | 126.9 | 4.30 | -3.20 |
| **J907** | 51 | 2.79 | -0.24 | **J1301** | 130.4 | 3.92 | -3.16 |
| **J907** | 52 | 2.04 | -2.45 | **J1301** | 133 | 4.27 | -2.59 |
| **J907** | 53 | 2.20 | -0.12 | **J1301** | 137.1 | 4.47 | -1.91 |
| **J907** | 54 | 3.51 | 1.11 | **J1301** | 140.3 | 4.39 | -1.59 |
| **J907** | 55 | 2.22 | -0.79 | **J1301** | 147.1 | 4.54 | -1.31 |
| **J907** | 56 | 1.32 | 0.72 | **J1301** | 149.8 | 4.69 | -1.26 |
| **J907** | 57 | -0.04 | 1.15 | **J1301** | 152.6 | 4.80 | -0.12 |
| **J907** | 58 | -2.24 | 3.09 | **J1301** | 165.3 | 4.53 | -0.45 |
| **J907** | 59 | -0.91 | 1.92 | **J1301** | 168 | 4.85 | 0.04 |
| **J907** | 60 | 0.36 | 0.20 | **J1301** | 171 | 4.86 | 0.50 |
| **J907** | 61 | -0.06 | -0.60 | **J1301** | 177.8 | 3.99 | -2.97 |
| **J907** | 62 | 1.42 | -0.67 | **J1301** | 176.7 | 4.69 | -0.19 |
| **J907** | 63 | 1.72 | 0.50 | **J1301** | 179.7 | 4.23 | -2.03 |
| **J907** | 64 | 1.48 | -2.60 | **J1301** | 185.2 | 4.24 | -1.62 |
| **J907** | 65 | 2.22 | -0.63 | **J1301** | 187.1 | 4.92 | 1.19 |
| **J907** | 66 | 0.96 | -4.19 | **J1301** | 190 | 4.58 | -0.40 |
| **J907** | 67 | 1.57 | -0.03 | **J1301** | 193 | 5.01 | 1.36 |
| **J907** | 68 | 0.20 | 1.35 | **J1301** | 196.2 | 4.72 | 0.40 |
| **J907** | 69 | -1.39 | 1.53 | **J1301** | 199.5 | 4.44 | -2.03 |
| **J907** | 70 | -2.12 | 2.08 | **J1301** | 202.3 | 4.52 | -1.22 |
| **J907** | 71 | -2.18 | 2.65 | **J1301** | 205.6 | 4.82 | 0.45 |
| **J907** | 72 | -1.34 | -0.03 | **J1301** | 208 | 4.51 | 0.22 |
| **J907** | 73 | -2.08 | 2.54 | **J1301** | 211 | 4.11 | -2.69 |
| **J907** | 74 | -1.76 | 1.85 | **J1301** | 214.5 | 5.06 | 1.77 |
| **J907** | 75 | -0.86 | 0.60 | **J1301** | 217.7 | 4.12 | -2.23 |
| **J907** | 76 | -1.33 | -2.97 | **J1301** | 220.3 | 4.36 | 1.44 |
| **J907** | 77 | -1.22 | -1.27 | **J1301** | 223 | 5.01 | 1.96 |
| **J907** | 78 | -1.77 | 1.66 | **J1301** | 226.1 | 5.13 | 3.22 |
| **J907** | 79 | -0.99 | -0.28 | **J1301** | 229.5 | 5.32 | 2.93 |
| **J907** | 80 | -1.15 | -0.09 | **J1301** | 232.1 | 5.08 | 1.04 |
| **J907** | 81 | -2.90 | 2.27 | **J1301** | 235.4 | 4.89 | 0.26 |
| **J907** | 82 | -3.28 | 2.00 | **J1301** | 238 | 4.99 | 1.48 |
| **J907** | 83 | -1.24 | -2.25 | **J1301** | 241 | 5.17 | 1.97 |
| **J907** | 84 | -0.89 | -0.53 | **J1301** | 243.1 | 4.92 | 0.66 |
| **J907** | 86 | 0.85 | 0.35 | **J1301** | 246 | 4.92 | 0.95 |
| **J907** | 88 | 0.54 | -0.07 | **J1301** | 248.3 | 4.91 | 1.41 |
| **J907** | 90 | 2.34 | -0.19 | **J1301** | 252 | 4.45 | 0.28 |
| **J907** | 92 | 2.58 | 2.34 | **J1301** | 255.1 | 4.70 | 1.09 |
| **J907** | 94 | 1.94 | 2.03 | **J1301** | 258.1 | 4.89 | 2.21 |
| **J907** | 96 | 1.82 | 2.56 | **J1301** | 261.2 | 4.75 | 1.72 |
| **J907** | 98 | 2.54 | 1.33 | **J1301** | 267 | 5.13 | 2.72 |
| **J907** | 100 | 1.71 | -3.02 | **J1301** | 267 | 5.14 | 2.70 |
| **J907** | 102 | 2.63 | 0.50 | **J1301** | 270.1 | 4.83 | 1.08 |
| **J907** | 104 | 2.43 | 1.43 | **J1301** | 273 | 4.82 | 2.16 |
| **J907** | 106 | 2.77 | 1.75 | **J1301** | 275.1 | 4.77 | 0.65 |
| **J907** | 108 | 2.41 | 1.43 | **J1301** | 279.2 | 4.89 | 2.58 |
| **J907** | 110 | 2.30 | 1.62 | **J1301** | 282 | 4.87 | 2.72 |
| **J907** | 112 | 2.67 | 0.64 | **J1301** | 285.1 | 4.64 | 1.17 |
| **J907** | 114 | 2.89 | 1.01 | **J1301** | 288.2 | 5.03 | 1.63 |
| **J907** | 116 | 2.59 | -0.13 | **J1301** | 291 | 4.99 | 1.46 |
| **J907** | 118 | 2.87 | 0.79 | **J1301** | 293 | 4.77 | 0.56 |
| **J907** | 120 | 3.08 | 2.04 | **J1301** | 296 | 4.95 | 2.30 |
| **J907** | 122 | 2.53 | 0.85 | **J1301** | 299.1 | 4.64 | -0.31 |
| **J907** | 124 | 2.68 | 0.39 | **J1301** | 302.2 | 4.84 | 2.73 |
| **J907** | 126 | 2.94 | 1.26 | **J1301** | 305 | 4.44 | -1.27 |
| **J907** | 128 | 2.73 | -0.01 | **J1301** | 307.8 | 5.17 | 3.36 |
| **J907** | 130 | 2.88 | 0.51 | **J1301** | 310.1 | 4.47 | 0.87 |

| | | | | | | | |
|---|---|---|---|---|---|---|---|
| **J907** | 132 | 2.71 | 0.57 | **J1301** | 312.9 | 4.68 | 2.52 |
| **J907** | 134 | 3.08 | 1.38 | **J1301** | 316 | 4.32 | 1.76 |
| **J907** | 136 | 3.18 | 1.37 | **J1301** | 319 | 4.71 | 1.88 |
| **J907** | 138 | 3.14 | 0.66 | **J1301** | 322.3 | 4.43 | 2.16 |
| **J907** | 140 | 2.22 | -1.09 | **J1301** | 325 | 4.08 | 1.34 |
| **J907** | 142 | 2.98 | 0.32 | **J1301** | 328.2 | 4.66 | -0.16 |
| **J907** | 144 | 3.04 | 0.07 | **J1301** | 331.1 | 4.45 | -0.10 |
| **J907** | 146 | 3.20 | -0.55 | **J1301** | 334 | 4.94 | 1.16 |
| **J907** | 148 | 3.17 | 0.21 | **J1301** | 337 | 4.78 | 0.84 |
| **J907** | 150 | 3.44 | 0.48 | **J1301** | 340 | 4.06 | -2.67 |
| **J907** | 152 | 3.01 | -0.33 | **J1301** | 343.1 | 4.53 | 0.05 |
| **J907** | 154 | 2.58 | -1.83 | **J1301** | 346 | 4.08 | -0.25 |
| **J907** | 156 | 3.11 | 0.78 | **J1301** | 349.4 | 4.78 | 2.10 |
| **J907** | 158 | 3.25 | 0.21 | **J1301** | 352 | 4.49 | 1.46 |
| **J907** | 160 | 3.05 | 1.26 | **J1301** | 355.7 | 4.57 | 2.97 |
| **J907** | 162 | 3.36 | -0.28 | **J1301** | 361.5 | 3.55 | 2.44 |
| **J907** | 164 | 3.31 | 0.24 | **J1301** | 364.6 | 3.77 | 0.25 |
| **J907** | 166 | 3.31 | 0.08 | **J1301** | 368.5 | 3.40 | -1.92 |
| **J907** | 168 | 3.07 | 0.30 | **J1301** | 371.2 | 3.61 | -1.02 |
| **J907** | 170 | 3.13 | 0.19 | **J1301** | 374.9 | 3.45 | -0.49 |
| **J907** | 172 | 2.41 | -0.21 | **J1301** | 377 | 3.66 | 1.25 |
| **J907** | 174 | 1.68 | -2.25 | **J1301** | 380 | 3.87 | 0.85 |
| **J907** | 176 | 2.38 | 0.73 | **J1301** | 385.5 | 4.09 | 1.54 |
| **J907** | 178 | 0.94 | 1.73 | **J1301** | 387.5 | 3.88 | 0.16 |
| **J907** | 180 | 0.49 | -1.47 | **J1301** | 389.7 | 3.44 | -0.28 |
| **J907** | 182 | 2.03 | 1.87 | **J1301** | 391.2 | 3.22 | 2.19 |
| **J907** | 184 | 1.70 | 2.32 | **J1301** | 393 | 3.05 | 1.08 |
| **J907** | 186 | 1.95 | 0.89 | **J1301** | 394.7 | 3.93 | 0.38 |
| **J907** | 186 | 1.93 | 0.89 | **J1301** | 396.4 | 3.83 | 0.70 |
| **J907** | 188 | 1.22 | 0.79 | **J1301** | 397.4 | 4.05 | 0.63 |
| **J907** | 190 | 2.73 | 1.59 | **J1301** | 401.3 | 1.37 | 1.13 |
| **J907** | 192 | 2.47 | 0.70 | **J1301** | 401.7 | 1.71 | 0.45 |
| **J907** | 194 | 2.87 | 1.03 | **J1301** | 402.9 | 0.04 | 0.85 |
| **J907** | 194 | 2.83 | 1.10 | | | | |
| **J907** | 196 | 2.62 | 0.19 | **J908** | 0.1 | 2.33 | -4.60 |
| **J907** | 198 | 2.79 | 1.00 | **J908** | 1 | 3.95 | -4.75 |
| **J907** | 200 | 2.69 | 0.94 | **J908** | 1.2 | 3.78 | -4.79 |
| **J907** | 202 | 2.33 | 0.31 | **J908** | 3 | 2.71 | -4.24 |
| **J907** | 204 | 1.64 | -1.47 | **J908** | 3.8 | 3.44 | -3.29 |
| **J907** | 205.5 | -0.93 | 1.67 | **J908** | 4.4 | 2.09 | -3.25 |
| **J907** | 206 | 0.44 | -0.09 | **J908** | 23.6 | 2.91 | -2.00 |
| **J907** | 208 | 0.43 | 1.51 | **J908** | 25.4 | 1.28 | -0.76 |
| **J907** | 210 | -0.08 | 3.13 | **J908** | 26 | 1.52 | 0.61 |
| **J907** | 212 | 0.06 | 1.51 | **J908** | 26.4 | 0.55 | 0.71 |
| **J907** | 214 | 0.40 | 0.58 | **J908** | 27 | 0.94 | 0.12 |
| **J907** | 216 | -0.24 | 1.12 | **J908** | 28.8 | 1.26 | -2.28 |
| **J907** | 218 | 0.02 | 1.17 | **J908** | 28.9 | 2.48 | -0.69 |
| **J907** | 218 | 0.04 | 1.17 | **J908** | 30 | 3.19 | 0.95 |
| **J907** | 220 | -0.49 | 2.23 | **J908** | 32 | 2.59 | -0.49 |
| **J907** | 222 | -0.28 | 2.07 | **J908** | 34 | 2.62 | -0.06 |
| **J907** | 224 | 1.54 | 0.91 | **J908** | 36 | 2.93 | 0.84 |
| **J907** | 226 | 1.13 | 1.18 | **J908** | 38 | 2.48 | -0.30 |
| **J907** | 228 | 1.59 | 0.63 | **J908** | 40 | 2.12 | -0.10 |
| **J907** | 230 | 1.98 | 0.16 | **J908** | 46 | 0.90 | -1.31 |
| **J907** | 232 | 1.62 | 1.98 | **J908** | 48 | 1.00 | -1.23 |
| **J907** | 234 | 1.07 | 1.61 | **J908** | 50 | 1.07 | -0.04 |
| **J907** | 236 | 1.51 | 1.18 | **J908** | 52 | 0.74 | -4.05 |
| **J907** | 238 | 1.52 | 1.33 | **J908** | 54.1 | -1.15 | 0.47 |

| | | | | | | | |
|---|---|---|---|---|---|---|---|
| **J907** | 240 | 1.68 | 0.73 | **J908** | 56.6 | -2.16 | -0.48 |
| **J907** | 242 | 2.14 | 1.49 | **J908** | 57.1 | -3.25 | 0.21 |
| **J907** | 244 | 1.84 | 4.04 | **J908** | 58 | -2.21 | -0.72 |
| **J907** | 246 | 1.53 | 0.90 | **J908** | 60.4 | -0.37 | -3.31 |
| **J907** | 248 | 0.52 | 0.22 | **J908** | 61.5 | 2.76 | 0.03 |
| **J907** | 250 | 1.02 | 1.19 | **J908** | 62.5 | 2.85 | -0.37 |
| **J907** | 252 | 1.07 | 2.43 | **J908** | 63.3 | 1.94 | 1.00 |
| **J907** | 254 | 1.22 | 2.38 | **J908** | 64.2 | 0.42 | -0.83 |
| **J907** | 256 | 0.81 | 1.65 | **J908** | 64.6 | 2.48 | -0.54 |
| **J907** | 258 | 0.75 | 1.54 | **J908** | 64.8 | -0.80 | -0.87 |
| **J907** | 260 | 0.80 | 2.11 | **J908** | 64.9 | 2.11 | 0.55 |
| **J907** | 262 | 1.00 | 2.05 | **J908** | 66.4 | -0.19 | 0.16 |
| **J907** | 264 | 0.52 | -0.49 | **J908** | 68.1 | 1.50 | 0.66 |
| **J907** | 266 | 0.09 | 1.99 | **J908** | 69.1 | 2.13 | 1.16 |
| **J907** | 268 | 0.35 | 0.75 | | | | |
| **J907** | 270 | 0.68 | 0.83 | **J1122** | 0.1 | 1.82 | -1.98 |
| **J907** | 272 | 0.09 | 2.56 | **J1122** | 2 | 2.05 | -1.38 |
| **J907** | 274 | 1.90 | 2.02 | **J1122** | 3.9 | 0.59 | -3.24 |
| **J907** | 276 | 1.95 | 1.45 | **J1122** | 6 | 1.60 | -0.59 |
| **J907** | 278 | 3.21 | 2.82 | **J1122** | 8 | 1.48 | -0.41 |
| **J907** | 280 | 2.69 | 2.74 | **J1122** | 12 | 0.12 | -0.98 |
| **J907** | 282 | 2.66 | 3.15 | **J1122** | 14 | -0.60 | -1.30 |
| **J907** | 284 | 2.40 | 2.64 | **J1122** | 16 | 1.33 | -3.50 |
| **J907** | 286 | 2.22 | 3.81 | **J1122** | 18 | 3.13 | 0.28 |
| **J907** | 288 | 3.31 | 4.25 | **J1122** | 20 | 2.86 | -0.89 |
| **J907** | 290 | 1.33 | 1.73 | **J1122** | 22 | 1.50 | -0.72 |
| **J907** | 292 | 1.10 | 2.04 | **J1122** | 24 | 1.41 | -1.40 |
| **J907** | 294 | 0.63 | 3.28 | **J1122** | 26 | 1.38 | -1.35 |
| **J907** | 296 | 2.89 | 3.71 | **J1122** | 28 | 1.53 | -1.31 |
| **J907** | 298 | 3.02 | 5.16 | **J1122** | 30 | 1.13 | -1.98 |
| **J907** | 300 | 1.57 | 3.38 | **J1122** | 32 | 0.84 | -2.55 |
| **J907** | 302 | 1.56 | 2.82 | **J1122** | 34 | 1.68 | -1.72 |
| **J907** | 304 | 3.09 | 3.74 | **J1122** | 36 | -0.23 | -2.52 |
| **J907** | 306 | 3.60 | 3.97 | **J1122** | 38 | -0.15 | -3.01 |
| **J907** | 308 | 1.24 | 3.27 | **J1122** | 40 | 1.37 | -3.25 |
| **J907** | 310 | -0.57 | 4.40 | **J1122** | 42 | 1.73 | -2.02 |
| **J907** | 312 | 0.99 | 2.92 | **J1122** | 44 | 1.29 | -1.78 |
| **J907** | 314 | 1.57 | 3.25 | **J1122** | 48 | 1.64 | -1.45 |
| **J907** | 316 | 1.74 | 2.28 | **J1122** | 50 | 1.45 | -1.84 |
| **J907** | 318 | 0.97 | 3.50 | **J1122** | 52 | 2.21 | -0.99 |
| **J907** | 320 | 3.11 | 2.49 | **J1122** | 54 | 2.01 | -1.39 |
| **J907** | 322 | 3.76 | 2.75 | **J1122** | 58 | 2.91 | -1.35 |
| **J907** | 324 | 3.03 | 1.76 | **J1122** | 60 | 2.69 | -1.39 |
| **J907** | 326 | 4.17 | 2.91 | **J1122** | 62 | 1.81 | -1.66 |
| **J907** | 328 | 3.17 | 3.99 | **J1122** | 64 | 0.59 | -0.94 |
| **J907** | 330 | 2.66 | 3.95 | **J1122** | 66 | 0.54 | -0.74 |
| **J907** | 332 | 3.18 | 2.12 | **J1122** | 68 | 0.87 | -1.96 |
| **J907** | 334 | 2.90 | 1.27 | **J1122** | 70 | -0.05 | -1.48 |
| **J907** | 336 | 1.81 | 3.69 | **J1122** | 73 | 0.14 | -1.13 |
| **J907** | 338 | 2.30 | 4.29 | **J1122** | 75 | 0.08 | -1.19 |
| | | | | **J1122** | 77 | 0.53 | -1.82 |
| **J1222** | 30.9 | 2.65 | -3.27 | **J1122** | 79 | 0.26 | -1.64 |
| **J1222** | 31.4 | 3.57 | -2.92 | **J1122** | 83 | 0.43 | -2.86 |
| **J1222** | 31.8 | 3.36 | -2.55 | **J1122** | 85 | 1.61 | -2.42 |
| **J1222** | 32.2 | 2.14 | -3.47 | **J1122** | 87 | 1.62 | -0.20 |
| **J1222** | 39.3 | 2.37 | -4.50 | **J1122** | 89 | 1.89 | -0.99 |
| **J1222** | 39.9 | 2.68 | -4.20 | **J1122** | 91 | 1.16 | -0.57 |
| **J1222** | 45.7 | 2.62 | -4.48 | **J1122** | 93 | 0.03 | -0.17 |

| | | | | | | | |
|---|---|---|---|---|---|---|---|
| **J1222** | 59.7 | 4.04 | -0.87 | **J1122** | 95 | -1.98 | -2.17 |
| **J1222** | 60.6 | 3.51 | -1.05 | **J1122** | 97 | -5.61 | -2.89 |
| **J1222** | 63.2 | 3.82 | -0.22 | **J1122** | 99 | -4.34 | -1.87 |
| **J1222** | 62.1 | 3.39 | 0.14 | **J1122** | 101 | -2.35 | -4.36 |
| **J1222** | 64.3 | 3.37 | -0.89 | **J1122** | 103 | -0.96 | -5.18 |
| **J1222** | 65.2 | 3.60 | -0.23 | **J1122** | 105 | -1.08 | -3.85 |
| **J1222** | 65.7 | 3.08 | 0.48 | **J1122** | 107 | -4.34 | -1.84 |
| **J1222** | 66.1 | -0.80 | -5.76 | **J1122** | 114 | -0.84 | -3.99 |
| **J1222** | 66.2 | 0.21 | -0.64 | **J1122** | 116 | -0.27 | -4.86 |
| **J1222** | 67 | 0.63 | 0.20 | **J1122** | 118 | 0.53 | -4.62 |
| **J1222** | 69.1 | 2.11 | 0.00 | **J1122** | 120 | 0.98 | -5.73 |
| **J1222** | 70.8 | 3.69 | 0.98 | **J1122** | 122 | 1.22 | -4.46 |
| **J1222** | 72.9 | 2.84 | -0.06 | **J1122** | 124 | 1.69 | -2.57 |
| **J1222** | 74.9 | 3.83 | 0.22 | **J1122** | 126 | 2.36 | -3.15 |
| **J1222** | 77.3 | 2.84 | -2.04 | | | | |
| **J1222** | 77.4 | 3.46 | 0.03 | **J1223** | 37.7 | 3.84 | -1.43 |
| **J1222** | 81.1 | 3.13 | -0.51 | **J1223** | 38.8 | 4.01 | -0.34 |
| **J1222** | 83.1 | 3.23 | -1.25 | **J1223** | 39.8 | 2.33 | -0.66 |
| **J1222** | 85 | 3.02 | -2.98 | **J1223** | 40.9 | 1.12 | 0.88 |
| **J1222** | 86.9 | 3.08 | -2.09 | **J1223** | 43.2 | -3.44 | -4.00 |
| **J1222** | 89.6 | 2.81 | -0.81 | **J1223** | 46.3 | -2.70 | -1.73 |
| **J1222** | 92.1 | 1.97 | 0.24 | **J1223** | 48.3 | 0.20 | -0.66 |
| **J1222** | 94 | 1.49 | -1.69 | **J1223** | 51.4 | -2.84 | 2.51 |
| **J1222** | 96 | 1.66 | -0.35 | **J1223** | 53.8 | 0.05 | 1.17 |
| **J1222** | 98.6 | 1.66 | -0.38 | **J1223** | 56.3 | 1.17 | -0.17 |
| **J1222** | 100 | 1.24 | -1.16 | **J1223** | 59.1 | 1.16 | 1.43 |
| **J1222** | 104.3 | 1.22 | -0.63 | **J1223** | 59.7 | 1.85 | 1.60 |
| **J1222** | 109.2 | 1.59 | -1.81 | **J1223** | 62.3 | 1.80 | -0.42 |
| **J1222** | 110.1 | 2.15 | -1.36 | **J1223** | 65.1 | 1.63 | 0.91 |
| **J1222** | 111.3 | 2.00 | -0.41 | **J1223** | 76 | 0.38 | -1.73 |
| **J1222** | 112.7 | 1.90 | -1.49 | **J1223** | 78.1 | 1.74 | -0.62 |
| **J1222** | 113.3 | 2.44 | -1.93 | **J1223** | 80 | 1.23 | -1.09 |
| **J1222** | 116.2 | -1.20 | -0.47 | **J1223** | 82.2 | 2.63 | -0.16 |
| **J1222** | 118 | 0.70 | -0.62 | **J1223** | 84.3 | 1.37 | -0.28 |
| **J1222** | 120.5 | 2.18 | 0.45 | **J1223** | 86.1 | 0.96 | 2.35 |
| **J1222** | 122 | 2.26 | 0.91 | **J1223** | 88.2 | 1.87 | -1.03 |
| **J1222** | 123.5 | 2.61 | 1.67 | **J1223** | 90 | 0.97 | -1.18 |
| **J1222** | 125.5 | -2.86 | 1.17 | **J1223** | 92.2 | 1.31 | 2.13 |
| **J1222** | 126.9 | 0.54 | -2.67 | **J1223** | 94.4 | 1.47 | 1.65 |
| **J1222** | 130.1 | 1.35 | -4.17 | **J1223** | 96.9 | 1.30 | 0.75 |
| **J1222** | 130.2 | 2.17 | -2.65 | **J1223** | 99 | 2.21 | 0.26 |
| **J1222** | 134 | 1.79 | -4.04 | **J1223** | 101.1 | 2.24 | -2.86 |
| **J1222** | 136.1 | 2.25 | -2.27 | **J1223** | 105.6 | 0.73 | -3.30 |
| **J1222** | 138.4 | 2.31 | -2.13 | **J1223** | 107.2 | 0.90 | -3.78 |
| **J1222** | 139.9 | 2.38 | -1.16 | **J1223** | 110.1 | 1.34 | -4.10 |
| **J1222** | 142 | 2.29 | -0.71 | **J1223** | 112.1 | 0.45 | -5.28 |
| **J1222** | 146.2 | 1.91 | -1.20 | **J1223** | 94 | 0.35 | -3.23 |
| **J1222** | 147.1 | 0.88 | 1.19 | **J1223** | 117.3 | 0.67 | -1.91 |
| **J1222** | 150.4 | 1.40 | 0.19 | **J1223** | 121.1 | -0.03 | -1.72 |
| **J1222** | 153.3 | 1.90 | -0.66 | **J1223** | 124.1 | 0.41 | -2.90 |
| **J1222** | 156.5 | 1.88 | -0.14 | **J1223** | 128.6 | -0.57 | -3.00 |
| **J1222** | 158.2 | 2.22 | -1.46 | **J1223** | 129.8 | -1.18 | -3.66 |
| **J1222** | 160 | 2.49 | -0.53 | **J1223** | 132.1 | -0.25 | -2.94 |
| **J1222** | 162.1 | 1.82 | 0.05 | **J1223** | 134.3 | 0.77 | -3.85 |
| **J1222** | 164.2 | 2.28 | -0.25 | **J1223** | 136 | 2.00 | -0.96 |
| **J1222** | 166 | 2.14 | -1.28 | **J1223** | 136 | 1.94 | -0.94 |
| **J1222** | 168 | 2.09 | -1.75 | **J1223** | 137.5 | 0.43 | 0.81 |
| **J1222** | 169.3 | 2.57 | -0.94 | **J1223** | 139.5 | 1.68 | -0.90 |

| | | | | | | | |
|---|---|---|---|---|---|---|---|
| **J1222** | 172.8 | 2.23 | -1.95 | **J1223** | 141.6 | 0.60 | -0.33 |
| **J1222** | 175.1 | 1.32 | -3.70 | **J1223** | 143.5 | -0.11 | 1.65 |
| **J1222** | 177 | 0.37 | -2.40 | | | | |
| **J1222** | 178.5 | -0.42 | -4.29 | **J1019** | 27.7 | 0.53 | -8.62 |
| **J1222** | 179 | -0.22 | -3.63 | **J1019** | 29.4 | 1.48 | -7.34 |
| **J1222** | 191.5 | -0.06 | 0.07 | **J1019** | 30.0 | 1.73 | -6.77 |
| **J1222** | 194.5 | -0.03 | -1.57 | **J1019** | 31.4 | -0.88 | -11.37 |
| **J1222** | 196.2 | -0.06 | -0.98 | **J1019** | 37.3 | 0.36 | -5.38 |
| **J1222** | 198 | 0.01 | -0.63 | **J1019** | 37.7 | 0.84 | -3.28 |
| **J1222** | 200 | -0.20 | -1.98 | **J1019** | 38.3 | 0.65 | -6.59 |
| **J1222** | 202 | -0.25 | -1.56 | **J1019** | 39.1 | 0.44 | -8.31 |
| **J1222** | 205 | 0.27 | -0.39 | **J1019** | 39.6 | 0.98 | -7.17 |
| **J1222** | 207.2 | 0.32 | 0.59 | **J1019** | 40.0 | 1.63 | -5.02 |
| **J1222** | 208.1 | 1.23 | 1.97 | **J1019** | 40.5 | 1.20 | -4.40 |
| **J1222** | 211.2 | 0.70 | 1.95 | **J1019** | 41.0 | 0.25 | -2.28 |
| **J1222** | 212.9 | 0.27 | 1.50 | **J1019** | 79.6 | 4.25 | -0.24 |
| **J1222** | 214.8 | 0.25 | 2.26 | **J1019** | 81.0 | 1.54 | 0.68 |
| **J1222** | 217.1 | -0.04 | 0.81 | **J1019** | 82.0 | 4.06 | 1.34 |
| **J1222** | 218.9 | -1.10 | -0.65 | **J1019** | 83.0 | 4.55 | -0.09 |
| **J1222** | 219.8 | 1.04 | -2.03 | **J1019** | 84.0 | 4.76 | 1.37 |
| **J1222** | 221.2 | 0.74 | 2.52 | **J1019** | 85.0 | 4.76 | 1.13 |
| **J1222** | 225.1 | -1.84 | -0.21 | **J1019** | 86.0 | 4.70 | -0.75 |
| **J1222** | 227.4 | -0.21 | -0.45 | **J1019** | 87.0 | 4.74 | -1.65 |
| **J1222** | 229.9 | -0.33 | -3.86 | **J1019** | 88.0 | 4.99 | -0.20 |
| **J1222** | 234.3 | -1.63 | -4.23 | **J1019** | 89.0 | 4.72 | -0.67 |
| **J1222** | 232.1 | -1.32 | -4.47 | **J1019** | 90.0 | 4.83 | 0.82 |
| **J1222** | 235.4 | -1.22 | -3.79 | **J1019** | 91.0 | 4.46 | 0.65 |
| **J1222** | 237.4 | -0.79 | -2.80 | **J1019** | 92.0 | 2.74 | -0.99 |
| **J1222** | 239.6 | -1.62 | -1.42 | **J1019** | 96.0 | 2.74 | -3.21 |
| **J1222** | 240.6 | -1.48 | -4.50 | **J1019** | 97.0 | 2.84 | -3.78 |
| **J1222** | 242.7 | -1.80 | -3.27 | **J1019** | 98.0 | 2.53 | -4.97 |
| **J1222** | 248.6 | -1.06 | -2.93 | **J1019** | 99.0 | 3.08 | -3.25 |
| **J1222** | 250.7 | -0.54 | -3.22 | **J1019** | 100.0 | 2.99 | -3.42 |
| **J1222** | 253.7 | -0.67 | -4.03 | **J1019** | 101.0 | 3.01 | -3.05 |
| **J1222** | 255.5 | -0.82 | -2.72 | **J1019** | 103.0 | 2.93 | -3.41 |
| **J1222** | 257.6 | -0.26 | -3.35 | **J1019** | 104.0 | 2.88 | -3.20 |
| **J1222** | 259.8 | -0.79 | -2.29 | **J1019** | 105.0 | 2.49 | -2.87 |
| **J1222** | 261.9 | -0.77 | -1.94 | **J1019** | 106.0 | 3.21 | -5.55 |
| **J1222** | 264.9 | -0.78 | -1.51 | **J1019** | 107.0 | 2.61 | -5.02 |
| **J1222** | 269 | -0.05 | -3.14 | **J1019** | 109.0 | 3.47 | -4.26 |
| **J1222** | 271.2 | -0.70 | -2.66 | **J1019** | 110.0 | 3.35 | -3.85 |
| **J1222** | 275.1 | -0.03 | -3.64 | **J1019** | 112.5 | 2.92 | -3.10 |
| **J1222** | 280.6 | -0.64 | -1.54 | **J1019** | 116.0 | 2.95 | -3.26 |
| **J1222** | 282.4 | -1.13 | -4.22 | **J1019** | 117.0 | 2.92 | -3.34 |
| **J1222** | 286.7 | -0.72 | -3.47 | **J1019** | 118.0 | 2.91 | -3.08 |
| **J1222** | 287.8 | -0.56 | -3.12 | **J1019** | 119.0 | 3.30 | -2.52 |
| **J1222** | 290.2 | -0.28 | -3.88 | **J1019** | 120.0 | 3.09 | -2.33 |
| **J1222** | 293.3 | -0.52 | -5.90 | **J1019** | 122.0 | 2.07 | -2.80 |
| **J1222** | 294.4 | 0.14 | -5.66 | **J1019** | 123.0 | 2.53 | -2.50 |
| **J1222** | 296.5 | 0.20 | -4.00 | **J1019** | 124.0 | 2.95 | -5.60 |
| **J1222** | 304.2 | -1.37 | -2.31 | **J1019** | 127.0 | 3.12 | -5.72 |
| **J1222** | 306.7 | -1.50 | -2.19 | **J1019** | 128.0 | 2.50 | -3.83 |
| **J1222** | 311.2 | 0.26 | -2.83 | **J1019** | 129.4 | 2.11 | -6.80 |
| **J1222** | 314 | 1.95 | -1.06 | **J1019** | 130.4 | 1.45 | -3.30 |
| **J1222** | 316.3 | -0.37 | -3.26 | **J1019** | 131.0 | 2.75 | -5.44 |
| **J1222** | 321.6 | 0.38 | 1.17 | **J1019** | 132.0 | 1.39 | -3.22 |
| **J1222** | 323.7 | 1.81 | 2.02 | **J1019** | 133.0 | 0.97 | -2.60 |
| **J1222** | 325.9 | 0.35 | 1.33 | **J1019** | 134.0 | 1.36 | -2.62 |

| | | | | | | | |
|---|---|---|---|---|---|---|---|
| **J1222** | 327.5 | 1.94 | 1.89 | **J1019** | 135.0 | 1.80 | -4.04 |
| **J1222** | 330.6 | 2.09 | 3.84 | **J1019** | 137.0 | 1.32 | -2.31 |
| **J1222** | 332.5 | 1.85 | 1.43 | **J1019** | 140.0 | 4.14 | 1.98 |
| **J1222** | 335 | 3.20 | 3.08 | **J1019** | 141.0 | 3.51 | 0.66 |
| **J1222** | 337.3 | 3.05 | 1.18 | **J1019** | 142.0 | 3.41 | 1.62 |
| **J1222** | 339.2 | 1.80 | 2.66 | **J1019** | 145.0 | 1.09 | 0.06 |
| **J1222** | 343.4 | 3.80 | 3.40 | **J1019** | 147.0 | 1.25 | -3.83 |
| **J1222** | 346.2 | 3.11 | 3.80 | **J1019** | 151.0 | 1.62 | -0.22 |
| **J1222** | 349.3 | 3.39 | 2.77 | **J1019** | 156.0 | 3.26 | 0.48 |
| **J1222** | 352.3 | 1.47 | 1.80 | **J1019** | 157.0 | 2.31 | -0.29 |
| **J1222** | 354.4 | 2.64 | 2.14 | **J1019** | 158.0 | 3.18 | -1.25 |
| **J1222** | 360.5 | 1.72 | 1.75 | **J1019** | 159.0 | 3.20 | -1.04 |
| **J1222** | 362.6 | 1.86 | 0.63 | **J1019** | 163.0 | 2.48 | -0.35 |
| **J1222** | 365.3 | 3.63 | 3.71 | **J1019** | 164.0 | 3.40 | 0.18 |
| **J1222** | 367.6 | 3.06 | 3.75 | **J1019** | 165.0 | 2.07 | -0.05 |
| **J1222** | 372.7 | 3.01 | 1.77 | **J1019** | 173.0 | 3.64 | -0.48 |
| **J1222** | 374.5 | 2.46 | 2.53 | **J1019** | 175.0 | 3.18 | 0.53 |
| **J1222** | 378.4 | 3.27 | 1.66 | **J1019** | 185.0 | 2.38 | 1.81 |
| **J1222** | 381.4 | 2.19 | 0.46 | **J1019** | 190.0 | 1.98 | 1.16 |
| **J1222** | 383.4 | 1.42 | 2.72 | **J1019** | 192.0 | -0.92 | 1.74 |
| **J1222** | 385.6 | 3.11 | 0.38 | **J1019** | 194.0 | -0.04 | -0.07 |
| **J1222** | 388.5 | 2.70 | 0.43 | **J1019** | 196.0 | 0.22 | -0.45 |
| **J1222** | 392.1 | 2.67 | 3.03 | **J1019** | 198.0 | 1.57 | -0.92 |
| **J1222** | 394.5 | 2.26 | -1.42 | **J1019** | 200.0 | 0.85 | -1.34 |
| **J1222** | 396.5 | 2.96 | 1.80 | **J1019** | 202.0 | 1.54 | -1.88 |
| **J1222** | 398.5 | 0.94 | -1.13 | **J1019** | 204.0 | 1.77 | -1.81 |
| **J1222** | 400.6 | 3.58 | 1.27 | **J1019** | 206.0 | 2.14 | -1.79 |
| **J1222** | 404.4 | 2.87 | 1.90 | **J1019** | 208.0 | 2.29 | -0.60 |
| **J1222** | 406.5 | 2.43 | 2.58 | **J1019** | 210.0 | 2.17 | -1.39 |
| **J1222** | 408.5 | 2.81 | 1.82 | **J1019** | 212.0 | 0.94 | -1.63 |
| **J1222** | 410.6 | 2.78 | 1.93 | **J1019** | 214.0 | 2.22 | -1.33 |
| **J1222** | 412.4 | 2.54 | 2.07 | **J1019** | 216.0 | 0.05 | 1.17 |
| **J1222** | 412.9 | 1.01 | -0.65 | **J1019** | 218.0 | -0.52 | -0.91 |
| **J1222** | 414.8 | 1.52 | -1.12 | **J1019** | 220.0 | -2.23 | 0.78 |
| | | | | **J1019** | 222.0 | 0.26 | -0.90 |
| **F928** | 6 | 3.19 | -0.83 | **J1019** | 224.0 | 1.23 | -2.68 |
| **F928** | 8 | 3.68 | 0.34 | **J1019** | 226.0 | -0.14 | -0.13 |
| **F928** | 10 | 3.66 | 0.34 | **J1019** | 228.0 | -0.10 | -0.26 |
| **F928** | 12 | 3.33 | -0.66 | **J1019** | 232.0 | 0.21 | -0.58 |
| **F928** | 14 | 3.28 | -1.58 | **J1019** | 234.0 | 1.54 | -6.80 |
| **F928** | 16 | 3.16 | -1.74 | **J1019** | 236.0 | 1.17 | -7.37 |
| **F928** | 18 | 3.55 | -1.17 | **J1019** | 238.0 | 0.28 | -4.88 |
| **F928** | 20 | 3.90 | -0.67 | **J1019** | 240.0 | 0.28 | -1.01 |
| **F928** | 22 | 3.29 | -1.84 | **J1019** | 242.0 | -2.35 | -2.85 |
| **F928** | 24 | 3.13 | -1.92 | **J1019** | 244.0 | 1.01 | -3.94 |
| **F928** | 28 | 3.52 | -1.20 | **J1019** | 248.0 | 2.55 | -4.28 |
| **F928** | 28 | 3.52 | -1.76 | **J1019** | 250.0 | 1.81 | -2.91 |
| **F928** | 30 | 3.75 | -0.82 | **J1019** | 252.0 | 1.90 | -6.21 |

| | | | | | | | |
|---|---|---|---|---|---|---|---|
| **F928** | 32 | 3.18 | -3.28 | **J1019** | 254.0 | 2.40 | -8.18 |
| **F928** | 34 | 3.50 | -0.85 | **J1019** | 258.0 | 3.34 | -4.46 |
| **F928** | 36 | 3.66 | 1.69 | **J1019** | 260.0 | 2.99 | 0.89 |
| **F928** | 38 | 3.26 | -0.74 | **J1019** | 262.0 | 4.03 | -1.71 |
| **F928** | 40 | 3.91 | -0.13 | **J1019** | 264.0 | 4.21 | -3.16 |
| **F928** | 42 | 3.27 | 0.85 | **J1019** | 266.0 | 5.77 | -2.13 |
| **F928** | 46 | 3.05 | -1.21 | **J1019** | 268.0 | 2.85 | -6.77 |
| **F928** | 50 | 2.81 | -2.12 | **J1019** | 269.0 | 2.62 | -6.77 |
| **F928** | 54 | 2.85 | -3.56 | **J1019** | 275.0 | 2.76 | -4.62 |
| **F928** | 58 | 3.16 | -2.03 | **J1019** | 279.0 | 1.81 | -5.17 |
| **F928** | 62 | 3.07 | -2.02 | **J1019** | 283.0 | 2.63 | -4.79 |
| **F928** | 66 | 2.78 | -0.05 | **J1019** | 287.0 | 1.96 | -4.42 |
| **F928** | 70 | 3.17 | -1.44 | **J1019** | 291.0 | 2.74 | -4.65 |
| **F928** | 74 | 3.05 | 0.62 | **J1019** | 295.0 | 1.84 | -4.66 |
| **F928** | 78 | 3.81 | -0.86 | **J1019** | 299.0 | 2.62 | -1.20 |
| **F928** | 82 | 3.25 | 1.73 | **J1019** | 303.0 | -0.27 | 0.79 |
| **F928** | 88 | 4.27 | 0.77 | **J1019** | 307.0 | 1.35 | -1.01 |
| **F928** | 92 | 3.65 | -0.69 | **J1019** | 311.0 | 0.82 | -2.02 |
| **F928** | 96 | 3.71 | 2.32 | **J1019** | 315.0 | 2.79 | 0.45 |
| **F928** | 100 | 4.75 | 2.35 | **J1019** | 323.0 | 1.89 | -0.50 |
| **F928** | 104 | 4.39 | 2.23 | **J1019** | 327.0 | 1.83 | -5.17 |
| **F928** | 108 | 4.92 | 2.73 | **J1019** | 331.0 | 3.30 | 1.82 |
| **F928** | 112 | 4.98 | -0.49 | **J1019** | 333.0 | 2.88 | 1.69 |
| **F928** | 116 | 4.32 | 1.27 | **J1019** | 337.0 | 3.58 | 1.86 |
| **F928** | 120 | 4.48 | 1.08 | **J1019** | 341.0 | 3.36 | 0.94 |
| **F928** | 124 | 3.94 | 2.66 | **J1019** | 345.0 | 2.89 | 1.30 |
| **F928** | 128 | 5.06 | 1.47 | **J1019** | 355.0 | 4.03 | 1.82 |
| **F928** | 130 | 4.84 | 3.18 | **J1019** | 365.0 | 4.00 | 0.03 |
| **F928** | 136 | 5.10 | 3.00 | **J1019** | 375.0 | 3.99 | 2.25 |
| **F928** | 140 | 4.79 | -0.35 | **J1019** | 385.0 | 3.43 | -1.80 |
| **F928** | 144 | 3.95 | 0.88 | **J1019** | 395.0 | 2.88 | 0.69 |
| **F928** | 148 | 4.51 | 0.28 | **J1019** | 405.0 | 2.97 | 0.75 |
| **F928** | 152 | 3.91 | 1.36 | **J1019** | 415.0 | 3.19 | -0.57 |
| **F928** | 156 | 4.35 | 3.13 | **J1019** | 425.0 | 3.72 | -0.30 |
| **F928** | 160 | 4.79 | -1.48 | **J1019** | 429.0 | 3.59 | -0.47 |
| **F928** | 164 | 3.65 | 2.89 | **J1019** | 433.0 | 3.70 | 0.11 |
| **F928** | 168 | 4.93 | 2.97 | **J1019** | 437.0 | 3.78 | 0.30 |
| **F928** | 172 | 4.66 | 2.43 | **J1019** | 441.0 | 3.63 | 0.79 |
| **F928** | 176 | 4.54 | 2.55 | **J1019** | 447.0 | 4.46 | 1.30 |
| **F928** | 180 | 4.63 | 2.62 | **J1019** | 451.0 | 4.08 | -0.43 |
| **F928** | 184 | 4.78 | 1.04 | **J1019** | 455.0 | 3.91 | 0.92 |
| **F928** | 188 | 3.75 | 1.40 | **J1019** | 459.0 | 4.14 | 2.63 |
| **F928** | 192 | 4.57 | 2.33 | **J1019** | 463.0 | 3.95 | 0.64 |
| **F928** | 196 | 4.80 | 0.11 | **J1019** | 465.0 | 3.47 | 0.09 |
| **F928** | 200 | 3.96 | -1.80 | **J1019** | 467.0 | 3.61 | 0.01 |
| **F928** | 204 | 4.00 | 1.18 | **J1019** | 471.0 | 3.75 | 1.87 |
| **F928** | 208 | 4.61 | 1.09 | | | | |
| **F928** | 212 | 4.65 | 0.44 | | | | |
| **F928** | 216 | 4.19 | 2.95 | | | | |
| **F928** | 220 | 4.54 | 1.88 | | | | |
| **F928** | 228 | 4.30 | 1.26 | | | | |
| **F928** | 232 | 3.70 | 0.92 | | | | |
| **F928** | 236 | 3.60 | 2.12 | | | | |
| **F928** | 240 | 3.50 | 0.49 | | | | |
| **F928** | 244 | 3.47 | 2.05 | | | | |
| **F928** | 248 | 3.44 | 0.94 | | | | |
| **F928** | 256 | 3.23 | 2.43 | | | | |
| **F928** | 260 | 3.88 | 2.31 | | | | |

TABLE 1. SUMMARY OF CALLISON LAKE FORMATION LITHOFACIES (PAGE 1)

| Lithofacies | Composition | Bedding Style/Structures | Depositional Environment | Distribution |
|---|---|---|---|---|
| **Siliciclastic Facies:** | | | | |
| F1: Pebble to granule conglomerate | Clast- to matrix-supported conglomerate; light grey to brown; dominated by quartz and chert with occasional lithics; well-rounded to subangular; moderate sorting; hematite and silica cement | Thin- to thick-bedded; occasionally forming distinct transgressive lags; faint ripple- to dune-scale trough and tabular cross-bedding up to 20 cm thick; erosional base, lenticular geometry, and fining-up packages common; associated with F2 and F3 | Braided fluvial channels. Tidal/Estuarine? Amalgamated channel deposits with abrupt lateral facies change; difficult to discern distinct point-bar or lateral accretion geometries; locally reworking underlying strata; transgressive lag | Restricted to HM |
| F2: Sandstone | Quartz and chert arenite and wacke; very fine- to coarse-grained with occasional granules; moderate sorting; well-rounded to subangular; abundant hematite staining; tan yellow to brown; silica cement | Thin- to medium-bedded; commonly with unidirectional and symmetrical ripple cross-bedding and parallel lamination; occasionally amalgamated; mud chip intraclasts common; interbedded with F3 and forming fining-up packages with F1 | Coastal plain/Estuarine. Maybe local shoreface? Evidence for floodplain or tidal flat deposition with clear tidal influence in the form of distinct tidal ravinement surfaces and fining-up packages | Restricted to HM |
| F3: Variegated siltstone and shale | Variegated shale (red, yellow, green, and purple) interbedded with siltstone; locally contains diagenetic dolostone lenses and iron formation; heavily silicified in certain horizons; occasional very-fine sand sized particles | Locally abundant mudcracks and scours; mostly planar-laminated and associated with F1 and F2; occasional coarsening-upward packages with ripple cross lamination; flaser-bedding and ball and pillows locally | Floodplain or peritidal mud flat/lagoon. Generally associated with transition into marginal marine inner ramp to lagoonal deposits; interbedded sandstone units could represent crevasse splays in a fluvial setting | Restricted to HM |
| F4: Black shale | Black to dark grey shale; TOC to 3.5 wt. %; occasionally silicified with abundant chert nodules; locally contains vase-shaped microfossils; minor silt and very-fine sand; Fe-oxides, pyrite, sphalerite, ankerite(?) locally | Planar-laminated and fissile; occasionally silicified and more resistant; locally interbedded with various lithofacies and no evidence for wave or storm activity; poor sorting with coarser grained horizons | Outer–inner ramp subtidal or lagoonal. Suspension depositon in a low-energy setting; elevated TOC tied to episodic restriction? | HM, TRM |
| **Evaporite/Talc Facies:** | | | | |
| F5: Talc-rich shale | Black talc-rich shale; commonly silicified with abundant chert nodules; organic-rich with TOC up to 4 wt% | Planar-laminated to nodular bedded; abundant diagenetic chert; occasional soft-sediment deformation; intimate association with F6 | Restricted lagoonal to sahbka. Playa lake? Suspension deposition in a low-energy setting; evidence for seismic or storm-generated disruption | TM, TRM? |
| F6: Interbedded talc and dolostone | Black talc-rich shale interbedded with microbial and sucrosic light to dark dolostone; commonly silicified with chert nodules | Nodular- to planar-bedded with microbial lamination; teepees structures, mudcracks, and evaporite pseudomorphs after anhydrite and gypsum common; horizons of talc-shale chip intraclast conglomerate common; local overturned stromatolites and seismites | Sahbka to peritidal mud flat. Evidence for intertidal to peritidal deposition; episodic restriction with sulfate deposition; wave-, storm-, and seismically-generated structures common; complex paragenetic history with multiple Mg-silicate and evaporite transformations | Restricted to TM |
| **Carbonate Facies:** | | | | |
| F7: Stromatolitic bioherm/biostrome | Orange-yellow to dark grey (fresh) stromatolitic doloboundstone; minor terriginous silt and frosted quartz grains; occasional vase-shaped microfossils in disseminated organic matter; microbial sheaths after cyanobacteria | Meter- to decimeter-thick stromatolitic biohermal/biostromal buildups interbedded with F3,4; stromatolites range from domal to columnar with both low- and high-inheritance forms; micritic, oolitic, and intraclastic fill; isolated to laterally linked forms | Middle- to inner-ramp subtidal or lagoonal. Isolated to linked stromatolitic patch reefs or buildups associated with a subtidal depositional setting; possibly lagoonal with no evidence for exposure or wave activity | HM, TRM |

HM – Heterolithic member, TM – Talc member, PM – Platformal member, TRM – Transitional member

TABLE 1. SUMMARY OF CALLISON LAKE FORMATION LITHOFACIES (PAGE 2)

| Lithofacies | Composition | Bedding Style/Structures | Depositional Environment | Distribution |
|---|---|---|---|---|
| F8: Stromatolitic doloboundstone | Light to dark grey stromatolitic doloboundstone; occasional black chert and ferruginous clay-rich laminae; close association with stromatolite-rich intraclast wackestone and grainstone | Centimeter- to meter-thick stromatolitic structures; forms range from laterally-linked, low relief, and domal to high-inheritance columnar structures; intercolumnal fill micritic, oolitic, pisolitic, and intraclasts; scours and corrosive structures common | Middle-Inner ramp subtidal. Heterogeneous assemblage of stromatolitic morphologies; common wave-generated scours and association with F9 and F10; meter-scale high relief domes suggest occasional deeper water setting | All members. |
| F9: Microbialite | Light to dark grey microbial doloboundstone; occasional black chert nodules, terriginous silt, fine- to medium-sized frosted quartz grains; distinguished from F8 by flat, crinkly lamination | Centimeter- to meter-thick microbialite; mm-scale undulatory and wavy lamination; locally containing fenestrae (birds' eye), teepee structures, and mudcracks; occasional seismically-disrupted and folded laminae; discrete intervals of intraclast conglomerate | Inner ramp intertidal to peritidal. Intertidal deposition evidenced by intimate association with F8 and wave- or storm-generated intraclasts; exposure surfaces common; discrete parasequences with F6,8, and 10 | All members. |
| F10: Intraclast grainstone/wackestone | Light to dark grey dolomitic intraclast grainstone and wackestone; almost exclusively composed of clasts from F8 and F9; minor rudstone | Thin- to thick-bedded, tabular to subrounded, sand- to cobble-sized intraclastic grainstone and wackestone matrix-supported with scoured and erosive bases, occasional crude lamination, and faint grading; commonly randomly oriented | Inner ramp subtidal. Subtidal deposits associated with high-energy storm- or wave-generated events that scour and rework material from F9 and F10; no evidence for subaerial exposure | PM, TRM |
| F11: Dolograinstone | Light to dark grey dolograinstone composed of ooids, peloids, pisoids, and/or oncoids; minor terriginous silt component | Thin- to thick-bedded and massive to finely laminated; occasional trough cross-bedding and planar laminated but generally quite massive and crudely stratified; intimately associated with F8, F9, and F10; occasional low-angle cross-bedding | Inner ramp subtidal to intertidal bar or shoal complex. High-energy subtidal deposition associated with tidal sand bars and/or migrating barrier complex; 3D morphology not worked out but commonly interbedded with diverse lithofacies | Restricted to PM |
| F12: Thin-bedded dolomicrite/siltite | Dark grey to black dolomicrite and dolosiltite; commonly composed of microcrystalline and neomorphosed dolospar and dolomicrite; occasional hints of peloidal precuser allochems; ferruginous clay drapes and black chert common | Thin-bedded and laminated with mm-scale parallel lamination; occasional erosional base; black chert commonly late diagenetic and fabric destructive; no evidence for grading or turbidite deposition; commonly resemble Phanerozoic ribbon-bedded limestone | Mid-outer ramp subtidal. Generally constrained to transgressive horizons associated with relatively low-energy deposition; ferruginous drapes could indicate hardground conditions or suspension rainout during highstand; occasionally deformed during seismic activity | PM, TRM |
| **Diagenetic Facies:** | | | | |
| F13: Recrystallized dolostone | Light grey to white sucrosic dolostone with fabric-destructive diagenetic recrystallization; occasional oolitic ghosts | Medium- to thick-bedded and massive; crude stratification and commonly impossible to tell precursor lithology; abundant secondary isopachus, drusy, and botryoidal cements; veins common; locally contains clotty secondary fabric that resembles "thrombolitic" texture | Unclear but commonly associated with subaerial exposure surfaces and coarser-grained lithofacies. | All members |
| F14: Breccia | Grey to white dolostone breccia; commonly silicified with angular clasts of dolostone; matrix composed of both terriginous silt, secondary dolomite spar, and dolosiltite; clasts range from sand- to boulder-sized; local well-rounded quartz sand within cavity fill | Massive and generally thick-bedded; crude stratification with clear horizons indicating subaerial exposure and karst development; clasts composed exclusively of underlying strata in puzzle-fitting fabric; local grykes and irregular cavities filled with terriginous silt and sand | Inner ramp intertidal to peritidal. Clearly associated with subaerial exposure and karst development in dolostone lithologies; possibly associated with uplift and fault breccia in certain localities | PM, TRM |

HM – Heterolithic member, TM – Talc member, PM – Platformal member, TRM – Transitional member